Univerzita Karlova v Praze, Přírodovědecká fakulta

Charles University in Prague, Faculty of Science

Doktorský studijní program: Parazitologie

PhD study program: Parasitology

Mgr. Luboš Voleman

Biogeneze mitosomů *Giardia intestinalis*

Biogenesis of *Giardia intestinalis* mitosomes

Ph.D. Thesis

Thesis supervisor: Mgr. Pavel Doležal, Ph.D.

PRAGUE, 2018

Declaration of the author

I declare that I elaborated this thesis independently. I also proclaim that the literary sources were cited properly and neither this work nor the substantial part of it have been used to reach the same or any other academic degree.

Prohlašuji, že jsem tuto práci zpracoval samostatně a že jsem uvedl všechny použité zdroje a literaturu. Tato práce ani její podstatná část nebyla předložena k získání jiného nebo stejného akademického titulu.

Mgr. Luboš Voleman

Declaration of the thesis supervisor

Data presented in this thesis resulted from a team collaboration at the Laboratory of Protein Transport and Biogenesis of Organelles and from a cooperation with other associates. I declare that the involvement of Mgr. Luboš Voleman in this work was substantial and that he contributed significantly to obtain the results.

Mgr. Pavel Doležal, Ph.D.

Thesis supervisor

Acknowledgements

Many thanks to my supervisor Pavel for his unwavering support and encouragement during all those years, to my lab fellows and all other people who supported and fueled me during my PhD study.

Table of Contents:

ABSTRACT

Mitochondria of opisthokonts undergo permanent fusion and fission throughout the cell cycle. Keeping these two processes in balance is vital for various aspects of mitochondrial and cellular homeostasis. Both mitochondrial fusion and division mechanisms are controlled by highly conserved dynamin-related GTPases that are present in all kingdoms of life. The aspects of mitochondrial dynamics outside the opisthokonts is, however, almost completely unexplored phenomenon.

In our work, we introduced a tool for live imaging of the reduced forms of mitochondria into model organisms *Giardia intestinalis* and *Trichomonas vaginalis*, anaerobic protist parasites from the Excavata supergroup of Eukaryotes. Using this technique, we investigated the dynamics of the mitosomes, the simplest forms of mitochondria, of *G. intestinalis*. The division of mitosomes is restricted to *Giardia* mitosis and is absolutely synchronized with the process. The synchrony of the nuclear and the mitosomal division persists also during the encystation of the parasite. Surprisingly, the sole dynamin-related protein of the parasite seems not to be involved in mitosomal division. However, throughout the cell cycle mitosomes associate with the endoplasmic reticulum, although none of the known ER tethering complexes are present. Instead, the mitosome-ER interface is occupied by lipid metabolism enzyme long chain acyl-CoA synthetase 4.

Additionally, we investigated mitosomal content using in vivo enzymatic tagging method, thereby discovering another component of mitosomal protein import machinery, GiTim44, together with several other mitosomal proteins.

ABSTRAKT

Mitochondrie opisthokont neustále fúzují a dělí se v průběhu celého buněčného cyklu. Udržení těchto dvou procesů v rovnováze je pro buňku zásadní. Mitochondriální fúze i dělení jsou řízeny dynaminovými GTPázami, které jsou konzervovány napříč všemi organismy. Jak mitochondriální fúze a dělení probíhá mimo zmíněnou skupinu organismů téměř není známo.

V naší práci jsme se zabývali zavedením fluorescenčního značení pro live imaging do organismů *G. intestinalis* a *T. vaginalis,* jednobuněčných parazitů ze skupiny Excavata. Pomocí této metody jsme poté zkoumali dynamiku mitosomů, nejjednodušších forem mitochondrií, u *G. intestinalis*. Zjistili jsme, že dělení mitosomů probíhá během mitozy, se kterou je absolutně synchronizováno, a že ke stejné synchronizaci dochází také během encystace parazita. Dále jsme objevili, že během buněčného cyklu jsou mitosomy spojené s endoplasmatickým retikulem, nicméně charakter tohoto spojení není znám, jelikož genom *Giardie* nekóduje žádný ze známých proteinů zodpovědných za zprostředkování tohoto kontaktu. Prozatím jediným proteinem nalezeným v místech kontaktu mitosomů a endoplasmatického retikula je acyl-CoA syntetáza 4, enzym biosyntézy lipidů.

Také jsme se zabývali hledáním dalších potenciálních mitosomálních proteinů pomocí *in vivo* enzymatického značení, díky němuž jsme objevili další komponentu komplexu proteinů transportujícího proteiny do mitosomů, protein Tim44. Spolu s ním jsme identifikovali několik dalších mitosomálních proteinů, jejichž funkce ale zatím zůstává neznámá.

1. INTRODUCTION

1.1 Mitochondrial dynamics and DRPs

In the past few decades, mitochondrial dynamics has been extensively studied using predominantly two model systems, baker's yeast *Saccharomyces cerevisiae*, and mammalian cells. Mitochondrial dynamics in these organisms shares common principles, however, differs in many molecular aspects. Although thoroughly studied, mitochondrial dynamics research outside mammals and fungi is limited only to a handful of studies, e.g. [1–4].

Typical mitochondria of yeast or humans are extremely dynamic organelles undergoing constant fusion and fission. These opposing processes act together to maintain mitochondrial morphology, number and function [5]. Overall, they are crucial for maintaining mitochondrial homeostasis, which is extremely important for the cells. Both mitochondrial fusion and division mechanisms are controlled by highly conserved dynamin-related GTPases (DRPs) that can be found in all kingdoms of life [6].

DRPs probably originate from bacterial ancestors of mitochondria which usually harbor two DRPs encoded in one operon [7]. These two genes are likely a product of a gene duplication [8]. Bacterial DRPs are most closely related to mitofusin and atlastin class of DRPs found in eukaryotes [8]. Unlike bacteria, which use tubulin homologue FtsZ for division [9], mitochondria of most eukaryotes divide using DRPs. Thus, it was suggested that DRPs replaced the role of FtsZ in mitochondrial fission during evolution [10]. This was further supported by the experimental studies showing that FtsZ is still used in mitochondrial division in some eukaryotes [11–15]. Newly published genomes of eukaryotes from several taxa including jakobids, heteroloboseans, malawimonads, stramenopiles, amoebozoans, a breviate, and apusomonads suggest that FtsZ-derived machinery together with MinCDE positioning system have been preserved in mitochondria of most major eukaryotic lineages and that these were replaced independently multiple times in evolution with the DRP-based machinery [16].

DRPs control membrane remodeling via their ability to self-assemble into spiral structures leading to GTP hydrolysis [17,18]. Dynamin, a prototypical member of DRPs, consist of five functional domains (Fig.1). On its N terminus, dynamin harbors GTPase domain capable of binding GDP/GTP, which is also responsible for GTP hydrolysis. This effector domain is followed by so called middle (MD) domain containing amino acid residues that drive dynamin's self-assembly [19]. Pleckstrin homology (PH) domain and proline/arginine-rich region (PRD) are responsible for protein-protein or protein-lipid interactions and binding of dynamin effectors and targeting the protein to plasma membrane where it mediates endocytosis, respectively [17,20–24]. PH and PRD are also, respectively, negative and positive regulators of dynamin's self-assembly and thus GTP hydrolysis.

The alpha helical domain interposed between PH and PRD, GTPase effector domain (GED), interacts with the N-terminal GTPase domain and also stimulates GTP hydrolysis [25].

In general, all DRPs exhibit conserved domain architecture similar to that of dynamin, however, the domains vary in function in different members of DRP family. N-terminal GTPase domain varies only slightly between individual DRPs. Apart from this domain, DRPs share the Middle domain, GED, sometimes called assembly domain, and Insert B, a region highly variable in structure and function, yet crucial for protein functioning. [25,26]. In dynamin, insert B is formed by PH domain. Fibroblasts lacking PH domain of dynamin exhibit impaired endocytosis, and point mutations in the first hydrophobic variable loop 1(VP1) of PH domain cause inability to bind phospholipids [27]. VP1 region is also essential for dynamin insertion into the membranes and efficient high membrane curvature generation, leading to vesicle fission [28,29]. Recent findings show that isolated PH domain of mammalian Dyn1 is a membrane curvature sensor independent on dynamin self-assembly but cannot generate the curvature on its own [30]. PH domains of two mammalian isoforms of dynamin, Dyn1 and Dyn2, are responsible for their different properties *in vivo* and *in vitro* [31]. Insert B region of other DRPs has different function. In mitochondrial outer and inner membrane fusion DRPs, Fzo1/MFNs and Mgm1/OPA1, respectively, insert B serves for anchoring or targeting of these proteins to their specific destination and, in case of Fzo1 and Mgm1, also serves for the interaction with their protein partners such as Ugo1 [32–34]. In addition, in Mgm1/OPA1, insert B binds cardiolipin, a mitochondria-specific lipid that is highly enriched in mitochondrial inner membrane, and is necessary for mitochondrial inner membrane fusion [35–37]. In yeast mitochondrial division DRP, Dnm1, insert B region was shown to harbor highly conserved motif of eight amino acids that is responsible for the interaction with its protein partner, Mdv1 [38]. In DRP1, mammalian homologue of yeast Dnm1, insert B binds its anchoring protein partner MFF, and is indispensable for mitochondrial recruitment and mitochondrial fragmentation [39]. Taken together, DRPs are capable of remodeling the biological membranes due to their shared domain architecture, however, minor differences in their variable domain composition enable them to act in such opposing processes like mitochondrial fusion and division.

Figure 1: Schematic representation of human dynamin-1 (AAA88025.1) domains. The insert B region of human dynamin1 harbors pleckstrin homology (PH) domain. GD, GTPase domain; MD, middle domain; GED, GTPase effector domain; PRD, proline-rich domain [6], modified.

1.1.1 Mitochondrial fusion

Although mitochondrial content transfer occurs also during transient kiss-and-run merging events [40], mixing of mitochondrial content is secured mainly by mitochondrial fusion. During mitochondrial fusion, DNA, mRNA, lipids and proteins are redistributed between organelles which ensures mitochondrial homogeneity and can complement defective mitochondria [5,6,41]. Furthermore, impaired fusion leads to mitochondrial heterogeneity, dysfunction, reduction and even loss of mitochondrial genome, and is lethal for the mouse model [33,34,42–44].

In yeast, mitochondrial fusion is facilitated by two DRPs, Fzo1 and Mgm1, and Ugo1 protein (Fig.2). Protein complex assembled from these components ensures functional coordination of the outer and inner mitochondrial membrane fusion, although how this process is regulated at molecular level is little understood. In addition, the outer and the inner membrane fusions are separable and mechanistically distinct [45].

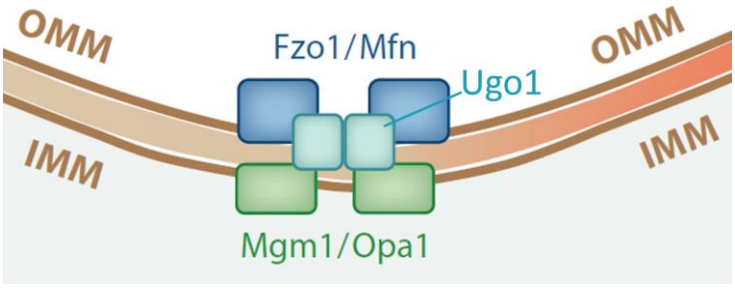

Figure 2: Mechanistic model of mitochondrial fusion. Mitochondrial outer and inner membrane (OMM and IMM) fusion is facilitated by two DRPs, Fzo1 and Mgm1 in the outer and inner membrane, respectively, and Ugo1 that connects the two membranes. Mammalian homologues of Fzo1 and Mgm1 are Mfn and OPA1, respectively. The connection of both membranes outside fungi remains to be clarified [6], modified.

Fzo1 is mitochondrial membrane protein, which is essential for mitochondrial outer membrane fusion. Although, the protein and its role in mitochondrial fusion had been discovered more than a decade ago, a structural model of Fzo1 was clarified only very recently [46]. The protein is anchored to the outer membrane by two membrane-spanning helices with the GTPase domain facing cytosol. The region between the two intramembrane segments is exposed to intermembrane space where it serves for connection between the two mitochondrial membranes [33,34,47]. GTPase domains of two different Fzo1 proteins connect outer membranes prior to mitochondrial fusion and recruit Mdm30, a major regulator of mitochondrial fusion. Mdm30 is an F-box protein that regulates mitochondrial fusion by ubiquitinylation of Fzo1. The ubiquitinylation of Fzo1 and subsequent GTP hydrolysis are enough to promote the outer membrane fusion [48–50].

Mammalian homologues of Fzo1 are mitofusins 1 and 2 (MFN1 and MFN2). Both proteins harbor N-terminal GTPase domain and two heptad repeats (HR1 and HR2) that beset two transmembrane segments close to the C-terminus. Similar to Fzo1, both MFNs are essential and are anchored to the

outer mitochondrial membrane by the two transmembrane regions [51,52]. The HR2 segments of both MFN1 and MFN2 interact with the same region of other MFN located at different mitochondrial membrane forming homotypic complexes, thereby anchoring the membranes which are ready to fuse [52]. Although, both mitofusins are sequentially and functionally redundant, they are also specialized. Only MFN2 interacts with proapoptotic protein Bax, activating assembly of the mitofusin, thus positively regulating mitochondrial fusion [53]. Although, MF1-MFN2 heterotypic complexes are more efficacious for mitochondrial fusion than MFN1- and MFN2- only complexes, Bax protein promotes fusion only in MFN2-MFN2 homotypic interaction [54]. Recent findings suggest that analogously to Fzo1, MFNs are also regulated by ubiquitinylation. E3 ubiquitin ligase Parkin ubiquitinylates MFNs which leads to proteasome-dependent degradation of MFNs and subsequent inhibition of mitochondrial fusion [55,56].

Mgm1 and its mammalian homologue, OPA1, exist in two different variants, long (l-Mgm1/OPA1) and short (s-Mgm1/OPA1), which are functionally distinct. In Mgm1, both variants originate from proteolytic cleavage of nascent protein and are essential for mitochondrial fusion, however, functional GTPase domain is required only for s-Mgm1. Mgm1 is cleaved by mitochondrial processing peptidase (MPP), leading to l-Mgm1, which is inserted to the inner mitochondrial membrane via TIM23 translocase. l-Mgm1 can be further processed by rhomboid protease Pcp1 which gives rise to s-Mgm1, that is a soluble protein of the intermembrane space (IMS) [57–60]. This alternative topogenesis is regulated by ATP levels in mitochondrial matrix [61] and the ratio of l-Mgm1 to s-Mgm1 is crucial for fusion competence of mitochondria [60]. Since l-Mgm1 isoform is located exclusively in mitochondrial cristae and its GTPase domain is not essential, it was proposed to anchor the fusion machinery to the inner membrane [60]. On the other hand, s-Mgm1 requires a functional GTPase domain, thus appears to regulate the inner membrane fusion in a GTP-dependent manner [60]. Moreover, s-Mgm1 is able to alter membrane topography, deform liposomes in vitro and, when bound to GTP, promote local membrane bending, suggesting its direct role in mitochondrial membrane fusion [62]. OPA1 processing is a way more complicated. Single *OPA1* gene encodes for eight protein isoforms [63]. The relative function of all the isoforms is still unclear. Different splicing of OPA1 gives rise to distinct cleavage sites recognized by different proteases. Splice variants 5 and 5b introduce two distinct cleavage sites, S1 and S2, which are cleaved by metalloprotease OMA1 and the intermembrane space protease YME1, respectively. Cleavage yields long, GTPase-active forms of OPA1 that retain the N-terminal transmembrane domain and short soluble forms that are further processed by the Rhomboid-like protease PARL releasing a soluble IMS fraction of OPA1s [64–68]. Furthermore, as a reaction to oxidative stress, OMA1 protease converts all l-OPA1 isoforms to s-OPA1, leading to the inhibition of mitochondrial fusion and subsequent mitochondrial fragmentation [69]. Recent findings show that l-OPA1 isoforms are sufficient to promote mitochondrial fusion while

expression of s-OPA1 isoforms only promotes mitochondrial fragmentation. In addition, short forms of OPA1 partially co-localize with the ER-mitochondria contact sites [70], suggesting the role of OPA1 processing not only in mitochondrial fusion but in mitochondrial dynamics in general. Consistent with these findings, s-OPA1 only is sufficient to maintain cristae morphology and mitochondrial energetics [71], demonstrating the complicated functional interconnection and the importance of both isoforms.

The only non-DRP protein directly mediating mitochondrial fusion is Ugo1. Ugo1 belongs to the superfamily of the inner membrane mitochondrial carrier proteins. However, Ugo1 is of double size when compared to the rest of family members, it is localized in the outer membrane and exhibits opposing N/C topology [72,73]. Ugo1 was shown to physically interact with both Fzo1 and Mgm1, thus coordinating outer and inner membrane fusion [32,74]. It facilitates Fzo1 assembly in a GTP-dependent manner, promoting tethering of the outer mitochondrial membranes [49]. In addition, Ugo1 was suggested to facilitate lipid mixing between the outer and the inner membranes during mitochondrial fusion [75]. Outside fungi, one homolog of Ugo1 has been found so far. It is mammalian SLC25A46, an integral outer membrane protein that also belongs to mitochondrial carrier proteins family [76–78]. According to [76], SLC25A46 does not interact with the outer and the inner membrane GTPases, although this result was questioned later by two independent studies that show its interaction with both mitofusins and OPA1 [79,80], suggesting similar role to Ugo1 protein in yeast. Interestingly, mitochondrial inner and outer membrane can fuse independently on each other in mammals [81], which questions the actual function of SLC25A46. Moreover, knockdown of SLC25A46 causes mitochondrial hyperfusion in HeLa cells, even more profound in fibroblasts [76,79], which is in strike contrast to Ugo1 function in yeast [73,75], thus arguing its pro-fission role. Furthermore, treated fibroblasts show accumulation of DRP1 protein and short OPA1 isoforms and, surprisingly, destabilization of MICOS, protein complex that is indispensable for the maintenance of mitochondrial cristae junctions. In fact, SLC25A46 interacts not only with the outer and the inner membrane GTPases but also with MICOS subunits MIC60, MIC27 and MIC19 [79,80]. These results strongly suggest that SLC25A46 is part of a larger interactome that integrates the major cristae organizing proteins with proteins of the outer mitochondrial membrane [79]. Moreover, SLC25A46 was shown to interact with the components of endoplasmic reticulum membrane protein complex, EMC, and its suppression leads to altered mitochondrial phospholipid composition and abnormal ER morphology [79], albeit these results were questioned later by another group [80]. A full knock out of the SLC25A46 gene is lethal for mice after 3-4 weeks. The mitochondria of affected mice show imbalanced fusion/fission dynamics and abnormalities in their architecture as well as metabolic defects [82].

1.1.2 Mitochondrial division

Mitochondrial division in yeast is facilitated by the member of DRP family, Dnm1, which forms helical structures that surround mitochondria and constrict upon GTP hydrolysis [83–85]. The same features imply for its mammalian homologue, DRP1 [86,87]. Dnm1/DRP1 is a cytosolic protein that needs to be recruited to the mitochondrial division site prior to division. In yeast, mitochondrial outer membrane protein Fis1 in concert with Mdv1 target Dnm1 to mitochondrial surface. The N-terminal cytosolic domain of Fis1 interacts directly with Mdv1 [88–90]. This interaction is facilitated by two interfaces in the coiled coil region of Mdv1 [91]. Mdv1 also binds to specific motif in the insert B region of Dnm1 [38,88–90], thus serving as a molecular bridge between mitochondria and cytosolic Dnm1 [92]. Surprisingly, Mdv1 alone is dispensable for Dnm1 recruitment to mitochondria but essential for the division itself [89], which indicates that Mdv1 acts downstream of Dnm1 recruitment. Consistent with this finding is a fact that Mdv1 interacts efficiently only with Dnm1 assembled in GTP-bound rings and spirals that are localized to mitochondrial surface [93]. The exact role of Mdv1 recruitment of Dnm1 is, however, not fully resolved. Caf4 is Mdv1 paralog that also interacts with Dnm1. It localizes to mitochondria in Fis1-dependent manner and interacts with each component of the fission apparatus, Fis1, Mdv1 and Dnm1. Moreover, yeast cells lacking both Mdv1 and Caf4 are not able to recruit Dnm1 to mitochondrial surface, demonstrating the possible role of Caf4 in this process [94]. Only minority of Dnm1-assemblies on mitochondrial surface are directly involved in mitochondrial fission. Most of the assemblies are dynamic and are not localized to mitochondrial constriction sites [95]. Many of the mitochondria-associated Dnm1 clusters point to the cell surface and this polarization is impaired in cells lacking Caf4 or Fis1 but not Mdv1 [96]. Surprisingly, structural orthologues of Mdv1 or Caf4 were not found in mammals, thus how the DRP1 is recruited to mitochondrial surface has not been completely clarified. There have been several candidate proteins identified so far. They are hFIS1, orthologue of yeast division element, mitochondrial fission factor MFF and mitochondrial dynamics proteins MiD49 and MiD51 (alternatively named Mief2 and Mief1, respectively) [97–103]. Contradictory studies published in the past decade reported on the role of MiD proteins in mitochondrial division or fusion. The overexpression of both MiDs impairs mitochondrial fission by sequestering DRP1 specifically at mitochondrial surface, thus promoting mitochondrial fusion. Moreover, targeting of either MiD49 or MiD51 to peroxisomal or lysosomal surface leads to DRP1 recruitment to these organelles [104]. Furthermore, when co-expressed with soluble DRP1 (variant 3, NCBI reference sequence number NP_005681.2) in yeast division-defective strain, both MiDs as well as MFF are capable of rescuing the mitochondrial morphology. However, this phenotype was not observed when soluble DRP1 was expressed alone or together with hFis1 [105]. MiD49 as well as MiD51 and MFF independently recruit

DRP1 to mitochondria and the loss of more than one adaptor protein confers resistance to cell death induced by CCCP, a mitochondrial fragmentation-inducing agent [106]. According to the proximity-based labeling technique [107], MiD51 and MFF assemble to the same division foci as DRP1 during mitochondrial division [106], as previously suggested by Elgass and colleagues, using FRET analysis and colocalization experiments [108]. In contrast to yeast mitochondria, the exact role of hFiS1 in the recruitment of DRP1 to mammalian mitochondria is uncertain. Although hFis1 has been shown to participate in the process, it is not an essential factor for the recruitment nor for the mitochondrial fission itself [100,103,105,106].

In addition to the interacting proteins, the activity of DRP1 is strongly influenced by the posttranslational modifications such as phosphorylation, nitrosylation, sumoylation and ubiquitinylation as reviewed by Wilson and colleagues [109].

Until recently, DRP1 was thought to be the only dynamin-like protein involved in mitochondrial fission in mammalian cells. However, recently a "classical" dynamin orthologue dynamin-2 (DYN2) (Sontag et al., 1994) was also shown to participate in the process (Lee et al., 2016). DYN2 is also recruited to mitochondrial constriction sites marked by DRP1 and the cells lacking DYN2 have impaired mitochondrial division. Interestingly, both dynamins, DRP1 and DYN2, behave differently during mitochondrial division event. Unlike DRP1, DYN2 is recruited to mitochondria only transiently just prior to the division event and the assembly of DYN2 requires pre-existing DRP1-dependent constriction of mitochondria. After division, DYN2 segregate to only one of the two generated mitochondrial tips [111].

The overall picture of mitochondrial division is summarized in Fig.3.

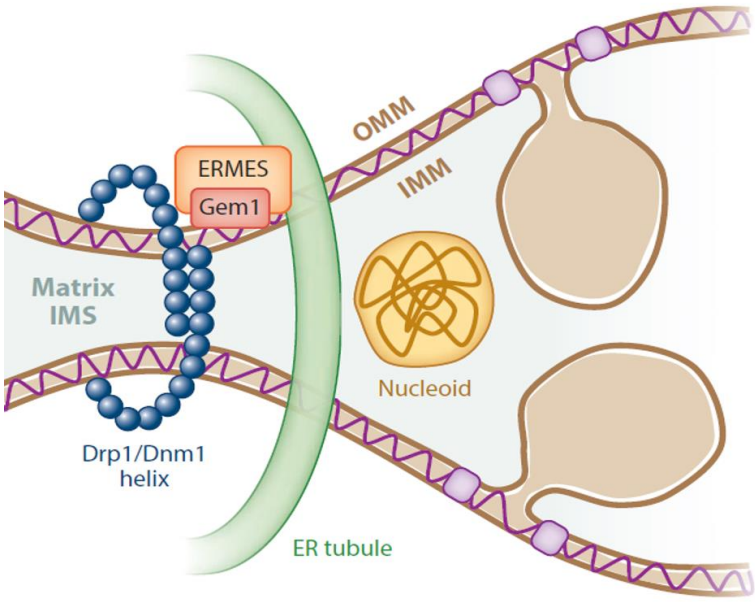

Figure 3: Mechanistic model of mitochondrial division apparatus. Mitochondrial division is facilitated by Drp1/Dnm1 in yeast and mammals, respectively, that forms helical structures around mitochondrial outer membrane that constrict upon GTP hydrolysis. The division is also driven by ER tubules via interaction with ERMES complex. Position of mitochondrial DNA nucleoids during division is shown. [6], modified.

1.2 The ER-mitochondria hotspots.

Recently, the endoplasmic reticulum (ER) was shown to play a prominent role in mitochondrial division. Simultaneous live imaging of the ER and mitochondria revealed that the ER tubules wrap around mitochondria prior to the mitochondrial division and suggested that the wrapping may cause mitochondrial pre-constriction in yeast and mammals [112]. The diameter of mitochondria at these sites was measured twice, resulting in 138nm and 146nm, which is in contrast to common mitochondrial diameter of 200nm to 400nm [113]. However, the earlier measurements of mitochondrial constriction sites gave slightly different values. In average, mitochondrial diameter at constriction sites was 109nm ± 24 nm [83]. More importantly, the division sites marked by the ER were positive for Dnm1/DRP1 and also contain MFF, which localizes to these hotspots independently of DRP1 [112].

The nature of the link between the ER and mitochondria has been characterized in *S. cerevisiae* where the connection is facilitated predominantly by the ER-mitochondria encounter structure (ERMES) [114]. ERMES is a protein complex localized in a few discrete foci in the cell consisting of four proteins with appropriate topology to build the proteinaceous bridge between the organelles (Fig.4). While Mmm1 and Mdm34/Mdm10 are membrane proteins anchored in the ER and mitochondrial outer membranes, respectively, Mdm12 is a soluble cytosolic protein [114,115]. Three of the ERMES components (Mdm12, Mdm34 and Mmm1) carry a synaptotagmin-like mitochondrial-lipid-binding protein (SMP) domain [116,117], pointing to the primary function of the complex to mediate lipid transfer between the two organelles. Unlike the other ERMES proteins, Mdm10 is a β-barrel protein functioning as part of the TOM and SAM complexes in the transport and assembly of the mitochondrial proteins [118–121].

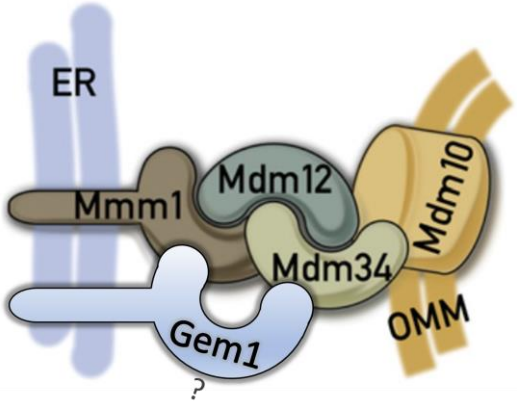

Figure 4: Mechanistic model of yeast ERMES complex topology. Mmm1, an ER residing protein interacts with Mdm34 and Mdm10, membrane anchored proteins in the outer mitochondrial membrane, via soluble Mdm12, thus forming the ER-mitochondria interface. Exact topology of Gem1 remains unclear [122], modified.

The actual organization and the precise function of the ERMES complex is still not fully understood. It was shown that Mmm1 and Mdm12 form a heterotetramer via direct association of SMP domains. Moreover, their SMP domains bind phospholipids, preferentially phosphatidylglycerol

and phosphatidylethanolamine, lipids that are transported between ER and mitochondria [123]. Recent crystal structure of Mdm12 proposed that Mmm1 forms a homodimer via a head-to-head interaction of each SMP domain in the center, and a heterodimer with Mdm12 through a tail-to-tail interaction of their respective SMP domains [124].

Additionally, Gem1 was identified as a component of ERMES complex [125]. Gem1 is a yeast orthologue of Miro GTPase that was originally found to regulate mitochondrial morphology [126]. In addition, Gem1 regulates the number and the size of the ERMES complexes as well as their ability to transfer phospholipids [125]. The live cell microscopy suggested that Gem1 serves as a negative regulator of the ER-mitochondria connections by mediating the segregation of mitochondrial ends upon the constriction [127]. However, an independent study questioned the direct role of Gem1 in the stability of the ERMES complex, suggesting that neither the phospholipid transport nor the mitochondrial division are the primary roles of the protein [128].

1.2.1 Lipid transport between ER and mitochondria.

According to current model, the primary function of ERMES complex is to mediate phospholipid transport between ER and mitochondria. ER-generated phosphatidylserine (PS) is transported to mitochondria where it is converted to phosphatidylethanolamine (PE) and transported back to the ER, as reviewed by [129]. However, conflicting information exists on the actual importance of the ERMES complex in the lipid transfer. While recently developed *in vitro* assay indicates that the complex is essential for PS transport from the ER to mitochondria [130], deletion of the ERMES complex subunits has only minimal effect on the lipid transfer *in vivo* [128,131]. In agreement with the uncovered non-essential character of the ERMES complex, other complexes were shown to partake in the lipid transport between the ER and mitochondria. The endoplasmic reticulum membrane protein complex (EMC) was discovered as another ER-mitochondria tethering complex deletion of which leads to decreased number of ER-mitochondria tethers and impaired phospholipid transfer between mitochondria and ER [132]. As for the ERMES, deletion of the whole EMC does not lead to cell death, however, cells lacking both complexes are inviable [114,132]. In yeast, the complex contains six subunits, all of which are associated with the TOM complex machinery via Tom5. It was also shown that this interaction is crucial for the transport of PS from ER to mitochondria [132]. Unlike ERMES, EMC is highly conserved in all major eukaryotic linages. So far only a handful of organisms have been shown to secondarily lack the entire EMC, namely two microsporidians, *Nosema ceranae* and *Encephalitozoon cuniculi*, the metamonad *Giardia intestinalis*, the stramenopile *Blastocystis hominis*, the alveolate *Theileria parva*, and the red alga *Cyanidioschyzon merolae* [133,134]. The abundance of the complex indicates its prominent cellular function.

The phospholipid transfer to mitochondria is also facilitated by the so-called vCLAMPs (vacuole and mitochondria patches) in yeast. These connections between mitochondria and vacuoles are formed by soluble Vps39, Rab GTPase Ypt7 in the vacuolar membrane and unknown mitochondrial component [135,136]. vCLAMPs and ERMES are both dynamic structures and likely serve as mutual backup system. The loss of vCLAMPs causes the increase in the number of ERMES complexes and vice-versa. The loss of both systems leads to the impaired mitochondrial phospholipid transfer [135]. Moreover, the ERMES/vCLAMP ratio depends on the physiological state of the yeast cells. Non-fermentable carbon source such as glycerol changes the ratio in favor of the ERMES complex, while the opposite occurs when cells are grown on glucose [136].

Surprisingly, recently identified Lam6 protein was found to be part of both vCLAMP and ERMES complexes [137]. Although Lam6 is not essential for contact sites generation, its overexpression causes the expansion of interorganellar contacts [137].

1.2.2 ERMES and mitochondrial division.

ERMES was shown to be directly involved in the ER-associated mitochondrial division in yeast (Fig.3). The ERMES foci localize to the mitochondrial constrictions and the eventual division sites [127]. Moreover, ERMES is linked to actively replicating mitochondrial nucleoids [138,139] and thus likely mediates the even segregation of mtDNA into daughter mitochondria [127]. The deletion of core ERMES components leads to nucleoid disruption and eventually to the loss of mitochondrial DNA [115].

Since ERMES complex is not present in metazoa [133], nature of the physical connection between ER and mitochondria in mammalian cells remains largely elusive. Originally, it had been thought that Mfn2 plays a role in tethering the two organelles together. Mfn2 was shown to localize to mitochondria-associated membranes (MAMs) and the cells lacking the protein showed impaired ER-mitochondria tethering. Moreover, ER residing Mfn2 was suggested to interact *in trans* with mitochondria-localized Mfn1 or Mfn2, thus bridging the two organelles [140]. Yet, the exact role of Mfn2 in ER-mitochondria tethering was recently debated [141,142]. In agreement with previous report, it was shown that ablation of Mfn2 truly affects morphology of both mitochondria and ER [141], however, to the contrary, the loss of Mfn2 lead to increased ER-mitochondria contacts and Ca^{2+} transfer from ER to mitochondria [141,142]. Based on these new reports, Mfn2 is considered as a ER-mitochondria tethering antagonist, preventing an excessive proximity between these organelles, which could be potentially toxic by triggering mitochondrial Ca^{2+} overload-dependent death [142]. Later in 2016, the original studies have been re-evaluated to clear the dispute. According to [143], Mfn2 really tethers ER to mitochondria and its ablation reduces ER-mitochondria juxtaposition as well as mitochondrial uptake of Ca^{2+} released from ER.

Recently, other factors have been proposed to physically connect ER with mitochondria in mammalian cells. MiD49 and MiD51 were shown to combine during constriction of mitochondria, co-localizing with other fission proteins at ER-mitochondrial contacts. However, not all ER-mitochondria contacts at MiD foci were located at constriction sites and not all MiD51-ER-marked constricted mitochondria led to actual mitochondrial division [108]. In addition, the metazoan homologue of Gem1, Miro1, was also localized to several foci per mitochondria and consistently coincided with the ER tubules, a pattern reminiscent of the ERMES components [125]. Interestingly, Miro1 homologues are absent in organisms lacking mitochondrial DNA [144] which corresponds to the phenotype of yeast cells lacking *gem1*, which rapidly lose mtDNA [126].

1.2.3 Actin and mitochondrial constriction.

The ER is not the only player facilitating mitochondrial pre-constriction. Recently, cytoskeletal machinery was shown to play in concert with the ER in mitochondrial division in mammalian cells. Actin polymerization at the ER-mitochondria contact sites is required for efficient mitochondrial fission. Actin filaments accumulate at the ER membranes enriched for the inverted formin 2 (INF2) at the mitochondrial constriction sites. Here, INF2 stimulates actin nucleation and elongation. Surprisingly, INF2 was shown to function upstream of DRP1, suggesting that actin polymerization may cause the initial mitochondrial constriction, which then allows the DRP-driven secondary constriction to happen [145]. Korobova and colleagues also showed that myosin II accumulates in puncta on mitochondria in an actin- and IF2-dependent manner. Moreover, the inhibition of myosin II leads to decreased accumulation of DRP1 at the mitochondrial division sites [146]. Based on these results, Korobova proposes a mechanistic model in which INF2-mediated actin polymerization leads to myosin II recruitment and initial constriction at the fission sites, enhancing subsequent DRP1 accumulation and mitochondrial fission [146].

1.3 Mitochondrial dynamics in parasitic protists

In general, mitochondria of parasitic protists are extremely intriguing organelles, structure of which often reflects their long independent evolutionary path as well as the metabolic adaptation of the parasite. E. g., in African trypanosomes, the single mitochondrion undergoes extreme morphological and metabolical changes during the life cycle of the parasite; mitochondrion of plasmodium needs to divide into thousands of individual organelles prior to cellular division and their precise segregation into daughter cells needs to be carefully orchestrated; in *Giardia intestinalis*,

mitochondria have adapted to the oxygen-poor environment and their dynamics got under full control of the cell cycle.

1.3.1 *Trypanosoma brucei*

Trypanosomes harbor single mitochondrion that extends throughout the whole cell. In concert with the mitochondrial metabolism, mitochondrial morphology differs dramatically in two trypanosomal life stages, the vertebrate bloodstream form (BSF) and the insect procyclic form (PCF). In BSF, the mitochondrion has acristate tubular morphology and is functionally repressed, while in PCF the mitochondrion has highly defined branched structure with cristae and is metabolically active. For detailed review on mitochondrial metabolism in *T. brucei*, see [147]. However, recently, a new major reservoir for *T. brucei* that differs from both BSF and PCF was discovered. It is a form living in an adipose tissue of its mammalian host, thus called the adipose tissue form (ATF) [148]. This form is able to replicate and is infective for naïve animal. Moreover, it is transcriptionally distinct from BSF, as evidenced by the upregulation of fatty acid β-oxidation enzymes [148]. Mitochondrion of ATFs occupies small volume of parasite body and is not highly branched, similar to that of the BSFs [148].

Mitochondrion of trypanosomes is physically connected to a basal body of the single flagellum via so-called tripartite attachment complex (TAC) [149]. This physical connection is crucial for trypanosomes as they need to orchestrate the flagellar and mitochondrial division prior to the cell division itself [150,151]. TAC consists of two sets of filaments that connect flagellar basal body with mitochondrial outer membrane and mitochondrial inner membrane with kinetoplast, a highly ordered unique mitochondrial DNA, respectively [149]. So far, four proteins were shown to localize to TAC, namely p166, AEP-1, p197 and β-barrel TAC40. Their ablation leads to the impaired kinetoplast inheritance by severing the connection between kinetoplast and basal body [152–155]. Unlike animal and fungal mitochondria that divide continuously throughout the cell cycle, mitochondrion of trypanosomes divides only once during the cell division [156]. Recent elaborate morphological observations of mitochondria during different stages of bloodstream form of *T. brucei* cell cycle showed that mitochondrion forms multiple branches and protrusions prior to cytokinesis. The fission itself occurs within the cytoplasmic bridge during the cell abscission [157]. Although these observations are thorough, no molecular background has been characterized. During the cell growth, the mitochondrion of *T. brucei* enlarges and branches out. The growing complexity of mitochondria correlates with cell cycle progression [158], however, it is not continuous throughout the cell cycle as described in other model organisms [159,160] but occurs in the last part of the cell cycle [158]. The branching occurs at specific spots: (i) posterior branches positioned close to the kinetoplast, (ii) branches close to the nuclei and (iii) branches emerging from the anterior part of the cell. Eventually,

as the cell cycle progresses, all the branches fuse together to form a complex network that separates after the cell division [158].

Genome of *Trypanosoma brucei* encodes homologues of two mitochondrial division proteins, Dnm1 and Fis1 [161,162] (Fig.5). Dynamin-like protein of *T. brucei*, TbDLP, is also conserved in other trypanosomatids and localizes to the mitochondrion and the flagellar pocket, which is the only site for the endocytosis and exocytosis [163]. The ablation of TbDLP leads to impaired mitochondrial morphology, lack of mitochondrial division and accumulation of mitochondrial constriction sites, finally leading to the arrest of cytokinesis [161,162]. *T. brucei* orthologue of Fis1 was shown to be targeted to the mitochondrial outer membrane in PCF [164]. The protein is expressed in both stages [165], however, its localization in BSF has not been characterized.

So far, mitochondrial fusion has not been observed in trypanosomes. Moreover, none of the known components of the fusion machinery were found in trypanosomes. This suggests that either the fusion does not occur in trypanosomes or it is mediated by a different molecular machinery. Moreover, the fusion may be limited to a specific life cycle stage of *T. brucei*, as haploid, gamete-like *T. brucei* cells that differentiate in tse-tse fly undergo cellular fusion [166]. Whether the cellular fusion involves mitochondrial fusion as well remains to be characterized. However, it was shown that mitochondrion of BSF of *T. brucei* artificially fragmented by expression of human pro-apoptotic protein Bax is capable of re-fusion into one single organelle after halting of Bax expression [167]. This strongly suggests the ability of trypanosomal mitochondrion to fuse also under physiological conditions.

Several components of the ERMES complex were identified in the genome of *T. brucei*, namely Mdm12, Mdm34 and Gem1 [133,164]. Both core ERMES components Mdm12 and Mdm34, however, localize to cytoplasm, thus suggesting that functional ERMES complex is probably not formed in trypanosomes [155]. In contrast, Gem1 homologue was shown to associate with the mitochondrial outer membrane [164].

Taken together, trypanosomes lack most of the proteins involved in mitochondrial dynamics known from yeast or mammals. However, the unicellular character of trypanosomes and the fact that they harbor only single mitochondrion suggest highly ordered synchronization of mitochondrial dynamics and cell cycle and communication of mitochondrion with other cellular components.

1.3.2 *Plasmodium spp.*

Plasmodium parasites go through series of dramatic morphological transformations during their life cycle, spanning the intermediate vertebrate host and the definitive host, the mosquito. In the human host, *P. falciparum*, the major causative agent of human malaria, replicates asexually first in

the hepatocytes and subsequently in the red blood cells. The intracellular trophozoites undergo schizogony, a series of nuclear divisions without cytokinesis, giving rise to multinucleated schizonts. Schizonts then divide to form up merozoites, which are able to reinvade new host cells [168]. Every cell of plasmodium contains only single mitochondrion. During the multitude of divisions, this mitochondrion needs to be segregated into every single merozoite generated. In erythrocytal stages, mitochondrion was shown to associate with apicoplast [168–170] which was confirmed later by biochemical analysis by [171]. Apicoplast is a secondary plastid harbored by most apicomplexans that is necessary for various metabolical processes such as fatty acid metabolism and isoprenoid synthesis etc., reviewed e.g. by [172]. Van Dooren and colleagues discovered that mitochondrion branches massively during schizogony, forming large single organelle that appears to have contact points with plasma membrane. Moreover, contact points between mitochondrion and apicoplast multiply during schizogony. The actual mitochondrial division occurs only after the apicoplast has been divided. The coordinated organelle divisions thus make sure that every daughter cell contains one mitochondrion associated with one apicoplast [168].

The liver stages of plasmodium undergo varied number of schyzogonies, forming thousands of infectious merozoites, thus achieving one of the fastest growth rates among eukaryotes [173]. Thus, cytokinesis and organellar segregation in these stages needs to be synchronized and controlled even more. Consistent with results discovered in erythrocytal stages, mitochondrion and apicoplast of rodent parasite *P. berghei* undergo similar morphological changes in hepatocytes, although on much higher scale [4,173]. Surprisingly, it seems that the association between the apicoplast and mitochondrion does not occur in liver stages [4,173].

Differentiation into sexual stages (gametocytogenesis) of the parasite starts in the erythrocytes, where macrogametocytes and microgametocytes are formed. Upon the transmission to the mosquito, these cells produce single female macrogamete or eight male microgametes, respectively, which fuse to produce a zygote that later develops into the infectious sporozites [174]. Mitochondria of plasmodium and other apicomplexans are inherited exclusively maternally which means that it divides only in macrogametocytes [174–177]. During the sexual development, mitochondrion of macrogametocyte undergoes serious morphological changes. It elongates and branches and forms a cluster around the apicoplast which, in contrast to the asexual cycle in erythrocyte or hepatocyte stages, does not develop at all [174]. As the gametogenesis continues, the mitochondrion elongates even more [174], which relates to its metabolic activation and formation of the inner membrane cristae [178,179].

So far, the fascinating dynamics of plasmodium mitochondria during the parasite life and cell cycle is not understood on the molecular level. Plasmodium species lack all known proteins involved in the mitochondrial fusion, fission and in the formation of the ER-mitochondria tethering complexes. *P.*

falciparum genome contains three homologues of dynamin, Pfdyn1, Pfdyn2, Pfdyn3 [180–182] (Fig.5). First two isoforms are typical dynamins with all the necessary domains and they both are expressed in mature erythrocytal stages [180,181]. Pfdyn3 harbors only GTPase domain typical for dynamins, however, lacks all other necessary features [182], thus its role as a dynamin is disputable. Pfdyn1 localizes partially to the endoplasmic reticulum and the protein is also present on parasite membrane as well as in host erythrocyte cytoplasm. Moreover, Pfdyn1 is essential for parasite survival during erythrocytic stage and also involved in hemoglobin trafficking [180,183]. Pfdyn2 was showed to localize to parasite cytoplasm, partially co-localize with ER membranes, apicoplast and Golgi apparatus [181]. No involvement of the dynamin homologues in mitochondrial dynamics has been found so far.

1.3.3 *Toxoplasma gondii*

Mitochondrion of *Toxoplasma gondii*, an apicomplexan parasite of mammals, has been described predominantly in rapidly proliferating life stage called tachyzoite. In this life stage, mitochondrion of *T. gondii* clusters at the anterior part of the cell with branches spanning towards its posterior part, forming a lasso shape [3]. Mitochondrial division in tachyzoites is tightly coupled with cellular division. During tachyzoite binary division, endodyogeny, mitochondrion branches at multiple locations. These extensions continue to grow, ultimately surrounding the growing daughter cells. Interestingly, mitochondrial branches enter the developing daughter cells at the last possible moment of cell division, migrating along the cytoskeletal scaffolding. A small amount of mitochondrial compartment is left behind in the residual body [184]. In *T. gondii*, mitochondrion was also reported to associate with apicoplast during the parasite division but this association was not maintained throughout the whole process [184]. Unlike in mammalian cells where actin is involved in mitochondrial division [145], actin of *T. gondii* was suggested not to play a role in the process [184].

Upon egress from the host cell, mitochondrial morphology of *T. gondii* changes dramatically [185]. Immediately after the egress, “lasso-shaped” mitochondrion concentrates from the cell periphery into “sperm-like” and “collapsed” morphologies, which are preserved until the induction of gliding movement and the invasion of the new host cell. Consistently, collapsed mitochondria of invading parasites were shown to re-expand and re-establish its lasso shape via the sperm-like intermediate and only parasites that harbor lasso-shaped mitochondrion are able to divide within the host cell [185]. Besides the association with apicoplast, mitochondrion of tachyzoites was shown to associate with the inner membrane complex, a unique complex of flattened membranes found directly below the plasma membrane of apicomplexans [185,186].

Of the three dynamin-related proteins encoded in *T. gondii* genome (Fig.5), TgDrpA was shown to control the division of apicoplast [187]. TgDrpB is required for the biogenesis of the secretory organelles, micronemes and rhoptries [182] and the role of TgDrpC has not been resolved so far as knock-down of the gene did not show any detectable phenotype [188]. Whether any of *T. gondii* dynamin related proteins partake in mitochondrial division has not been investigated.

1.3.4 *Trichomonas vaginalis*

In *Trichomonas vaginalis*, mitochondria-related organelles called hydrogenosomes are found [189]. Morphological studies describe hydrogenosomal division and their association with endoplasmic reticulum [190]. It was even suggested that the hydrogenosomes divide by distinct processes called segmentation, partition and the formation of a "heart-form". According to Benchimol and colleagues, the division of hydrogenosomes begins by an invagination of the inner membrane, forming a transversal septum and separating the organelle matrix into two compartments [190,191]. However, given that this is a unique observation, it is still unclear whether this morphology represents actual hydrogenosomal division or a distinct cellular process.

There are eight DRPs in the genome of *T. vaginalis* (Fig.5). One of them was localized to the hydrogenosomes and the expression of the mutant form of the protein (K38A) generated a dominant negative phenotype observed as an increase in size and decrease in number of hydrogenosomes. This was likely a consequence of the impared hydrogenosomal division, hence strongly suggesting the role of this single DRP in the process [192].

1.3.5 *Giardia intestinalis*

Giardia intestinalis possesses mitosomes, the most reduced form of mitochondria which have been shown to contain several proteins that are involved predominantly in the Fe-S clusters assembly and the protein import [193–196]. Two main populations of mitosomes are recognized in *G. intestinalis*. They are defined by their position to the karyomastigont as the central mitosomes (CMs), between the two giardia nuclei, and the peripheral mitosomes (PMs) in the rest of the cell [197]. Until recently, only scarce morphological data regarding the mitosomal dynamics were available [197,198]. Regarding the conserved position of CMs, Regoes and colleagues proposed that CMs might be connected to the basal bodies and that their division could be coordinated with the cell-cycle [194,197].

The single dynamin-related protein of *G. intestinalis*, GlDRP (Fig.5), contains all the necessary domains for its proper function, however their position is atypical [199]. In contrast to "classical"

dynamins, the PRD of GlDRP is inserted between the middle domain and GED. The initial report on the function of GlDRP showed its localization at the cytoplasmic membrane, corresponding to the role of GlDRP in the scission of the endocytic vesicles. Moreover, the protein is necessary during the encystation of the parasite, which was efficiently blocked by the expression of dominant negative form of GlDRP [199]. However, recent data have also suggested possible involvement of GlDRP in the mitosomal division [200]. The dominant-negative form of GlDRP partially co-localized with the mitosomal marker Tom40 and the cells containing the mutant protein contained enlarged, dumbbell-shaped mitosomes, indicating impaired mitosomal division [200].

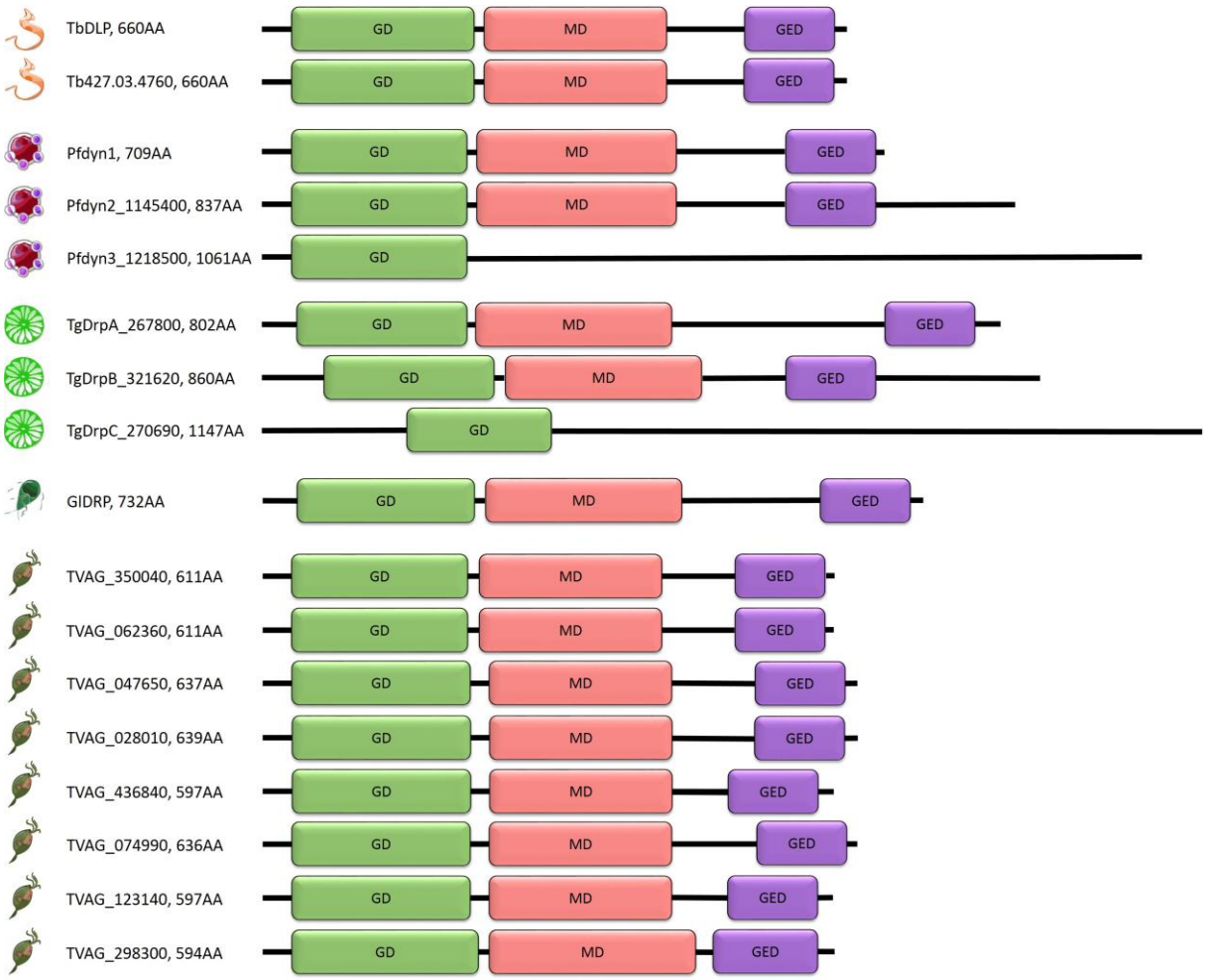

Figure 5: Schematic representation of dynamin-related proteins from different parasitic protists. Protein candidates were found by HMMER searches [201]. Depicted domains were found by Pfam database searches [202]. Protein lengths are indicated in amino acids (AA). Parasite strains were selected as following: *Trypanosoma brucei* strain 427, *Plasmodium falciparum* strain 3D7, *Toxoplasma gondii* strain GT1, *Giardia intestinalis* assamblage A strain WB, *Trichomonas vaginalis* strain G3. GD, GTPase domain; MD, middle domain; GED, GTPase effector domain. Parasite cartoons were modified from http://eupathdb.org/eupathdb/.

2. AIMS

1. To introduce technology for life imaging of mitochondria-like organelles in anaerobic protists *Giardia intestinalis* and *Trichomonas vaginalis*.
2. To characterize mitosomal dynamics in *G. intestinalis* and their behavior during *Giardia* cell cycle.
3. To characterize new mitosomal proteins of *G. intestinalis* discovered previously by [196].

3. LIST OF PUBLICATIONS AND AUTHOR CONTRIBUTION

Martincová, E., L. Voleman, V. Najdrová, M. De Napoli, S. Eshar, M. Gualdron, C.S. Hopp, D.E. Sanin, D.L. Tembo, D. Van Tyne, D. Walker, M. Marcinčiková, J. Tachezy, and P. Doležal. 2012. **Live Imaging of Mitosomes and Hydrogenosomes by HaloTag Technology**. *PLoS One*. 7:e36314. doi:10.1371/journal.pone.0036314.

Together with Eva Martincová: Cloning of used constructs; analysis of acquired imaging data; writing the manuscript.

Martincová, E., L. Voleman, J. Pyrih, V. Žárský, P. Vondráčková, M. Kolísko, J. Tachezy, and P. Doležal. 2015. **Probing the Biology of *Giardia intestinalis* Mitosomes Using In Vivo Enzymatic Tagging**. *Mol. Cell. Biol.* 35:2864–2874. doi:10.1128/MCB.00448-15.

Cloning of several constructs based on pull-down experiments; localization of several proteins in *G. intestinalis* by immunofluorescence; characterization of GiMOMP35; precipitation of GiMOMP35 interacting protein partners.

Voleman, L., V. Najdrová, Á. Ástvaldsson, P. Tůmová, E. Einarsson, Z. Švindrych, G.M. Hagen, J. Tachezy, S.G. Svärd, and P. Doležal. 2017. ***Giardia intestinalis* mitosomes undergo synchronized fission but not fusion and are constitutively associated with the endoplasmic reticulum**. *BMC Biol.* 15:27. doi:10.1186/s12915-017-0361-y.

Performing of all the experiments; analysing the data; writing the manuscript.

4. SUMMARY

4.1 A new tool for live imaging of anaerobic protists

HaloTag technology is relatively new to cell biology. Although it has been discovered quite recently [203], it is used massively since then in various fields, e.g. [204–206]. It is chemical tag-based technology which works *in vivo* and, unlike GFP and its derivatives, does not require oxygen for its activation [203]. This makes it a potentially great tool for imaging of anaerobic or microaerophilic organisms. Although GFP had been used for anaerobes including *G. intestinalis* in the past, e.g. [200,207–209], its activation requires oxygenation of the media or use of alternate buffers, which are not fully compatible with the parasite physiology. We introduced the HaloTag technology to label mitosomes and hydrogenosomes of *Giardia intestinalis* and *Trichomonas vaginalis*, respectively. The HaloTag was fused with IscU of *G. intestinalis* and Frataxin of *T. vaginalis* and the chimeric genes were expressed episomaly in *G. intestinalis* and *T. vaginalis* cells, respectively. The expression of both proteins as well as their localization to mitosomes and hydrogenosomes were confirmed by western blotting and immunofluorescence using specific antibodies. Using HaloTag TMR ligand for live-cell imaging, we were able to observe hydrogenosomes and mitosomes *in vivo* for more than 60 minutes without any visible signal loss [2]. The introduction of HaloTag technology to the cell systems of anaerobic protists should be of great assistance in the field.

4.2 Dynamics of *Giardia intestinalis* mitosomes

4.2.1 Mitosomes during interphase

Mitochondria are dynamic organelles undergoing constant fusion and division events throughout the cell cycle [6]. We used the HaloTag technology we had introduced earlier to *G. intestinalis* [2] to follow the mitosomes during *Giardia* cell cycle. *Giardia* trophozoites expressing GiIscU-Halo were incubated with HaloTag TMR ligand and observed for several hours using confocal microscope. Surprisingly, the number as well as distribution of mitosomes did not change during the time, suggesting no mitosomal fusion nor division occur in the interphase [210].

4.2.2 Mitosomal division

We hypothesized that the organelles need to divide prior to cell division, hence, we followed the GiIscU-Halo expressing cells during mitosis using spinning disk confocal microscope. However, live-cell microscopy of mitotic *G. intestinalis* cells is hampered by the rapid movement of the dividing cells, as their adhesive disc depolymerizes during division. Thus, instead, fixed *G. intestinalis* cultures

enriched for mitotic cells were examined by immunofluorescence microscopy. Indeed, we discovered that mitosomes divide during mitosis and the division is not restricted to individual phases of the division [210]. The only exception was the central mitosomes, division of which occurred exclusively in prophase, before the basal bodies, which mitosomes are attached to [211], moved toward the opposite spindle poles [212]. Moreover, we showed that central mitosomes divide through a V-shaped morphology, which likely represents the early separation of two sets of central mitosomes. We also showed that peripheral mitosomes divide by forming dumbbell-shaped intermediate [210], which is a typical configuration for dividing vesicular structures [213–215]. Furthermore, by immunofluorescence with fixed encysting cells, we showed that mitosomes divide also during *Giardia* encystation, showing that, in addition to two pairs of nuclei, *G. intestinalis* cysts contain a double set of mitosomes, which enable the parasite to undergo rapid cell division during excystation in a new host [210].

4.2.3 Mitosomal fusion

To ensure that no mitosomal fusion occurs in *Giardia*, we checked if the organelles exhibit some degree of heterogeneity which is typical for cells with impaired mitochondrial fusion [33,42]. Indeed, cells episomaly expressing HA-tagged IscU protein harbor two populations of mitosomes, one containing both IscU-HA and endogenous protein GL50803_9296 and another containing GL50803_9296 only, suggesting no content mixing within individual organelles occurs [210].

4.2.4 GlDRP

Mitochondrial division is controlled by dynamin GTPases, out of which *Giardia* genome encodes only one homologue, GlDRP [6,199]. Two studies exist concerning the role of GlDRP in mitosomal division [199,200]. According to our data, disruption of GlDRP GTPase fuction has no effect on mitosomal division. Encysting cells expressing non-functional version of GlDRP, K43E GlDRP [199], harbor the same number of mitosomes as the wild type encysting cells [210].

4.2.5 Association of mitosomes and endoplasmic reticulum

Recently, it was shown that mitochondrial division is associated with ER membranes in mammalian and yeast cells [112,127]. However, the direct evidence of this interaction is still missing outside the supergroup of Opisthoconta where mammals and fungi belong. Using antibodies against mitosomal and ER-resident proteins, we showed that the association between these organelles occurs in *G. intestinalis* and is maintained throughout the cell division. Moreover, we showed that mitosomes elongate along ER tubules, which may thus serve as a scaffold for mitosomal division [210]. In yeast, the interaction between ER and mitochondria is facilitated by ERMES and EMC

complexes [114,132], however, these complexes are not present in *Giardia* genome [133,134]. In addition, several proteins are enriched in the so-called mitochondria-associated membranes (MAMs), a specific region of the ER which comes into contact with mitochondria and mainly accommodates enzymes involved in lipid and fatty acid metabolism as summarized in [216]. By bioinformatic searches, out of all the proteins present in MAMs, we found only single candidate in *Giardia* genome, a long-chain acyl-CoA synthetase 4,GiLACS4 [217]. By immunofluorescence microscopy, we showed that the V5-tagged GiLACS4 localizes to distinct foci along the ER network, which are proximal to the mitosomes. We also showed that the protein is maintained in the membrane upon treatment with sodium carbonate and is exposed to the cytoplasm. Altogether, these data suggest that the mitosome–ER contact sites are occupied by the fatty acid activating enzyme, GiLACS4 [210].

4.3 Mitosomal proteome

In 2011, we published the first mitosomal proteome of *G. intestinalis* [195]. Because it is not possible to obtain pure mitosomal fraction devoid of contamination by other membrane structures by differential centrifugation, we used comparative mass spectrometry to exclude the protein contaminants. Using this two-step approach, we identified 139 putative mitosomal proteins, however, we confirmed the correct localization only to 20 of those [195]. To improve the resolution, we used another approach for isolation of mitosomal proteins [196]. By using known mitosomal proteins as a bait for biotinylation *in vivo* [218], we isolated putative protein partners of GiPam18, GiTom40, and GiHsp70. In the pull-down experiments, we identified novel component of mitosomal protein import machinery GL50803_14845, according to profile sequence comparison by HHpred homologous to Tim44, and mitosomal outer membrane protein, GL50803_14939, that we named GiMOMP35. Moreover, by using GiTim44 as a query for bioinformatic searches, we found its orthologue in free living metamonads, *Carpediemonas membranifera* and *Ergobibamus cyprinoides*. Furthermore, by combining the results from all pull-down experiments (GiPam18, GiTom40, GiHsp70, GiTim44 and GiMOMP35), we identified 17 putative mitosomal proteins, localization of which was confirmed by epitope tagging with HA tag and expression in *Giardia* cells. Out of those 17 candidates, 13 were confirmed to localize to mitosomes, however no recognizable homology could be identified for the most of them, thus they possibly represent *Giardia*-specific molecules [196]. The only exception stays for GL50803_27910 and GL50803_16424. The first represents an orthologue of rhodanese, a protein involved in various aspects of sulfur metabolism [219]. The later appears to be a member of the myelodysplasia-myeloid leukemia factor 1-interacting protein (Mlf1IP) family, which has been considered exclusive to metazoans [220]. 5 of those 13 mitosomal proteins seem to be outer membrane-specific, as these were co-precipitated with GiTom40 and GiMOMP35 only.

Altogether, further characterization of the newly identified mitosomal proteins may shed more light on mitosomal biogenesis and metabolism.

5. REFERENCES

1. Luz AL, Rooney JP, Kubik LL, Gonzalez CP, Song DH, Meyer JN. Mitochondrial Morphology and Fundamental Parameters of the Mitochondrial Respiratory Chain Are Altered in *Caenorhabditis elegans* Strains Deficient in Mitochondrial Dynamics and Homeostasis Processes. López Lluch G, editor. PLoS One. 2015;10: e0130940. doi:10.1371/journal.pone.0130940
2. Martincová E, Voleman L, Najdrová V, De Napoli M, Eshar S, Gualdron M, et al. Live Imaging of Mitosomes and Hydrogenosomes by HaloTag Technology. Waller RF, editor. PLoS One. 2012;7: e36314. doi:10.1371/journal.pone.0036314
3. Melo EJL, Attias M, De Souza W. The Single Mitochondrion of Tachyzoites of *Toxoplasma gondii*. J Struct Biol. 2000;130: 27–33. doi:10.1006/jsbi.2000.4228
4. Stanway RR, Mueller N, Zobiak B, Graewe S, Froehlke U, Zessin PJM, et al. Organelle segregation into *Plasmodium* liver stage merozoites. Cell Microbiol. 2011;13: 1768–1782. doi:10.1111/j.1462-5822.2011.01657.x
5. Nunnari J, Marshall WF, Straight A, Murray A, Sedat JW, Walter P. Mitochondrial transmission during mating in *Saccharomyces cerevisiae* is determined by mitochondrial fusion and fission and the intramitochondrial segregation of mitochondrial DNA. Mol Biol Cell. 1997;8: 1233–1242. doi:10.1091/mbc.8.7.1233
6. Labbé K, Murley A, Nunnari J. Determinants and Functions of Mitochondrial Behavior. Annu Rev Cell Dev Biol. Annual Reviews; 2014;30: 357–391. doi:10.1146/annurev-cellbio-101011-155756
7. Bürmann F, Ebert N, van Baarle S, Bramkamp M. A bacterial dynamin-like protein mediating nucleotide-independent membrane fusion. Mol Microbiol. 2011;79: 1294–1304. doi:10.1111/j.1365-2958.2011.07523.x
8. Bramkamp M. Structure and function of bacterial dynamin-like proteins. Biol Chem. 2012;393: 1203–1214. doi:10.1515/hsz-2012-0185
9. Egan AJF, Vollmer W. The physiology of bacterial cell division. Ann N Y Acad Sci. 2013;1277: 8–28. doi:10.1111/j.1749-6632.2012.06818.x
10. Erickson HP. Dynamin and Ftsz: Missing Links in Mitochondrial and Bacterial Division. J Cell Biol. 2000;148: 1103–1106. doi:10.1083/jcb.148.6.1103
11. Beech PL. Mitochondrial FtsZ in a Chromophyte Alga. Science (80-). 2000;287: 1276–1279. doi:10.1126/science.287.5456.1276
12. Gilson PR, Yu X-C, Hereld D, Barth C, Savage A, Kiefel BR, et al. Two *Dictyostelium* Orthologs of the Prokaryotic Cell Division Protein FtsZ Localize to Mitochondria and Are Required for the Maintenance of Normal Mitochondrial Morphology. Eukaryot Cell. 2003;2: 1315–1326. doi:10.1128/EC.2.6.1315–1326.2003
13. Kiefel BR, Gilson PR, Beech PL. Diverse eukaryotes have retained mitochondrial homologues of the bacterial division protein FtsZ. Protist. 2004;155: 105–15. doi:10.1078/1434461000168
14. Takahara M, Takahashi H, Matsunaga S, Miyagishima S, Takano H, Sakai A, et al. A putative mitochondrial ftsZ gene is present in the unicellular primitive red alga *Cyanidioschyzon merolae*. Mol Gen Genet MGG. 2000;264: 452–460. doi:10.1007/s004380000307
15. Takahara M, Kuroiwa H, Miyagishima S, Mori T, Kuroiwa T. Localization of the Mitochondrial FtsZ Protein in a Dividing Mitochondrion. Cytologia (Tokyo). 2001;66: 421–425. doi:10.1508/cytologia.66.421
16. Leger MM, Petrů M, Žárský V, Eme L, Vlček Č, Harding T, et al. An ancestral bacterial division system is widespread in eukaryotic mitochondria. Proc Natl Acad Sci. 2015;112: 10239–10246. doi:10.1073/pnas.1421392112
17. Sweitzer SM, Hinshaw JE. Dynamin Undergoes a GTP-Dependent Conformational Change

Causing Vesiculation. Cell. 1998;93: 1021–1029. doi:10.1016/S0092-8674(00)81207-6
18. Hinshaw JE. Dynamin Self-assembly Stimulates Its GTPase Activity. J Biol Chem. American Society for Biochemistry and Molecular Biology; 1996;271: 22310–22314. doi:10.1074/jbc.271.37.22310
19. Ramachandran R, Surka M, Chappie JS, Fowler DM, Foss TR, Song BD, et al. The dynamin middle domain is critical for tetramerization and higher-order self-assembly. EMBO J. 2007;26: 559–566. doi:10.1038/sj.emboj.7601491
20. Warnock DE, Schmid SL. Dynamin GTPase, a force-generating molecular switch. BioEssays. 1996;18: 885–893. doi:10.1002/bies.950181107
21. Shaw G. The pleckstrin homology domain: An intriguing multifunctional protein module. BioEssays. 1996;18: 35–46. doi:10.1002/bies.950180109
22. Zheng J, Cahill SM, Lemmon MA, Fushman D, Schlessinger J, Cowburn D. Identification of the Binding Site for Acidic Phospholipids on the PH Domain of Dynamin: Implications for Stimulation of GTPase Activity. J Mol Biol. 1996;255: 14–21. doi:10.1006/jmbi.1996.0002
23. Herskovits JS, Shpetner HS, Burgess CC, Vallee RB. Microtubules and Src homology 3 domains stimulate the dynamin GTPase via its C-terminal domain. Proc Natl Acad Sci U S A. 1993;90: 11468–72. Available: http://www.ncbi.nlm.nih.gov/pubmed/7505438
24. Shpetner HS, Herskovits JS, Vallee RB. A Binding Site for SH3 Domains Targets Dynamin to Coated Pits. J Biol Chem. American Society for Biochemistry and Molecular Biology; 1996;271: 13–16. doi:10.1074/jbc.271.1.13
25. Muhlberg AB. Domain structure and intramolecular regulation of dynamin GTPase. EMBO J. 1997;16: 6676–6683. doi:10.1093/emboj/16.22.6676
26. van der Bliek AM. Functional diversity in the dynamin family. Trends Cell Biol. 1999;9: 96–102. doi:10.1016/S0962-8924(98)01490-1
27. Vallis Y, Wigge P, Marks B, Evans PR, McMahon HT. Importance of the pleckstrin homology domain of dynamin in clathrin-mediated endocytosis. Curr Biol. 1999;9: 257–263. doi:10.1016/S0960-9822(99)80114-6
28. Ramachandran R, Schmid SL. Real-time detection reveals that effectors couple dynamin's GTP-dependent conformational changes to the membrane. EMBO J. 2008;27: 27–37. doi:10.1038/sj.emboj.7601961
29. Dudek SM, Chiang ET, Camp SM, Guo Y, Zhao J, Brown ME, et al. Abl tyrosine kinase phosphorylates nonmuscle Myosin light chain kinase to regulate endothelial barrier function. Mol Biol Cell. 2010;21: 4042–56. doi:10.1091/mbc.E09-10-0876
30. Mehrotra N, Nichols J, Ramachandran R. Alternate pleckstrin homology domain orientations regulate dynamin-catalyzed membrane fission. Mol Biol Cell. 2014;25: 879–890. doi:10.1091/mbc.E13-09-0548
31. Liu Y-W, Neumann S, Ramachandran R, Ferguson SM, Pucadyil TJ, Schmid SL. Differential curvature sensing and generating activities of dynamin isoforms provide opportunities for tissue-specific regulation. Proc Natl Acad Sci. 2011;108: E234–E242. doi:10.1073/pnas.1102710108
32. Sesaki H, Jensen RE. Ugo1p Links the Fzo1p and Mgm1p GTPases for Mitochondrial Fusion. J Biol Chem. in Press; 2004;279: 28298–28303. doi:10.1074/jbc.M401363200
33. Hermann GJ, Thatcher JW, Mills JP, Hales KG, Fuller MT, Nunnari J, et al. Mitochondrial Fusion in Yeast Requires the Transmembrane GTPase Fzo1p. J Cell Biol. 1998;143: 359–373. doi:10.1083/jcb.143.2.359
34. Rapaport D, Brunner M, Neupert W, Westermann B. Fzo1p Is a Mitochondrial Outer Membrane Protein Essential for the Biogenesis of Functional Mitochondria in Saccharomyces cerevisiae. J Biol Chem. 1998;273: 20150–20155. doi:10.1074/jbc.273.32.20150
35. Ban T, Heymann JAW, Song Z, Hinshaw JE, Chan DC. OPA1 disease alleles causing dominant optic atrophy have defects in cardiolipin-stimulated GTP hydrolysis and membrane tubulation. Hum Mol Genet. 2010;19: 2113–2122. doi:10.1093/hmg/ddq088
36. DeVay RM, Dominguez-Ramirez L, Lackner LL, Hoppins S, Stahlberg H, Nunnari J. Coassembly

of Mgm1 isoforms requires cardiolipin and mediates mitochondrial inner membrane fusion. J Cell Biol. 2009;186: 793–803. doi:10.1083/jcb.200906098
37. Rujiviphat J, Meglei G, Rubinstein JL, McQuibban GA. Phospholipid Association Is Essential for Dynamin-related Protein Mgm1 to Function in Mitochondrial Membrane Fusion. J Biol Chem. 2009;284: 28682–28686. doi:10.1074/jbc.M109.044933
38. Bui HT, Karren MA, Bhar D, Shaw JM. A novel motif in the yeast mitochondrial dynamin Dnm1 is essential for adaptor binding and membrane recruitment. J Cell Biol. 2012;199: 613–622. doi:10.1083/jcb.201207079
39. Strack S, Cribbs JT. Allosteric Modulation of Drp1 Mechanoenzyme Assembly and Mitochondrial Fission by the Variable Domain. J Biol Chem. 2012;287: 10990–11001. doi:10.1074/jbc.M112.342105
40. Liu X, Weaver D, Shirihai O, Hajnóczky G. Mitochondrial "kiss-and-run": interplay between mitochondrial motility and fusion–fission dynamics. EMBO J. 2009;28: 3074–3089. doi:10.1038/emboj.2009.255
41. Chen H, Detmer SA, Ewald AJ, Griffin EE, Fraser SE, Chan DC. Mitofusins Mfn1 and Mfn2 coordinately regulate mitochondrial fusion and are essential for embryonic development. J Cell Biol. Rockefeller University Press; 2003;160: 189–200. doi:10.1083/jcb.200211046
42. Chen H. Disruption of Fusion Results in Mitochondrial Heterogeneity and Dysfunction. J Biol Chem. 2005;280: 26185–26192. doi:10.1074/jbc.M503062200
43. Davies VJ, Hollins AJ, Piechota MJ, Yip W, Davies JR, White KE, et al. Opa1 deficiency in a mouse model of autosomal dominant optic atrophy impairs mitochondrial morphology, optic nerve structure and visual function. Hum Mol Genet. 2007;16: 1307–1318. doi:10.1093/hmg/ddm079
44. Chen H, Vermulst M, Wang YE, Chomyn A, Prolla TA, McCaffery JM, et al. Mitochondrial Fusion Is Required for mtDNA Stability in Skeletal Muscle and Tolerance of mtDNA Mutations. Cell. 2010;141: 280–289. doi:10.1016/j.cell.2010.02.026
45. Meeusen S. Mitochondrial Fusion Intermediates Revealed in Vitro. Science (80-). 2004;305: 1747–1752. doi:10.1126/science.1100612
46. De Vecchis D, Cavellini L, Baaden M, Hénin J, Cohen MM, Taly A. A membrane-inserted structural model of the yeast mitofusin Fzo1. Sci Rep. 2017;7: 10217. doi:10.1038/s41598-017-10687-2
47. Fritz S, Rapaport D, Klanner E, Neupert W, Westermann B. Connection of the Mitochondrial Outer and Inner Membranes by Fzo1 Is Critical for Organellar Fusion. J Cell Biol. 2001;152: 683–692. doi:10.1083/jcb.152.4.683
48. Cohen MMJ, Leboucher GP, Livnat-Levanon N, Glickman MH, Weissman AM. Ubiquitin-Proteasome-dependent Degradation of a Mitofusin, a Critical Regulator of Mitochondrial Fusion. Mol Biol Cell. 2008;19: 2457–2464. doi:10.1091/mbc.E08-02-0227
49. Anton F, Fres JM, Schauss A, Pinson B, Praefcke GJK, Langer T, et al. Ugo1 and Mdm30 act sequentially during Fzo1-mediated mitochondrial outer membrane fusion. J Cell Sci. 2011;124: 1126–1135. doi:10.1242/jcs.073080
50. Cohen MM, Amiott EA, Day AR, Leboucher GP, Pryce EN, Glickman MH, et al. Sequential requirements for the GTPase domain of the mitofusin Fzo1 and the ubiquitin ligase SCFMdm30 in mitochondrial outer membrane fusion. J Cell Sci. 2011;124: 1403–1410. doi:10.1242/jcs.079293
51. Ishihara N, Eura Y, Mihara K. Mitofusin 1 and 2 play distinct roles in mitochondrial fusion reactions via GTPase activity. J Cell Sci. 2004;117: 6535–6546. doi:10.1242/jcs.01565
52. Koshiba T, Detmer SA, Kaiser JT, Chen H, Mccaffery JM, Chan DC. Structural Basis of Mitochondrial Tethering by Mitofusin Complexes. Science (80-). 2004;305: 858–862. doi:10.1126/science.1099793
53. Karbowski M, Norris KL, Cleland MM, Jeong S-Y, Youle RJ. Role of Bax and Bak in mitochondrial morphogenesis. Nature. 2006;443: 658–662. doi:10.1038/nature05111
54. Hoppins S, Edlich F, Cleland MM, Banerjee S, McCaffery JM, Youle RJ, et al. The Soluble Form

of Bax Regulates Mitochondrial Fusion via MFN2 Homotypic Complexes. Mol Cell. 2011;41: 150–160. doi:10.1016/j.molcel.2010.11.030
55. Chan NC, Salazar AM, Pham AH, Sweredoski MJ, Kolawa NJ, Graham RLJ, et al. Broad activation of the ubiquitin-proteasome system by Parkin is critical for mitophagy. Hum Mol Genet. 2011;20: 1726–1737. doi:10.1093/hmg/ddr048
56. Gegg ME, Cooper JM, Chau K-Y, Rojo M, Schapira AH V, Taanman J-W. Mitofusin 1 and mitofusin 2 are ubiquitinated in a PINK1/parkin-dependent manner upon induction of mitophagy. Hum Mol Genet. 2010;19: 4861–4870. doi:10.1093/hmg/ddq419
57. Herlan M, Vogel F, Bornhovd C, Neupert W, Reichert AS. Processing of Mgm1 by the Rhomboid-type Protease Pcp1 Is Required for Maintenance of Mitochondrial Morphology and of Mitochondrial DNA. J Biol Chem. in Press; 2003;278: 27781–27788. doi:10.1074/jbc.M211311200
58. Meeusen S, DeVay R, Block J, Cassidy-Stone A, Wayson S, McCaffery JM, et al. Mitochondrial Inner-Membrane Fusion and Crista Maintenance Requires the Dynamin-Related GTPase Mgm1. Cell. 2006;127: 383–395. doi:10.1016/j.cell.2006.09.021
59. Schäfer A, Zick M, Kief J, Steger M, Heide H, Duvezin-Caubet S, et al. Intramembrane Proteolysis of Mgm1 by the Mitochondrial Rhomboid Protease Is Highly Promiscuous Regarding the Sequence of the Cleaved Hydrophobic Segment. J Mol Biol. 2010;401: 182–193. doi:10.1016/j.jmb.2010.06.014
60. Zick M, Duvezin-Caubet S, Schäfer A, Vogel F, Neupert W, Reichert AS. Distinct roles of the two isoforms of the dynamin-like GTPase Mgm1 in mitochondrial fusion. FEBS Lett. Federation of European Biochemical Societies; 2009;583: 2237–2243. doi:10.1016/j.febslet.2009.05.053
61. Herlan M, Bornhövd C, Hell K, Neupert W, Reichert AS. Alternative topogenesis of Mgm1 and mitochondrial morphology depend on ATP and a functional import motor. J Cell Biol. Rockefeller University Press; 2004;165: 167–173. doi:10.1083/jcb.200403022
62. Rujiviphat J, Wong MK, Won A, Shih Y, Yip CM, McQuibban GA. Mitochondrial Genome Maintenance 1 (Mgm1) Protein Alters Membrane Topology and Promotes Local Membrane Bending. J Mol Biol. Elsevier Ltd; 2015;427: 2599–2609. doi:10.1016/j.jmb.2015.03.006
63. Delettre C, Griffoin J-M, Kaplan J, Dollfus H, Lorenz B, Faivre L, et al. Mutation spectrum and splicing variants in the OPA1 gene. Hum Genet. 2001;109: 584–591. doi:10.1007/s00439-001-0633-y
64. Griparic L, Kanazawa T, van der Bliek AM. Regulation of the mitochondrial dynamin-like protein Opa1 by proteolytic cleavage. J Cell Biol. 2007;178: 757–764. doi:10.1083/jcb.200704112
65. Song Z, Chen H, Fiket M, Alexander C, Chan DC. OPA1 processing controls mitochondrial fusion and is regulated by mRNA splicing, membrane potential, and Yme1L. J Cell Biol. 2007;178: 749–755. doi:10.1083/jcb.200704110
66. Ishihara N, Fujita Y, Oka T, Mihara K. Regulation of mitochondrial morphology through proteolytic cleavage of OPA1. EMBO J. 2006;25: 2966–2977. doi:10.1038/sj.emboj.7601184
67. Ehses S, Raschke I, Mancuso G, Bernacchia A, Geimer S, Tondera D, et al. Regulation of OPA1 processing and mitochondrial fusion by m -AAA protease isoenzymes and OMA1. J Cell Biol. 2009;187: 1023–1036. doi:10.1083/jcb.200906084
68. Cipolat S, Rudka T, Hartmann D, Costa V, Serneels L, Craessaerts K, et al. Mitochondrial Rhomboid PARL Regulates Cytochrome c Release during Apoptosis via OPA1-Dependent Cristae Remodeling. Cell. 2006;126: 163–175. doi:10.1016/j.cell.2006.06.021
69. Baker MJ, Lampe PA, Stojanovski D, Korwitz A, Anand R, Tatsuta T, et al. Stress-induced OMA1 activation and autocatalytic turnover regulate OPA1-dependent mitochondrial dynamics. EMBO J. 2014;33: 578–593. doi:10.1002/embj.201386474
70. Anand R, Wai T, Baker MJ, Kladt N, Schauss AC, Rugarli E, et al. The i -AAA protease YME1L and OMA1 cleave OPA1 to balance mitochondrial fusion and fission. J Cell Biol. 2014;204: 919–929. doi:10.1083/jcb.201308006
71. Lee H, Smith SB, Yoon Y. The short variant of the mitochondrial dynamin OPA1 maintains

mitochondrial energetics and cristae structure. J Biol Chem. 2017;292: 7115–7130. doi:10.1074/jbc.M116.762567
72. Sesaki H, Jensen RE. UGO1 Encodes an Outer Membrane Protein Required for Mitochondrial Fusion. J Cell Biol. 2001;152: 1123–1134. doi:10.1083/jcb.152.6.1123
73. Coonrod EM, Karren MA, Shaw JM. Ugo1p Is a Multipass Transmembrane Protein with a Single Carrier Domain Required for Mitochondrial Fusion. Traffic. 2007;8: 500–511. doi:10.1111/j.1600-0854.2007.00550.x
74. Herrera-Cruz MS, Simmen T. Of yeast, mice and men: MAMs come in two flavors. Biol Direct. Rockefeller University Press; 2017;12: 3. doi:10.1186/s13062-017-0174-5
75. Hoppins S, Horner J, Song C, McCaffery JM, Nunnari J. Mitochondrial outer and inner membrane fusion requires a modified carrier protein. J Cell Biol. 2009;184: 569–581. doi:10.1083/jcb.200809099
76. Abrams AJ, Hufnagel RB, Rebelo A, Zanna C, Patel N, Gonzalez MA, et al. Mutations in SLC25A46, encoding a UGO1-like protein, cause an optic atrophy spectrum disorder. Nat Genet. 2015;47: 926–932. doi:10.1038/ng.3354
77. Palmieri F. The mitochondrial transporter family SLC25: Identification, properties and physiopathology. Mol Aspects Med. 2013;34: 465–484. doi:10.1016/j.mam.2012.05.005
78. Terzenidou ME, Segklia A, Kano T, Papastefanaki F, Karakostas A, Charalambous M, et al. Novel insights into SLC25A46-related pathologies in a genetic mouse model. Kunji E, editor. PLOS Genet. 2017;13: e1006656. doi:10.1371/journal.pgen.1006656
79. Janer A, Prudent J, Paupe V, Fahiminiya S, Majewski J, Sgarioto N, et al. SLC25A46 is required for mitochondrial lipid homeostasis and cristae maintenance and is responsible for Leigh syndrome. EMBO Mol Med. 2016;8: 1019–1038. doi:10.15252/emmm.201506159
80. Steffen J, Vashisht AA, Wan J, Jen JC, Claypool SM, Wohlschlegel JA, et al. Rapid degradation of mutant SLC25A46 by the ubiquitin-proteasome system results in MFN1/2-mediated hyperfusion of mitochondria. Fox TD, editor. Mol Biol Cell. 2017;28: 600–612. doi:10.1091/mbc.E16-07-0545
81. Song Z, Ghochani M, McCaffery JM, Frey TG, Chan DC. Mitofusins and OPA1 Mediate Sequential Steps in Mitochondrial Membrane Fusion. Mol Biol Cell. 2009;20: 3525–3532. doi:10.1091/mbc.E09-03-0252
82. Duchesne A, Vaiman A, Castille J, Beauvallet C, Gaignard P, Floriot S, et al. Bovine and murine models highlight novel roles for SLC25A46 in mitochondrial dynamics and metabolism, with implications for human and animal health. Kunji E, editor. PLOS Genet. 2017;13: e1006597. doi:10.1371/journal.pgen.1006597
83. Ingerman E, Perkins EM, Marino M, Mears JA, McCaffery JM, Hinshaw JE, et al. Dnm1 forms spirals that are structurally tailored to fit mitochondria. J Cell Biol. 2005;170: 1021–1027. doi:10.1083/jcb.200506078
84. Otsuga D, Keegan BR, Brisch E, Thatcher JW, Hermann GJ, Bleazard W, et al. The Dynamin-related GTPase, Dnm1p, Controls Mitochondrial Morphology in Yeast. J Cell Biol. 1998;143: 333–349. doi:10.1083/jcb.143.2.333
85. Sesaki H, Jensen RE. Division versus Fusion: Dnm1p and Fzo1p Antagonistically Regulate Mitochondrial Shape. J Cell Biol. 1999;147: 699–706. doi:10.1083/jcb.147.4.699
86. Yoon Y, Pitts KR, McNiven MA. Mammalian Dynamin-like Protein DLP1 Tubulates Membranes. Mol Biol Cell. 2001;12: 2894–2905. doi:10.1091/mbc.12.9.2894
87. Labrousse AM, Zappaterra MD, Rube DA, van der Bliek AM. C. elegans Dynamin-Related Protein DRP-1 Controls Severing of the Mitochondrial Outer Membrane. Mol Cell. 1999;4: 815–826. doi:10.1016/S1097-2765(00)80391-3
88. Mozdy AD, McCaffery JM, Shaw JM. Dnm1p Gtpase-Mediated Mitochondrial Fission Is a Multi-Step Process Requiring the Novel Integral Membrane Component Fis1p. J Cell Biol. 2000;151: 367–380. doi:10.1083/jcb.151.2.367
89. Tieu Q, Nunnari J. Mdv1p Is a Wd Repeat Protein That Interacts with the Dynamin-Related Gtpase, Dnm1p, to Trigger Mitochondrial Division. J Cell Biol. 2000;151: 353–366.

doi:10.1083/jcb.151.2.353
90. Cerveny KL. The WD-repeats of Net2p Interact with Dnm1p and Fis1p to Regulate Division of Mitochondria. Mol Biol Cell. 2003;14: 4126–4139. doi:10.1091/mbc.E03-02-0092
91. Zhang Y, Chan NC, Ngo HB, Gristick H, Chan DC. Crystal Structure of Mitochondrial Fission Complex Reveals Scaffolding Function for Mitochondrial Division 1 (Mdv1) Coiled Coil. J Biol Chem. 2012;287: 9855–9861. doi:10.1074/jbc.M111.329359
92. Tieu Q, Okreglak V, Naylor K, Nunnari J. The WD repeat protein, Mdv1p, functions as a molecular adaptor by interacting with Dnm1p and Fis1p during mitochondrial fission. J Cell Biol. Rockefeller University Press; 2002;158: 445–452. doi:10.1083/jcb.200205031
93. Naylor K, Ingerman E, Okreglak V, Marino M, Hinshaw JE, Nunnari J. Mdv1 Interacts with Assembled Dnm1 to Promote Mitochondrial Division. J Biol Chem. 2006;281: 2177–2183. doi:10.1074/jbc.M507943200
94. Griffin EE, Graumann J, Chan DC. The WD40 protein Caf4p is a component of the mitochondrial fission machinery and recruits Dnm1p to mitochondria. J Cell Biol. 2005;170: 237–248. doi:10.1083/jcb.200503148
95. Legesse-Miller A, Massol RH, Kirchhausen T. Constriction and Dnm1p Recruitment Are Distinct Processes in Mitochondrial Fission. Mol Biol Cell. 2003;14: 1953–1963. doi:10.1091/mbc.E02-10-0657
96. Schauss AC, Bewersdorf J, Jakobs S. Fis1p and Caf4p, but not Mdv1p, determine the polar localization of Dnm1p clusters on the mitochondrial surface. J Cell Sci. 2006;119: 3098–3106. doi:10.1242/jcs.03026
97. Gandre-Babbe S, van der Bliek AM. The Novel Tail-anchored Membrane Protein Mff Controls Mitochondrial and Peroxisomal Fission in Mammalian Cells. Mol Biol Cell. 2008;19: 2402–2412. doi:10.1091/mbc.E07-12-1287
98. James DI, Parone PA, Mattenberger Y, Martinou J-C. hFis1, a Novel Component of the Mammalian Mitochondrial Fission Machinery. J Biol Chem. in Press; 2003;278: 36373–36379. doi:10.1074/jbc.M303758200
99. Palmer CS, Osellame LD, Laine D, Koutsopoulos OS, Frazier AE, Ryan MT. MiD49 and MiD51, new components of the mitochondrial fission machinery. EMBO Rep. 2011;12: 565–573. doi:10.1038/embor.2011.54
100. Otera H, Wang C, Cleland MM, Setoguchi K, Yokota S, Youle RJ, et al. Mff is an essential factor for mitochondrial recruitment of Drp1 during mitochondrial fission in mammalian cells. J Cell Biol. 2010;191: 1141–1158. doi:10.1083/jcb.201007152
101. Yoon Y, Krueger EW, Oswald BJ, McNiven MA. The Mitochondrial Protein hFis1 Regulates Mitochondrial Fission in Mammalian Cells through an Interaction with the Dynamin-Like Protein DLP1. Mol Cell Biol. 2003;23: 5409–5420. doi:10.1128/MCB.23.15.5409-5420.2003
102. Zhao J, Liu T, Jin S, Wang X, Qu M, Uhlén P, et al. Human MIEF1 recruits Drp1 to mitochondrial outer membranes and promotes mitochondrial fusion rather than fission. EMBO J. 2011;30: 2762–2778. doi:10.1038/emboj.2011.198
103. Loson OC, Song Z, Chen H, Chan DC. Fis1, Mff, MiD49, and MiD51 mediate Drp1 recruitment in mitochondrial fission. Mol Biol Cell. 2013;24: 659–667. doi:10.1091/mbc.E12-10-0721
104. Palmer CS, Elgass KD, Parton RG, Osellame LD, Stojanovski D, Ryan MT. Adaptor Proteins MiD49 and MiD51 Can Act Independently of Mff and Fis1 in Drp1 Recruitment and Are Specific for Mitochondrial Fission. J Biol Chem. 2013;288: 27584–27593. doi:10.1074/jbc.M113.479873
105. Koirala S, Guo Q, Kalia R, Bui HT, Eckert DM, Frost A, et al. Interchangeable adaptors regulate mitochondrial dynamin assembly for membrane scission. Proc Natl Acad Sci. 2013;110: E1342–E1351. doi:10.1073/pnas.1300855110
106. Osellame LD, Singh AP, Stroud DA, Palmer CS, Stojanovski D, Ramachandran R, et al. Cooperative and independent roles of the Drp1 adaptors Mff, MiD49 and MiD51 in mitochondrial fission. J Cell Sci. 2016;129: 2170–2181. doi:10.1242/jcs.185165
107. Roux KJ, Kim DI, Burke B. BioID: A Screen for Protein-Protein Interactions. Current Protocols in

Protein Science. Hoboken, NJ, USA: John Wiley & Sons, Inc.; 2013. p. 19.23.1-19.23.14. doi:10.1002/0471140864.ps1923s74
108. Elgass KD, Smith EA, LeGros M a., Larabell CA, Ryan MT. Analysis of ER-mitochondria contacts using correlative fluorescence microscopy and soft X-ray tomography of mammalian cells. J Cell Sci. 2015;128: 2795–2804. doi:10.1242/jcs.169136
109. Wilson TJ, Slupe AM, Strack S. Cell signaling and mitochondrial dynamics: Implications for neuronal function and neurodegenerative disease. Neurobiol Dis. 2013;51: 13–26. doi:10.1016/j.nbd.2012.01.009
110. Sontag JM, Fykse EM, Ushkaryov Y, Liu JP, Robinson PJ, Südhof TC. Differential expression and regulation of multiple dynamins. J Biol Chem. 1994;269: 4547–54. Available: http://www.jbc.org/content/269/6/4547.full.pdf
111. Lee JE, Westrate LM, Wu H, Page C, Voeltz GK. Multiple dynamin family members collaborate to drive mitochondrial division. Nature. 2016;540: 139–143. doi:10.1038/nature20555
112. Friedman JR, Lackner LL, West M, DiBenedetto JR, Nunnari J, Voeltz GK. ER Tubules Mark Sites of Mitochondrial Division. Science (80-). 2011;334: 358–362. doi:10.1126/science.1207385
113. Schmidt R, Wurm CA, Punge A, Egner A, Jakobs S, Hell SW. Mitochondrial Cristae Revealed with Focused Light. Nano Lett. 2009;9: 2508–2510. doi:10.1021/nl901398t
114. Kornmann B, Currie E, Collins SR, Schuldinner M, Nunnari J, Weissman JS, et al. An ER-Mitochondria Tethering Complex Revealed by a Synthetic Biology Screen. Science. 2009;325: 477–81. doi:10.1126/science.1175088
115. Boldogh IR, Nowakowski DW, Yang H-C, Chung H, Karmon S, Royes P, et al. A Protein Complex Containing Mdm10p, Mdm12p, and Mmm1p Links Mitochondrial Membranes and DNA to the Cytoskeleton-based Segregation Machinery. Mol Biol Cell. 2003;14: 4618–4627. doi:10.1091/mbc.E03-04-0225
116. Lee I, Hong W. Diverse membrane-associated proteins contain a novel SMP domain. FASEB J. 2006;20: 202–206. doi:10.1096/fj.05-4581hyp
117. Kopec KO, Alva V, Lupas AN. Homology of SMP domains to the TULIP superfamily of lipid-binding proteins provides a structural basis for lipid exchange between ER and mitochondria. Bioinformatics. 2010;26: 1927–1931. doi:10.1093/bioinformatics/btq326
118. Meisinger C, Rissler M, Chacinska A, Szklarz LKS, Milenkovic D, Kozjak V, et al. The Mitochondrial Morphology Protein Mdm10 Functions in Assembly of the Preprotein Translocase of the Outer Membrane. Dev Cell. 2004;7: 61–71. doi:10.1016/j.devcel.2004.06.003
119. Meisinger C, Pfannschmidt S, Rissler M, Milenkovic D, Becker T, Stojanovski D, et al. The morphology proteins Mdm12/Mmm1 function in the major β-barrel assembly pathway of mitochondria. EMBO J. 2007;26: 2229–2239. doi:10.1038/sj.emboj.7601673
120. Yamano K, Tanaka-Yamano S, Endo T. Tom7 Regulates Mdm10-mediated Assembly of the Mitochondrial Import Channel Protein Tom40. J Biol Chem. 2010;285: 41222–41231. doi:10.1074/jbc.M110.163238
121. Yamano K, Tanaka-Yamano S, Endo T. Mdm10 as a dynamic constituent of the TOB/SAM complex directs coordinated assembly of Tom40. EMBO Rep. 2010;11: 187–193. doi:10.1038/embor.2009.283
122. Michel AH, Kornmann B. The ERMES complex and ER–mitochondria connections. Biochem Soc Trans. 2012;40: 445–450. doi:10.1042/BST20110758
123. AhYoung AP, Jiang J, Zhang J, Khoi Dang X, Loo JA, Zhou ZH, et al. Conserved SMP domains of the ERMES complex bind phospholipids and mediate tether assembly. Proc Natl Acad Sci. 2015;112: E3179–E3188. doi:10.1073/pnas.1422363112
124. Jeong H, Park J, Lee C. Crystal structure of Mdm12 reveals the architecture and dynamic organization of the ERMES complex. EMBO Rep. 2016;17: 1857–1871. doi:10.15252/embr.201642706
125. Kornmann B, Osman C, Walter P. The conserved GTPase Gem1 regulates endoplasmic reticulum-mitochondria connections. Proc Natl Acad Sci U S A. 2011;108: 14151–14156.

doi:10.1073/pnas.1111314108
126. Frederick RL, McCaffery JM, Cunningham KW, Okamoto K, Shaw JM. Yeast Miro GTPase, Gem1p, regulates mitochondrial morphology via a novel pathway. J Cell Biol. 2004;167: 87–98. doi:10.1083/jcb.200405100
127. Murley A, Lackner LL, Osman C, West M, Voeltz GK, Walter P, et al. ER-associated mitochondrial division links the distribution of mitochondria and mitochondrial DNA in yeast. Elife. 2013;2013: 1–16. doi:10.7554/eLife.00422
128. Nguyen TT, Lewandowska A, Choi J-Y, Markgraf DF, Junker M, Bilgin M, et al. Gem1 and ERMES Do Not Directly Affect Phosphatidylserine Transport from ER to Mitochondria or Mitochondrial Inheritance. Traffic. 2012;13: 880–890. doi:10.1111/j.1600-0854.2012.01352.x
129. Flis V V, Daum G. Lipid Transport between the Endoplasmic Reticulum and Mitochondria. Cold Spring Harb Perspect Biol. 2013;5: a013235–a013235. doi:10.1101/cshperspect.a013235
130. Kojima R, Endo T, Tamura Y. A phospholipid transfer function of ER-mitochondria encounter structure revealed in vitro. Sci Rep. Nature Publishing Group; 2016;6: 30777. doi:10.1038/srep30777
131. Voss C, Lahiri S, Young BP, Loewen CJ, Prinz WA. ER-shaping proteins facilitate lipid exchange between the ER and mitochondria in S. cerevisiae. J Cell Sci. 2012;125: 4791–4799. doi:10.1242/jcs.105635
132. Lahiri S, Chao JT, Tavassoli S, Wong AKO, Choudhary V, Young BP, et al. A Conserved Endoplasmic Reticulum Membrane Protein Complex (EMC) Facilitates Phospholipid Transfer from the ER to Mitochondria. Schmid SL, editor. PLoS Biol. 2014;12: e1001969. doi:10.1371/journal.pbio.1001969
133. Wideman JG, Gawryluk RMR, Gray MW, Dacks JB. The ancient and widespread nature of the ER-mitochondria encounter structure. Mol Biol Evol. 2013;30: 2044–2049. doi:10.1093/molbev/mst120
134. Wideman JG. The ubiquitous and ancient ER membrane protein complex (EMC): tether or not? F1000Research. 2015;4: 624. doi:10.12688/f1000research.6944.2
135. Elbaz-Alon Y, Rosenfeld-Gur E, Shinder V, Futerman AH, Geiger T, Schuldiner M. A Dynamic Interface between Vacuoles and Mitochondria in Yeast. Dev Cell. 2014;30: 95–102. doi:10.1016/j.devcel.2014.06.007
136. Hönscher C, Mari M, Auffarth K, Bohnert M, Griffith J, Geerts W, et al. Cellular Metabolism Regulates Contact Sites between Vacuoles and Mitochondria. Dev Cell. 2014;30: 86–94. doi:10.1016/j.devcel.2014.06.006
137. Elbaz-Alon Y, Eisenberg-Bord M, Shinder V, Stiller SB, Shimoni E, Wiedemann N, et al. Lam6 Regulates the Extent of Contacts between Organelles. Cell Rep. 2015;12: 7–14. doi:10.1016/j.celrep.2015.06.022
138. Hobbs AEA, Srinivasan M, McCaffery JM, Jensen RE. Mmm1p, a Mitochondrial Outer Membrane Protein, Is Connected to Mitochondrial DNA (Mtdna) Nucleoids and Required for Mtdna Stability. J Cell Biol. 2001;152: 401–410. doi:10.1083/jcb.152.2.401
139. Meeusen S, Nunnari J. Evidence for a two membrane-spanning autonomous mitochondrial DNA replisome. J Cell Biol. 2003;163: 503–510. doi:10.1083/jcb.200304040
140. de Brito OM, Scorrano L. Mitofusin 2 tethers endoplasmic reticulum to mitochondria. Nature. 2008;456: 605–610. doi:10.1038/nature07534
141. Cosson P, Marchetti A, Ravazzola M, Orci L. Mitofusin-2 Independent Juxtaposition of Endoplasmic Reticulum and Mitochondria: An Ultrastructural Study. van der Goot FG, editor. PLoS One. 2012;7: e46293. doi:10.1371/journal.pone.0046293
142. Filadi R, Greotti E, Turacchio G, Luini A, Pozzan T, Pizzo P. Mitofusin 2 ablation increases endoplasmic reticulum–mitochondria coupling. Proc Natl Acad Sci. 2015;112: E2174–E2181. doi:10.1073/pnas.1504880112
143. Naon D, Zaninello M, Giacomello M, Varanita T, Grespi F, Lakshminaranayan S, et al. Critical reappraisal confirms that Mitofusin 2 is an endoplasmic reticulum–mitochondria tether. Proc Natl Acad Sci. 2016;113: 11249–11254. doi:10.1073/pnas.1606786113

144. Vlahou G, Eliáš M, von Kleist-Retzow JC, Wiesner RJ, Rivero F. The Ras related GTPase Miro is not required for mitochondrial transport in *Dictyostelium discoideum*. Eur J Cell Biol. 2011;90: 342–355. doi:10.1016/j.ejcb.2010.10.012
145. Korobova F, Ramabhadran V, Higgs HN. An Actin-Dependent Step in Mitochondrial Fission Mediated by the ER-Associated Formin INF2. Science (80-). 2013;339: 464–467. doi:10.1126/science.1228360
146. Korobova F, Gauvin TJ, Higgs HN. A Role for Myosin II in Mammalian Mitochondrial Fission. Curr Biol. 2014;24: 409–414. doi:10.1016/j.cub.2013.12.032
147. Smith TK, Bringaud F, Nolan DP, Figueiredo LM. Metabolic reprogramming during the *Trypanosoma brucei* life cycle. F1000Research. 2017;6: 683. doi:10.12688/f1000research.10342.1
148. Trindade S, Rijo-Ferreira F, Carvalho T, Pinto-Neves D, Guegan F, Aresta-Branco F, et al. *Trypanosoma brucei* Parasites Occupy and Functionally Adapt to the Adipose Tissue in Mice. Cell Host Microbe. 2016;19: 837–848. doi:10.1016/j.chom.2016.05.002
149. Ogbadoyi EO, Robinson DR, Gull K. A High-Order Trans-Membrane Structural Linkage Is Responsible for Mitochondrial Genome Positioning and Segregation by Flagellar Basal Bodies in Trypanosomes. Mol Biol Cell. 2003;14: 1769–1779. doi:10.1091/mbc.E02-08-0525
150. Woodward R, Gull K. Timing of nuclear and kinetoplast DNA replication and early morphological events in the cell cycle of *Trypanosoma brucei*. J Cell Sci. 1990;95 (Pt 1): 49–57. Available: http://jcs.biologists.org/content/joces/95/1/49.full.pdf
151. Robinson DR, Gull K. Basal body movements as a mechanism for mitochondrial genome segregation in the trypanosome cell cycle. Nature. 1991;352: 731–733. doi:10.1038/352731a0
152. Zhao Z, Lindsay ME, Roy Chowdhury A, Robinson DR, Englund PT. p166, a link between the trypanosome mitochondrial DNA and flagellum, mediates genome segregation. EMBO J. 2008;27: 143–154. doi:10.1038/sj.emboj.7601956
153. Ochsenreiter T, Anderson S, Wood ZA, Hajduk SL. Alternative RNA Editing Produces a Novel Protein Involved in Mitochondrial DNA Maintenance in Trypanosomes. Mol Cell Biol. 2008;28: 5595–5604. doi:10.1128/MCB.00637-08
154. Gheiratmand L, Brasseur A, Zhou Q, He CY. Biochemical Characterization of the Bi-lobe Reveals a Continuous Structural Network Linking the Bi-lobe to Other Single-copied Organelles in *Trypanosoma brucei*. J Biol Chem. 2013;288: 3489–3499. doi:10.1074/jbc.M112.417428
155. Schnarwiler F, Niemann M, Doiron N, Harsman A, Kaser S, Mani J, et al. Trypanosomal TAC40 constitutes a novel subclass of mitochondrial -barrel proteins specialized in mitochondrial genome inheritance. Proc Natl Acad Sci. 2014;111: 7624–7629. doi:10.1073/pnas.1404854111
156. Hammarton TC. Cell cycle regulation in *Trypanosoma brucei*. Mol Biochem Parasitol. 2007;153: 1–8. doi:10.1016/j.molbiopara.2007.01.017
157. Hughes L, Borrett S, Towers K, Starborg T, Vaughan S. Patterns of organelle ontogeny through a cell cycle revealed by whole-cell reconstructions using 3D electron microscopy. J Cell Sci. 2017;130: 637–647. doi:10.1242/jcs.198887
158. Jakob M, Hoffmann A, Amodeo S, Peitsch C, Zuber B, Ochsenreiter T. Mitochondrial growth during the cell cycle of *Trypanosoma brucei* bloodstream forms. Sci Rep. 2016;6: 36565. doi:10.1038/srep36565
159. Posakony JW, England JM, Attardi G. Mitochondrial growth and division during the cell cycle in HeLa cells. J Cell Biol. 1977;74: 468–91. Available: http://jcb.rupress.org/content/jcb/74/2/468.full.pdf
160. Tanaka K, Kanbe T, Kuroiwa T. Three-dimensional behaviour of mitochondria during cell division and germ tube formation in the dimorphic yeast *Candida albicans*. J Cell Sci. 1985;73: 207–20. Available: http://jcs.biologists.org/content/joces/73/1/207.full.pdf
161. Morgan GW, Goulding D, Field MC. The Single Dynamin-like Protein of *Trypanosoma brucei* Regulates Mitochondrial Division and Is Not Required for Endocytosis. J Biol Chem. 2004;279: 10692–10701. doi:10.1074/jbc.M312178200
162. Chanez A-L, Hehl AB, Engstler M, Schneider A. Ablation of the single dynamin of *T. brucei*

blocks mitochondrial fission and endocytosis and leads to a precise cytokinesis arrest. J Cell Sci. 2006;119: 2968–2974. doi:10.1242/jcs.03023
163. Field MC, Carrington M. The trypanosome flagellar pocket. Nat Rev Microbiol. Nature Publishing Group; 2009;7: 775–786. doi:10.1038/nrmicro2221
164. Niemann M, Wiese S, Mani J, Chanfon A, Jackson C, Meisinger C, et al. Mitochondrial Outer Membrane Proteome of *Trypanosoma brucei* Reveals Novel Factors Required to Maintain Mitochondrial Morphology. Mol Cell Proteomics. 2013;12: 515–528. doi:10.1074/mcp.M112.023093
165. Urbaniak MD, Guther MLS, Ferguson MAJ. Comparative SILAC Proteomic Analysis of *Trypanosoma brucei* Bloodstream and Procyclic Lifecycle Stages. Li Z, editor. PLoS One. 2012;7: e36619. doi:10.1371/journal.pone.0036619
166. Peacock L, Ferris V, Bailey M, Gibson W. Mating compatibility in the parasitic protist *Trypanosoma brucei*. Parasit Vectors. 2014;7: 78. doi:10.1186/1756-3305-7-78
167. Esseiva AC, Chanez A-L, Bochud-Allemann N, Martinou J-C, Hemphill A, Schneider A. Temporal dissection of Bax-induced events leading to fission of the single mitochondrion in *Trypanosoma brucei*. EMBO Rep. EMBO Press; 2004;5: 268–273. doi:10.1038/sj.embor.7400095
168. van Dooren GG, Marti M, Tonkin CJ, Stimmler LM, Cowman AF, McFadden GI. Development of the endoplasmic reticulum, mitochondrion and apicoplast during the asexual life cycle of *Plasmodium falciparum*. Mol Microbiol. 2005;57: 405–419. doi:10.1111/j.1365-2958.2005.04699.x
169. Kohler S, Delwiche CF, Denny PW, Tilney LG, Webster P, Wilson RJM, et al. A Plastid of Probable Green Algal Origin in Apicomplexan Parasites. Science (80-). 1997;275: 1485–1489. doi:10.1126/science.275.5305.1485
170. Hopkins J, Fowler R, Krishna S, Wilson I, Mitchell G, Bannister L. The Plastid in *Plasmodium falciparum* Asexual Blood Stages: a Three-Dimensional Ultrastructural Analysis. Protist. 1999;150: 283–295. doi:10.1016/S1434-4610(99)70030-1
171. Kobayashi T, Sato S, Takamiya S, Komaki-Yasuda K, Yano K, Hirata A, et al. Mitochondria and apicoplast of *Plasmodium falciparum*: Behaviour on subcellular fractionation and the implication. Mitochondrion. 2007;7: 125–132. doi:10.1016/j.mito.2006.11.021
172. Arisue N, Hashimoto T. Phylogeny and evolution of apicoplasts and apicomplexan parasites. Parasitol Int. Elsevier B.V.; 2015;64: 254–259. doi:10.1016/j.parint.2014.10.005
173. Stanway RR, Witt T, Zobiak B, Aepfelbacher M, Heussler VT. GFP-targeting allows visualization of the apicoplast throughout the life cycle of live malaria parasites. Biol Cell. 2009;101: 415–435. doi:10.1042/BC20080202
174. Okamoto N, Spurck TP, Goodman CD, McFadden GI. Apicoplast and Mitochondrion in Gametocytogenesis of *Plasmodium falciparum*. Eukaryot Cell. 2009;8: 128–132. doi:10.1128/EC.00267-08
175. Creasey A, Mendis K, Carlton J, Williamson D, Wilson I, Carter R. Maternal inheritance of extrachromosomal DNA in malaria parasites. Mol Biochem Parasitol. 1994;65: 95–98. doi:10.1016/0166-6851(94)90118-X
176. Ferguson DJP, Henriquez FL, Kirisits MJ, Muench SP, Prigge ST, Rice DW, et al. Maternal Inheritance and Stage-Specific Variation of the Apicoplast in *Toxoplasma gondii* during Development in the Intermediate and Definitive Host. Eukaryot Cell. 2005;4: 814–826. doi:10.1128/EC.4.4.814-826.2005
177. Ferguson DJP, Campbell SA, Henriquez FL, Phan L, Mui E, Richards TA, et al. Enzymes of type II fatty acid synthesis and apicoplast differentiation and division in *Eimeria tenella*. Int J Parasitol. 2007;37: 33–51. doi:10.1016/j.ijpara.2006.10.003
178. Young JA, Fivelman QL, Blair PL, de la Vega P, Le Roch KG, Zhou Y, et al. The Plasmodium falciparum sexual development transcriptome: A microarray analysis using ontology-based pattern identification. Mol Biochem Parasitol. 2005;143: 67–79. doi:10.1016/j.molbiopara.2005.05.007

179. Krungkrai J, Prapunwattana P, Krungkrai SR. Ultrastructure and function of mitochondria in gametocytic stage of *Plasmodium falciparum*. Parasite. 2000;7: 19–26. doi:10.1051/parasite/2000071019
180. Li H, Han Z, Lu Y, Lin Y, Zhang L, Wu Y, et al. Isolation and functional characterization of a dynamin-like gene from *Plasmodium falciparum*. Biochem Biophys Res Commun. 2004;320: 664–671. doi:10.1016/j.bbrc.2004.06.010
181. Charneau S, Dourado Bastos IM, Mouray E, Ribeiro BM, Santana JM, Grellier P, et al. Characterization of PfDYN2, a dynamin-like protein of *Plasmodium falciparum* expressed in schizonts. Microbes Infect. 2007;9: 797–805. doi:10.1016/j.micinf.2007.02.020
182. Breinich MS, Ferguson DJP, Foth BJ, van Dooren GG, Lebrun M, Quon D V, et al. A Dynamin Is Required for the Biogenesis of Secretory Organelles in *Toxoplasma gondii*. Curr Biol. 2009;19: 277–286. doi:10.1016/j.cub.2009.01.039
183. Milani KJ, Schneider TG, Taraschi TF. Defining the Morphology and Mechanism of the Hemoglobin Transport Pathway in *Plasmodium falciparum*-Infected Erythrocytes. Eukaryot Cell. 2015;14: 415–426. doi:10.1128/EC.00267-14
184. Nishi M, Hu K, Murray JM, Roos DS. Organellar dynamics during the cell cycle of *Toxoplasma gondii*. J Cell Sci. 2008;121: 1559–1568. doi:10.1242/jcs.021089
185. Ovciarikova J, Lemgruber L, Stilger KL, Sullivan WJ, Sheiner L. Mitochondrial behaviour throughout the lytic cycle of *Toxoplasma gondii.* Sci Rep. Nature Publishing Group; 2017;7: 42746. doi:10.1038/srep42746
186. Harding CR, Meissner M. The inner membrane complex through development of *Toxoplasma gondii* and *Plasmodium*. Cell Microbiol. 2014;16: 632–641. doi:10.1111/cmi.12285
187. van Dooren GG, Reiff SB, Tomova C, Meissner M, Humbel BM, Striepen B. A Novel Dynamin-Related Protein Has Been Recruited for Apicoplast Fission in *Toxoplasma gondii*. Curr Biol. 2009;19: 267–276. doi:10.1016/j.cub.2008.12.048
188. Pieperhoff MS, Pall GS, Jiménez-Ruiz E, Das S, Melatti C, Gow M, et al. Conditional U1 Gene Silencing in *Toxoplasma gondii*. Knoll LJ, editor. PLoS One. 2015;10: e0130356. doi:10.1371/journal.pone.0130356
189. Lindmark DG, Müller M. Hydrogenosome, a cytoplasmic organelle of the anaerobic flagellate *Tritrichomonas foetus*, and its role in pvruvate metabolism. J Biol Chem. 1973;248: 7724–7729. Available: http://www.jbc.org/content/248/22/7724.full.pdf
190. Benchimol M, Johnson PJ, Souza W. Morphogenesis of the hydrogenosome: An ultrastructural study. Biol Cell. 1996;87: 197–205. doi:10.1111/j.1768-322X.1996.tb00981.x
191. Benchimol M. Hydrogenosomes under microscopy. Tissue Cell. 2009;41: 151–168. doi:10.1016/j.tice.2009.01.001
192. Wexler-Cohen Y, Stevens GC, Barnoy E, van der Bliek AM, Johnson PJ. A dynamin-related protein contributes to *Trichomonas vaginalis* hydrogenosomal fission. FASEB J. 2014;28: 1113–1121. doi:10.1096/fj.13-235473
193. Tovar J, León-Avila G, Sánchez LB, Sutak R, Tachezy J, van der Giezen M, et al. Mitochondrial remnant organelles of *Giardia* function in iron-sulphur protein maturation. Nature. 2003;426: 172–176. doi:10.1038/nature01945
194. Dolezal P, Smíd O, Rada P, Zubácová Z, Bursać D, Suták R, et al. *Giardia* mitosomes and trichomonad hydrogenosomes share a common mode of protein targeting. Proc Natl Acad Sci U S A. 2005;102: 10924–10929. doi:10.1073/pnas.0500349102
195. Jedelský PL, Doležal P, Rada P, Pyrih J, Šmíd O, Hrdý I, et al. The minimal proteome in the reduced mitochondrion of the parasitic protist *Giardia intestinalis*. PLoS One. 2011;6: 15–21. doi:10.1371/journal.pone.0017285
196. Martincová E, Voleman L, Pyrih J, Žárský V, Vondráčková P, Kolísko M, et al. Probing the Biology of *Giardia intestinalis* Mitosomes Using In Vivo Enzymatic Tagging. Mol Cell Biol. 2015;35: 2864–2874. doi:10.1128/MCB.00448-15
197. Regoes A. Protein Import, Replication, and Inheritance of a Vestigial Mitochondrion. J Biol Chem. 2005;280: 30557–30563. doi:10.1074/jbc.M500787200

198. Midlej V, Penha L, Silva R, de Souza W, Benchimol M. Mitosomal chaperone modulation during the life cycle of the pathogenic protist *Giardia intestinalis*. Eur J Cell Biol. 2016;95: 531–542. doi:10.1016/j.ejcb.2016.08.005
199. Gaechter V, Schraner E, Wild P, Hehl AB. The Single Dynamin Family Protein in the Primitive Protozoan *Giardia lamblia* Is Essential for Stage Conversion and Endocytic Transport. Traffic. 2008;9: 57–71. doi:10.1111/j.1600-0854.2007.00657.x
200. Rout S, Zumthor JP, Schraner EM, Faso C, Hehl AB. An Interactome-Centered Protein Discovery Approach Reveals Novel Components Involved in Mitosome Function and Homeostasis in *Giardia lamblia*. Kumar K, editor. PLOS Pathog. 2016;12: e1006036. doi:10.1371/journal.ppat.1006036
201. Finn RD, Clements J, Arndt W, Miller BL, Wheeler TJ, Schreiber F, et al. HMMER web server: 2015 update. Nucleic Acids Res. 2015;43: W30–W38. doi:10.1093/nar/gkv397
202. Finn RD, Coggill P, Eberhardt RY, Eddy SR, Mistry J, Mitchell AL, et al. The Pfam protein families database: towards a more sustainable future. Nucleic Acids Res. 2016;44: D279–D285. doi:10.1093/nar/gkv1344
203. Los G V, Encell LP, McDougall MG, Hartzell DD, Karassina N, Zimprich C, et al. HaloTag: A Novel Protein Labeling Technology for Cell Imaging and Protein Analysis. ACS Chem Biol. 2008;3: 373–382. doi:10.1021/cb800025k
204. Barlag B, Beutel O, Janning D, Czarniak F, Richter CP, Kommnick C, et al. Single molecule super-resolution imaging of proteins in living *Salmonella enterica* using self-labelling enzymes. Sci Rep. 2016;6: 31601. doi:10.1038/srep31601
205. Garranzo-Asensio M, Guzman-Aranguez A, Povés C, Fernández-Aceñero MJ, Torrente-Rodríguez RM, Ruiz-Valdepeñas Montiel V, et al. Toward Liquid Biopsy: Determination of the Humoral Immune Response in Cancer Patients Using HaloTag Fusion Protein-Modified Electrochemical Bioplatforms. Anal Chem. 2016;88: 12339–12345. doi:10.1021/acs.analchem.6b03526
206. Döbber J, Pohl M. HaloTag™: Evaluation of a covalent one-step immobilization for biocatalysis. J Biotechnol. 2017;241: 170–174. doi:10.1016/j.jbiotec.2016.12.004
207. Morin-Adeline V, Šlapeta J. The past, present and future of fluorescent protein tags in anaerobic protozoan parasites. Parasitology. 2016;143: 260–275. doi:10.1017/S0031182015001663
208. Zumthor JP, Cernikova L, Rout S, Kaech A, Faso C, Hehl AB. Static Clathrin Assemblies at the Peripheral Vacuole—Plasma Membrane Interface of the Parasitic Protozoan *Giardia lamblia*. Johnson PJ, editor. PLOS Pathog. 2016;12: e1005756. doi:10.1371/journal.ppat.1005756
209. Hagen KD, Hirakawa MP, House SA, Schwartz CL, Pham JK, Cipriano MJ, et al. Novel Structural Components of the Ventral Disc and Lateral Crest in *Giardia intestinalis*. Jones MK, editor. PLoS Negl Trop Dis. 2011;5: e1442. doi:10.1371/journal.pntd.0001442
210. Voleman L, Najdrová V, Ástvaldsson Á, Tůmová P, Einarsson E, Švindrych Z, et al. *Giardia intestinalis* mitosomes undergo synchronized fission but not fusion and are constitutively associated with the endoplasmic reticulum. BMC Biol. 2017;15: 27. doi:10.1186/s12915-017-0361-y
211. Hehl AB, Regos A, Schraner E, Schneider A. Bax Function in the Absence of Mitochondria in the Primitive Protozoan *Giardia lamblia*. Rutherford J, editor. PLoS One. 2007;2: e488. doi:10.1371/journal.pone.0000488
212. Sagolla MS, Dawson SC, Mancuso JJ, Cande WZ. Three-dimensional analysis of mitosis and cytokinesis in the binucleate parasite *Giardia intestinalis*. J Cell Sci. 2006;119: 4889–4900. doi:10.1242/jcs.03276
213. Striepen B, Crawford MJ, Shaw MK, Tilney LG, Seeber F, Roos DS. The Plastid of *Toxoplasma gondii* Is Divided by Association with the Centrosomes. J Cell Biol. 2000;151: 1423–1434. doi:10.1083/jcb.151.7.1423
214. Nishida K, Takahara M, Miyagishima S -y., Kuroiwa H, Matsuzaki M, Kuroiwa T. Dynamic recruitment of dynamin for final mitochondrial severance in a primitive red alga. Proc Natl

Acad Sci. 2003;100: 2146–2151. doi:10.1073/pnas.0436886100
215. Pucadyil TJ, Schmid SL. Real-Time Visualization of Dynamin-Catalyzed Membrane Fission and Vesicle Release. Cell. 2008;135: 1263–1275. doi:10.1016/j.cell.2008.11.020
216. Vance JE. MAM (mitochondria-associated membranes) in mammalian cells: Lipids and beyond. Biochim Biophys Acta - Mol Cell Biol Lipids. 2014;1841: 595–609. doi:10.1016/j.bbalip.2013.11.014
217. Yichoy M, Duarte TT, De Chatterjee A, Mendez TL, Aguilera KY, Roy D, et al. Lipid metabolism in *Giardia*: a post-genomic perspective. Parasitology. 2011;138: 267–278. doi:10.1017/S0031182010001277
218. Howarth M, Ting AY. Imaging proteins in live mammalian cells with biotin ligase and monovalent streptavidin. Nat Protoc. 2008;3: 534–545. doi:10.1038/nprot.2008.20
219. Cipollone R, Ascenzi P, Visca P. Common themes and variations in the rhodanese superfamily. IUBMB Life. 2007;59: 51–59. doi:10.1080/15216540701206859
220. Ohno K, Takahashi Y, Hirose F, Inoue YH, Taguchi O, Nishida Y, et al. Characterization of a *Drosophila* homologue of the human myelodysplasia/myeloid leukemia factor (MLF). Gene. 2000;260: 133–143. doi:10.1016/S0378-1119(00)00447-9

OPEN ACCESS Freely available online

PLoS one

Live Imaging of Mitosomes and Hydrogenosomes by HaloTag Technology

Eva Martincová[1☯], Luboš Voleman[1☯], Vladimíra Najdrová[1], Maximiliano De Napoli[2], Shiri Eshar[3], Melisa Gualdron[4], Christine S. Hopp[5], David E. Sanin[6], Dumizulu L. Tembo[7], Daria Van Tyne[8], Dawn Walker[9], Michaela Marcinčiková[1], Jan Tachezy[1], Pavel Doležal[1]*

1 Department of Parasitology, Faculty of Science, Charles University, Prague, Czech Republic, **2** Laboratorio de Parasitología Molecular, IIB-INTECH, CONICET-UNSAM, Chascomús, Provincia de Buenos Aires, Argentina, **3** Department of Microbiology and Molecular Genetics, The Kuvin Center for the Study of Infectious and Tropical Diseases, IMRIC, The Hebrew University-Hadassah Medical School, Jerusalem, Israel, **4** Christian De Duve Institute of Cellular Pathology, Brussels, Belgium, **5** Malaria Centre, London School of Hygiene & Tropical Medicine, London, United Kingdom, **6** Department of Biology, University of York, York, United Kingdom, **7** Malawi-Liverpool Wellcome Trust Clinical Research Programme, Chichiri, Blantyre, Malawi, **8** Department of Immunology and Infectious Diseases, Harvard School of Public Health, Boston, Massachusetts, United States of America, **9** Integrated Biomedical Sciences Center for Microbial Interface Biology Department of Internal Medicine, Columbus, Ohio, United States of America

Abstract

Hydrogenosomes and mitosomes represent remarkable mitochondrial adaptations in the anaerobic parasitic protists such as *Trichomonas vaginalis* and *Giardia intestinalis*, respectively. In order to provide a tool to study these organelles in the live cells, the HaloTag was fused to *G. intestinalis* IscU and *T. vaginalis* frataxin and expressed in the mitosomes and hydrogenosomes, respectively. The incubation of the parasites with the fluorescent Halo-ligand resulted in highly specific organellar labeling, allowing live imaging of the organelles. With the array of available ligands the HaloTag technology offers a new tool to study the dynamics of mitochondria-related compartments as well as other cellular components in these intriguing unicellular eukaryotes.

Citation: Martincová E, Voleman L, Najdrová V, De Napoli M, Eshar S, et al. (2012) Live Imaging of Mitosomes and Hydrogenosomes by HaloTag Technology. PLoS ONE 7(4): e36314. doi:10.1371/journal.pone.0036314

Editor: Ross Frederick Waller, University of Melbourne, Australia

Received January 21, 2012; **Accepted** April 2, 2012; **Published** April 27, 2012

Funding: Funding was provided by grants from the Czech Science Agency P305/10/0651 and LC07032 and from the Ministry of Education of the Czech Republic MSM 0021620858 and from the funders of the Biology of Parasitism course in Woods Hole (Burroughs Wellcome Fund, Howard Hughes Medical Institute and Wellcome Trust). The funders had no role in study design, data collection and analysis, decision to publish, or preparation of the manuscript.

Competing Interests: The authors have declared that no competing interests exist.

* E-mail: paveldolezal@yahoo.com

☯ These authors contributed equally to this work.

Introduction

In recent years studies of anaerobic protists such as *Giardia intestinalis* and *Trichomonas vaginalis* have revealed a number of exciting aspects of their cell biology, including cytoskeleton structures, vesicular transport and organelle biogenesis [1–5]. Besides unique cellular structures [6–8], many of the common eukaryotic processes have been stripped to their essentials in these protists e.g. [9,10]. The combination of their parasitic lifestyle, anaerobic metabolism and their evolutionary position [11] makes them attractive objects to study.

One of the features typical to anaerobic protists is the absence of 'classical' mitochondria, herein represented by organelles called mitosomes in *G. intestinalis* and hydrogenosomes in *T. vaginalis* [12]. Mitosomes, the simplest mitochondria-related compartments, seem to have lost all but the single pathway of iron-sulfur cluster assembly [4]. Compared to mitosomes, hydrogenosomes are more elaborate organelles, possessing substrate level ATP synthesis as well as iron and amino acid metabolism [13,14]. Moreover, recent proteomic studies of hydrogenosomes suggest that many more pathways are yet to be described [10,15].

Characterization of cellular organelles and their dynamics strongly relies on the concerted action of reverse genetics and live cell imaging. While particular advancements have been achieved in the former (e.g. gene silencing and protein overexpression) [16–20], only limited technical innovations have been introduced into the latter [21,22].

GFP and its derivatives are the first choice of reporters for live imaging in aerobic eukaryotes. They offer great protein stability as well as a broad range of spectral variants that enable multichannel studies. However the major drawback for their widespread use in anaerobic protists is the formation of the GFP fluorophore [22,23]: upon translation and protein folding the fluorophore is formed from the tripeptide Ser 65-Tyr 66-Gly 67 by an intramolecular cyclization, which requires the presence of molecular oxygen [24,25]. This reaction does not require additional proteins and occurs spontaneously in all eukaryotic compartments, except within anaerobic cells, which employ oxygen scavenging pathways in order to limit its toxic effects [26,27]. Cells can be temporarily oxygenated and observed under the microscope [7,28] . While this approach has proven to be efficient for large cellular structures such as the cytoskeleton [21,29], the organelles like mitosomes and hydrogenosomes exhibit only very weak labeling. Additionally, the double membrane surrounding the organelles may have limited capacity to import GFP.

Alternative approaches for live cell imaging exploit the use of chemical fluorescent tags, which form covalent or noncovalent bonds with the reporter protein or peptide [30]. Of these, SNAP and CLIP tags are commonly used for both extra- and intracellular labeling [31,32]. The SNAP tag was successfully used to track the distribution of *G. intestinalis* RabA homologue in the live parasite [22]. However, the use of the tag has been limited to this single study so far.

In this work, we decided to test a newly developed tag termed HaloTag, which utilizes a mutant form of haloalkane dehalogenase as a reporter protein. While the original enzyme hydrolyzes alkylhalides into a free halide and a primary alcohol, the H289Q mutant form of the protein (HaloTag) leaves free halide but remains covalently bound to the alkyl chain [33]. Thus, when a ligand with the alkylhalide chain is exposed to the native HaloTag, it is specifically bound by a covalent bond. The lack of dehalogenase activity among eukaryotes guarantees very low unspecific background labeling.

Here, we report the successful introduction of the HaloTag into vectors for stable expression in *G. intestinalis* and *T. vaginalis*. Moreover, using a TMR-halo ligand we were able to show live images of mitochondria-related compartments in these two anaerobic protists for the first time.

Materials and Methods

Cell strains

The *G. intestinalis* strain WB (ATCC 30957) was grown in TYI-S-33 medium supplemented with 10% heat-inactivated bovine serum, 0.1% bovine bile, and antibiotics. The *T. vaginalis* strain T1 was grown in TYM pH 6,2 medium supplemented with 10% heat inactivated horse serum. Both organisms were cultured at 37°C.

Preparation of cell fractions

G. intestinalis trophozoites were harvested in ice-cold PBS, washed once in ST buffer (250 mM sucrose, 0.5 mM KCl, 10 mM Tris [pH 7.2]) and suspended in ST buffer with protease inhibitors 50 μg/ml *N*-a-tosyl-L-lysine chloromethyl ketone and 10 μg/ml of leupeptin. Cells were lysed on ice using sonication, during which the cell integrity was checked under the microscope. The lysate was centrifuged twice at 2450× g for 10 minutes to remove unbroken cells, nuclei and residual cytoskeleton. Supernatant was transferred to a new tube and the centrifugation step repeated twice. The resulting supernatant was spun down at 180 000× g for 30 minutes. Final supernatant and pellet contained the cytosolic and high-speed pellet fraction, respectively.

T. vaginalis cells were harvested, washed once in ST buffer and suspended in ST buffer containing protease inhibitors (see above). Cells were sonicated on ice and the lysate was twice centrifuged at 2450× g (see above). Supernatant was spun down at 180 000× g for 30 minutes. The final supernatant corresponded to the cytosolic fraction. The pellet was resuspended in 1 ml of ST buffer, transferred to a new microcentrifuge tube and spun down at 30 000× g for 10 minutes. The Resulting pellet contained a white layer of lysosomes resting on top of a brown pellet of hydrogenosomes. Lysosomes were carefully removed using a pipette and this step was repeated once more. The final pellet corresponded to the hydrogenosomal fraction.

Cloning and stable cell transformation

***G. intestinalis*.** First, pTG vector (gift from Francis D. Gillin, [34]) was modified to contain NdeI PstI sites. The polylinker containing EcoRV, NdeI, XhoI, PstI, NsiI, MluI and ApaI sites was introduced into the vector using 5′-CATGGATATCCATATGCTCGAGCTGCAGATGCATACGCGTATGGTGAGCAAGGGCGAGGAG-3′ and 5′-GATCGGGCCCTCACTTGTACAGCTCGTCCAT-3′ primers. The PCR product was digested by EcoRV and ApaI and ligated into EcoRV/ApaI linearized pTG vector. The 300 bp of 5′UTR of *G. intestinalis* ornithine carbamoyl transferase (OCT) DNA sequence was amplified using 5′-CATGGATATCGAATTCGATGCTTCG-3′ and 5′-CATGCATATGTTTAATTTTCAGCCTCTACTG-3′ primers, digested by EcoRV and NdeI primers and ligated into modified pTG vector. The HaloTag DNA sequence was amplified from pHT2 vector (Promega) using 5′-ATGCTGCAGATGGGATCCGAAATCGGTACA-3′and 5′-CATGGGGCCCTTAGCCGGCCAGCCCGGGGAG-3′ oligonucleotides. The resulting PCR product was digested by PstI and ApaI and ligated into modified pTG vector. *G. intestinalis* IscU was amplified from genomic DNA using 5′-CTAGCATATGATGACTTCTGATGCCGCAGAT-3′ and 5′-GACTATGCATAGAAGACTTTGATACCTGTAT-3′ oligonucleotides. The product was digested by NdeI and NsiI and ligated into modified pTG vector containing HaloTag coding sequence.

***T. vaginalis*.** For expression in *T. vaginalis*, the HaloTag DNA sequence was amplified from pHT2 vector using 5′-CATGAGATCTATGGGATCCGAAATCGGTACA-3′ and 5′-GCTACTCGAGTTAAGCGTAATCTGGAACATCGTATGGGTAGCCGGCCAGCCCGGGGAGCCA-3′. The C-terminal hemagglutinin (HA)-tag was introduced into the construct as a part of the reverse primer. The PCR product was digested by BglII and XhoI and ligated into BamHI/XhoI linearized TagVag2 vector containing a gene encoding hydrogenosomal frataxin. Both organism were electroporated using modified protocols published in [35,36]. Briefly, three hundred micro liters of *T. vaginalis* and *G. intestinalis* at approximate concentration $2{,}5\times10^8$ cells/ml and $3{,}3\times10^8$ cells/ml, respectively, were electroporated with 50 ug of the plasmid using a Biorad Gene Pulser under the time constant protocol (Tc = 175 ms, U = 350 V). Transfectants were maintained under pressure of selective antibiotics (57 ug/ml of puromycin for *G. intestinalis* and 200 ug/ml for *T. vaginalis*).

Halo-labeling and immunofluorescence microscopy

Cell were incubated for 30 minutes in regular growth media supplemented with HaloTag TMR Ligand (1: 500 dilution) at 37°C. After the incubation the cells were pelleted at 1500× g and washed twice with fresh media. Cells were then incubated for 60 minutes at 37°C, pelleted and resuspended in fresh media or PBS. For immunofluorescence, the cells were incubated on slides for 15 minutes, fixed in −20°C methanol for 5 minutes and transferred to −20°C acetone for 5 minutes. Blocking and immunolabeling was performed in 0,25% Gelatin, 0,25% BSA, 0,05%.

Tween20 in PBS 7,4 using specific rabbit polyclonal antibodies raised against *T. vaginalis* malic enzyme and *G.intestinalis* Tom40 . Primary antibodies were decorated by Alexa Fluor 488 anti-rabbit antibody. Slides were mounted in hard set Vectashield containing DAPI. For live cell imaging, labeled *G. intestinalis* cells were allowed to attach to the surface of 96 well optical bottom plates and imaged directly. Labeled *T. vaginalis* cells were mounted in low temperature-melting 2% agarose dissolved in PBS and analyzed by microscopy. Cells were observed using an OLYMPUS Cell-R, IX81 microscope system and images processed by Fiji (http://fiji.sc/wiki/index.php/Fiji). During all steps cells were protected from light.

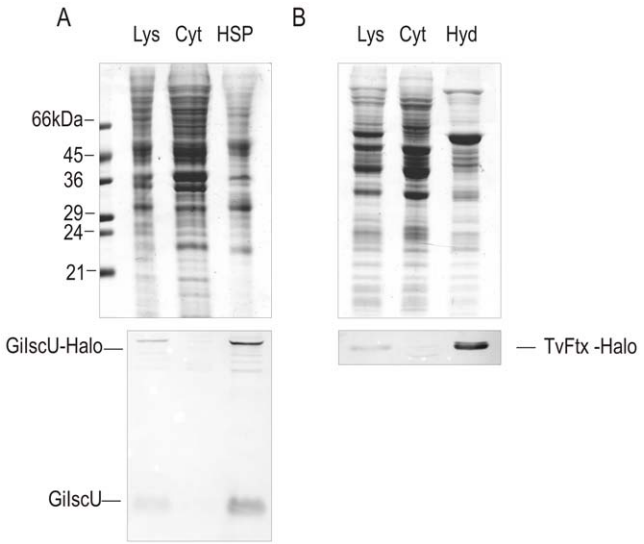

Figure 1. Expression of HaloTagged proteins in *G. intestinalis* and *T. vaginalis*. Western blot analyses of cellular fractions of *G. intestinalis* and *T. vaginalis* transformants expressing GilscU-Halo and TvFtx-Halo fusions, respectively. A) GilscU-Halo was detected by specific anti-IscU polyclonal antibodies in cell lysate and high-speed pellet (HSP). Two bands in these fractions represent the nuclear encoded (GilscU) and episomally encoded HaloTag fusion (GilscU-Halo). B) TvFtx-Halo product was detected by anti-HA monoclonal antibodies in *T. vaginalis* cellular fractions. The fusion protein was found exclusively in cell lysate and in hydrogenosomes. The upper panels demonstrate the protein profile on the coomassie stained SDS-PAGE gel. Lys-lysate, Cyt-cytosol, HSP-high-speed pellet, Hyd-hydrogenosomes.
doi:10.1371/journal.pone.0036314.g001

Results and Discussion

Mitosomes and hydrogenosomes can be found in anaerobic protists from different eukaryotic lineages. Recent phylogenetic and functional data have shown that these double membrane bound organelles represent long evolved mitochondrial forms adjusted to anaerobic environments [12]. While devoid of many typical mitochondrial functions, they contain unique metabolic adaptations as well as simplified versions of intricate molecular processes occurring in mitochondria [37–39]. To date only limited information is available on their biogenesis, inheritance and related membrane dynamics [40]. In order to follow these processes in living cells we have introduced HaloTag technology into both *G. intestinalis* and *T. vaginalis*.

The coding sequence of HaloTag was introduced into *G. intestinalis* and *T. vaginalis* episomal vectors pTG and TagVag2, respectively [34,39] . Transcription from these vectors is driven by promotor regions in 5′ UTRs of highly expressed ornithine carbamoyl transferase and succinyl-CoA thiokinase [34,41], respectively, which ensure strong constitutive protein expression in both organisms. For specific labeling of mitochondria-related organelles in these anaerobic protists, the HaloTag was inserted as a C-terminal fusion to the mitosomal and hydrogenosomal marker proteins GiIscU and TvFtx, respectively [13,42].

Expression of proteins fused to the HaloTag was determined on western blots of cellular fractions (Figure 1). *G. intestinalis* IscU-HaloTag fusion was detected by specific polyclonal antibody raised against mitosomal IscU. Two dominant protein bands of approximately 15 kDa and 50 kDa were detected, which is consistent with the expected molecular weights (the size of HaloTag is 33 kDa) (Figure 1A). While the lower band corresponded to the mature form of nuclear encoded IscU, the

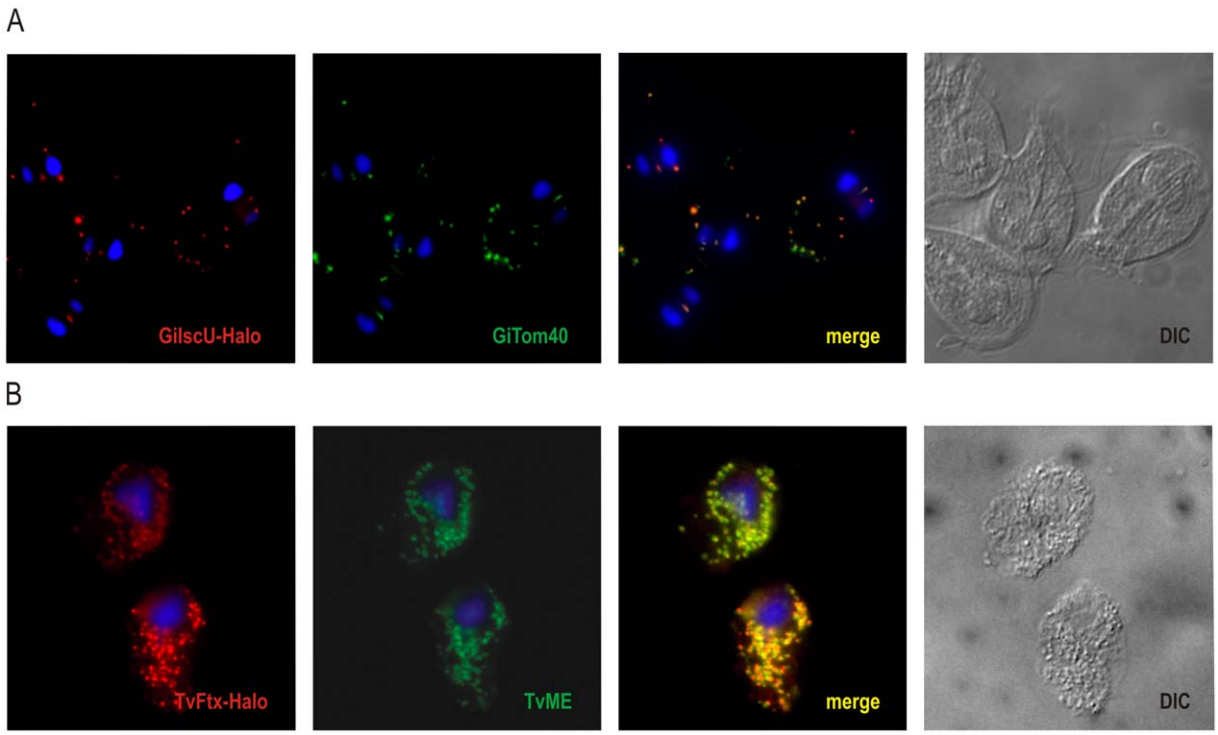

Figure 2. Mitosomal and hydrogenosomal localization of HaloTagged proteins. Immunofluorescence analyses of *G. intestinalis* and *T. vaginalis* transformants expressing GilscU-Halo and TvFtx-Halo fusion, respectively. Cells were incubated with TMR-Halo ligand (red), washed and fixed for immunofluorescence analysis. A) TMR-Halo labeled *G. intestinalis* cells were fixed and labeled by anti-Tom40 specific polyclonal antibodies (green). B) TMR-Halo labeled *T. vaginalis* cells were fixed and decorated by anti-malic enzyme specific polyclonal antibodies (green). Nuclei were stained with DAPI (blue).
doi:10.1371/journal.pone.0036314.g002

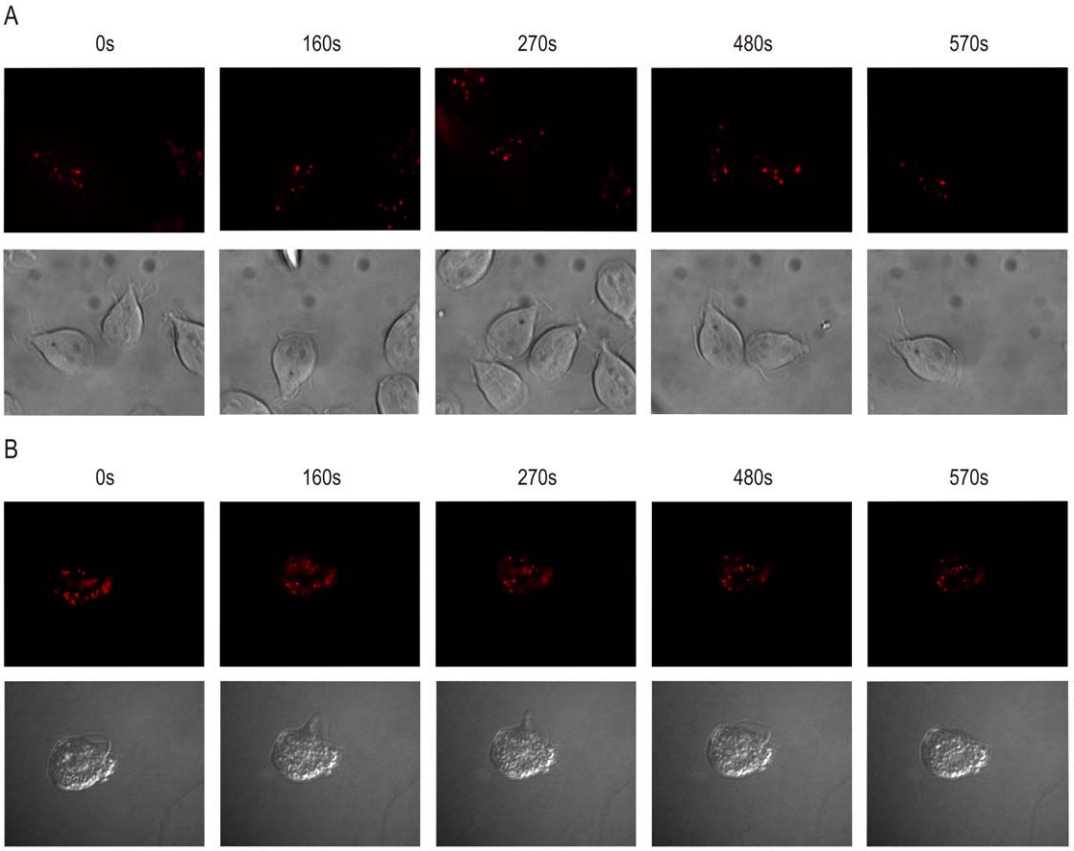

Figure 3. Live imaging of mitosomes and hydrogenosomes. Halo-TMR labeled organelles were followed in living cells. A) Labeled *G. intestinalis* cells were allowed to attach to the bottom of the well and directly observed while B) the labeled *T. vaginalis* cells were mounted in 2% agarose and then submitted to microscopy. Five different snapshots in time are shown. The original movies are part of the supplementary data.
doi:10.1371/journal.pone.0036314.g003

upper band represented IscU-HaloTag fusion. The specific signal was present in the lysate and high speed pellet fraction, which is in addition to other vesicular structures enriched for mitosomes. Additional weak protein bands were detected, which likely corresponded to partially proteolytically degraded protein forms.

In order to detect HaloTagged hydrogenosomal frataxin in *T. vaginalis*, an additional single hemagglutinin (HA)-tag was introduced to the C-terminus of the HaloTag sequence. Using anti-HA antibodies the protein band of about 47 kDa, corresponding to the expected protein fusion size, was detected in the cell lysate and hydrogenosomal fractions (Figure 1B).

In both organisms, the HaloTag fusion proteins were expressed at a moderate level with no growth defect obvious in daily culturing, indicating that the tag does not interfere with the cellular metabolism of the anaerobic eukaryotes, similar to what has been shown in mammalian cells [33].

In order to confirm that the fusion protein is targeted to mitochondria-related compartments of *G. intestinalis* and *T. vaginalis*, cells were labeled with HaloTag TMR ligand, fixed and immunolabeled with specific antibodies raised against organellar marker proteins. In *G. intestinalis*, mitosomes were labeled by Tom40-specific antibody [37]. Tom40 is a conserved protein of the outer mitochondrial/mitosomal membrane and its detection revealed typical mitosomal distribution within *G. intestinalis* cells: the central array of mitosomes between the two nuclei as well as the peripheral ones scattered throughout the cytoplasm. The HaloTag signal from GiIscU was found to be in perfect agreement with Tom40, revealing highly specific mitosomal compartment labeling in *G. intestinalis* (Figure 2A).

In contrast to mitosomes, which are scarce, *T. vaginalis* hydrogenosomes are abundant organelles distributed along the major cytoskeletal structures such as the costa and axostyle. Malic enzyme is the most dominant hydrogenosomal protein [43] and its detection in fixed TMR-Halo ligand-labeled cells revealed typical hydrogenosomal distribution. The same pattern was obtained with TMR labeled HaloTag, as indicated in the merged image (Figure 2B).

These experiments showed that the HaloTag TMR ligand is a membrane-permeable ligand in both organisms, capable of diffusing across the cell membrane as well as the two membranes surrounding the mitosomes and hydrogenosomes. Although some background labeling was detected using HaloTag in mammalian cells [31], no such signal was found in two anaerobic organisms used in this study.

Following the co-localization experiments, labeled cells were observed live for various time periods (Figure 3). While attached *G. intestinalis* trophozoites could be observed directly in optical bottom plates filled with medium (Figure 3A, Supplementary Movie S1 and S2), *T. vaginalis* were mounted in 2% low melting agarose in order to slow down the rapidly moving cells (Figure 3B, Supplementary Movie S3 and S4). In both parasites, the specific fluorescence signal could be followed visually for more than 60 minutes. Notably, for prolonged cell observation an anaerobic chamber would be necessary.

In summary, these experiments demonstrate the applicability of HaloTag in labeling the mitochondria-related organelles of *G. intestinalis* and *T. vaginalis*. These tiny double membrane bound organelles have been some of the most challenging cellular structures for live imaging in anaerobic eukaryotes, and to our knowledge this work is the first report of its kind.

HaloTag technology is relatively new to the cell biology. It exhibits excellent specificity and fast chemistry but as true for other large protein tags such as the fluorescent proteins or SNAP-tag, its major drawback is the size, which may interfere with the function of the carrier protein [30]. When possible the imaging studies rely on GFP and other recently characterized fluorescent proteins e.g. [44,45]. In these cases, the chemical tags such as HaloTag, SNAP-tag or tetracystein helix motif [46] offer additional customizable labeling, especially suitable for pulse-chase [47] or FRET experiments. In the anaerobic unicellular organisms or the anaerobic tissues of some invertebrates the GFP maturation requires an extra oxygenation step, which may perturb narrow physiological conditions. In these cases, the chemical tags may be the first choice protein-labeling approach. Moreover, the speed and the specificity of the formation of the covalent bond between the HaloTag and the ligand provides new means of protein purification from not easily tractable organisms [48].

Mitochondria are known to be very dynamic organelles undergoing constant antagonist fusion and fission reactions [49]. Several GTPases drive these opposing reactions in a highly regulated manner and the defects in the fusion or fission result in disintegration or collapse of the organelles, respectively. So far no information has been obtained on the machinery controlling the dynamics of mitosomes and hydrogenosomes. Given that neither the components of the mitochondrial division cycle nor the homologues of bacterial division proteins were found in the genomes of mitosome- and hydrogenosome-bearing eukaryotes, the HaloTag has the potential to be a means of identifying the different components driving these processes in these protists.

This opens up more fundamental questions regarding the evolution of the mitochondrial division apparatus, the transition from a FtsZ- to a dynamin-based system as well as the origin of mitochondrial fusion. We believe that the introduction of HaloTag technology to the cell biology of anaerobic protists will be of assistance in the process of answering these questions.

Supporting Information

Movie S1 *Giardia intestinalis* expressing mitosomal IscU-HaloTag fusion was labeled with TMR-Halo ligand. Images were taken every at 10 second intervals, movie is displayed at 2 frames per second.
(AVI)

Movie S2 Nomarski differential contrast of the same visual field as in Movie S1.
(AVI)

Movie S3 *Trichomonas vaginalis* expressing hydrogenosomal frataxin-HaloTag fusion was labeled with TMR-Halo ligand. Images were taken every at 10 second intervals, movie is displayed at 2 frames per second.
(AVI)

Movie S4 Nomarski differential contrast of the same visual field as in Movie S3.
(AVI)

Acknowledgments

We would like to thank the organizers (Boris Striepen and Dan Godlberg) of the Biology of Parasitism course in Woods Hole.

Author Contributions

Conceived and designed the experiments: JT PD. Performed the experiments: EM LM VN MN SE MG CH DS DT DT DW MM. Analyzed the data: EM LV. Wrote the paper: EM LV PD.

References

1. Hehl AB, Marti M (2004) Secretory protein trafficking in Giardia intestinalis. Mol Microbiol 53: 19–28.
2. Paredez AR, Assaf ZJ, Sept D, Timofejeva L, Dawson SC, et al. (2011) An actin cytoskeleton with evolutionarily conserved functions in the absence of canonical actin-binding proteins. Proc Natl Acad Sci U S A 108: 6151–6156.
3. Poxleitner MK, Carpenter ML, Mancuso JJ, Wang C-JR, Dawson SC, et al. (2008) Evidence for karyogamy and exchange of genetic material in the binucleate intestinal parasite Giardia intestinalis. Science 319: 1530–1533.
4. Tovar J, León-Avila G, Sánchez LB, Sutak R, Tachezy J, et al. (2003) Mitochondrial remnant organelles of Giardia function in iron-sulphur protein maturation. Nature 426: 172–176.
5. Ankarklev J, Jerlström-Hultqvist J, Ringqvist E, Troell K, Svärd SG (2010) Behind the smile: cell biology and disease mechanisms of Giardia species. Nat Rev Microbiol 8: 413–422.
6. Elmendorf HG, Dawson SC, McCaffery JM (2003) The cytoskeleton of Giardia lamblia. Int J Parasitol 33: 3–28.
7. Konrad C, Spycher C, Hehl AB (2010) Selective condensation drives partitioning and sequential secretion of cyst wall proteins in differentiating Giardia lamblia. PLoS Pathog 6: e1000835.
8. Prucca CG, Slavin I, Quiroga R, Elías EV, Rivero FD, et al. (2008) Antigenic variation in Giardia lamblia is regulated by RNA interference. Nature 456: 750–754.
9. Jedelský PL, Doležal P, Rada P, Pyrih J, Smíd O, et al. (2011) The minimal proteome in the reduced mitochondrion of the parasitic protist Giardia intestinalis. PLoS One 6: e17285.
10. Rada P, Doležal P, Jedelský PL, Bursac D, Perry AJ, et al. (2011) The Core Components of Organelle Biogenesis and Membrane Transport in the Hydrogenosomes of Trichomonas vaginalis. PLoS ONE 6: e24428.
11. Simpson AGB (2003) Cytoskeletal organization, phylogenetic affinities and systematics in the contentious taxon Excavata (Eukaryota). Int J Syst Evol Microbiol 53: 1759–1777.
12. Embley TM, Martin W (2006) Eukaryotic evolution, changes and challenges. Nature 440: 623–630.
13. Dolezal P, Dancis A, Lesuisse E, Sutak R, Hrdý I, et al. (2007) Frataxin, a conserved mitochondrial protein, in the hydrogenosome of Trichomonas vaginalis. Eukaryot Cell 6: 1431–1438.
14. Mukherjee M, Brown MT, McArthur AG, Johnson PJ (2006) Proteins of the glycine decarboxylase complex in the hydrogenosome of Trichomonas vaginalis. Eukaryot Cell 5: 2062–2071.
15. Schneider RE, Brown MT, Shiflett AM, Dyall SD, Hayes RD, et al. (2011) The Trichomonas vaginalis hydrogenosome proteome is highly reduced relative to mitochondria, yet complex compared with mitosomes. Int J Parasitol 41: 1421–1434.
16. Carpenter ML, Cande WZ (2009) Using morpholinos for gene knockdown in Giardia intestinalis. Eukaryot Cell 8: 916–919.
17. Davis-Hayman SR, Nash TE (2002) Genetic manipulation of Giardia lamblia. Mol Biochem Parasitol 122: 1–7.
18. Gourguechon S, Cande WZ (2011) Rapid tagging and integration of genes in Giardia intestinalis. Eukaryot Cell 10: 142–145.
19. Saraiya AA, Wang CC (2008) snoRNA, a novel precursor of microRNA in Giardia lamblia. PLoS Pathog 4: e1000224.
20. Yu DC, Wang AL, Wu CH, Wang CC (1995) Virus-mediated expression of firefly luciferase in the parasitic protozoan Giardia lamblia. Mol Cell Biol 15: 4867–4872.
21. Dawson SC, House SA (2010) Imaging and analysis of the microtubule cytoskeleton in giardia. Methods Cell Biol 97: 307–339.
22. Regoes A, Hehl A (2005) SNAP-tag™ mediated live cell labeling as an alternative to GFP in anaerobic organisms. Biotechniques 39: 809–812.
23. Elias EV, Quiroga R, Gottig N, Nakanishi H, Nash TE, et al. (2008) Characterization of SNAREs determines the absence of a typical Golgi apparatus in the ancient eukaryote Giardia lamblia. J Biol Chem 283: 35996–36010.
24. Chudakov DM, Matz MV, Lukyanov S, Lukyanov KA (2010) Fluorescent proteins and their applications in imaging living cells and tissues. Physiol Rev 90: 1103–1163.
25. Tsien RY (1998) The green fluorescent protein. Annu Rev Biochem 67: 509–544.

26. Lloyd D, Harris JC, Maroulis S, Biagini GA, Wadley RB, et al. (2000) The microaerophilic flagellate Giardia intestinalis: oxygen and its reaction products collapse membrane potential and cause cytotoxicity. Microbiology 146 Pt 12: 3109–3118.
27. Smutná T, Gonçalves VL, Saraiva LM, Tachezy J, Teixeira M, et al. (2009) Flavodiiron protein from Trichomonas vaginalis hydrogenosomes: the terminal oxygen reductase. Eukaryot Cell 8: 47–55.
28. Stefanic S, Morf L, Kulangara C, Regös A, Sonda S, et al. (2009) Neogenesis and maturation of transient Golgi-like cisternae in a simple eukaryote. J Cell Sci 122: 2846–2856.
29. House S a, Richter DJ, Pham JK, Dawson SC (2011) Giardia flagellar motility is not directly required to maintain attachment to surfaces. PLoS Pathog 7: e1002167.
30. Wombacher R, Cornish VW (2011) Chemical tags: Applications in live cell fluorescence imaging. J Biophotonics 4: 391–402.
31. Gautier A, Juillerat A, Heinis C, Corrêa IR, Kindermann M, et al. (2008) An engineered protein tag for multiprotein labeling in living cells. Chem Biol 15: 128–136.
32. Keppler A, Pick H, Arrivoli C, Vogel H, Johnsson K (2004) Labeling of fusion proteins with synthetic fluorophores in live cells. Proc Natl Acad Sci U S A 101: 9955–9959.
33. Los GV, Encell LP, McDougall MG, Hartzell DD, Karassina N, et al. (2008) HaloTag: a novel protein labeling technology for cell imaging and protein analysis. ACS Chem Biol 3: 373–382.
34. Lauwaet T, Davids BJ, Torres-Escobar A, Birkeland SR, Cipriano MJ, et al. (2007) Protein phosphatase 2A plays a crucial role in Giardia lamblia differentiation. Mol Biochem Parasitol 152: 80–89.
35. Yu DC, Wang AL, Wang CC (1996) Stable coexpression of a drug-resistance gene and a heterologous gene in an ancient parasitic protozoan Giardia lamblia. Mol Biochem Parasitol 83: 81–91.
36. Delgadillo MG, Liston DR, Niazi K, Johnson PJ (1997) Transient and selectable transformation of the parasitic protist Trichomonas vaginalis. Proc Natl Acad Sci U S A 94: 4716–4720.
37. Dagley MJ, Dolezal P, Likic VA, Smid O, Purcell AW, et al. (2009) The protein import channel in the outer mitosomal membrane of Giardia intestinalis. Mol Biol Evol 26: 1941–1947.
38. Dolezal P, Dagley MJ, Kono M, Wolynec P, Likić VA, et al. (2010) The essentials of protein import in the degenerate mitochondrion of Entamoeba histolytica. PLoS Pathog 6: e1000812.
39. Hrdy I, Hirt RP, Dolezal P, Bardonová L, Foster PG, et al. (2004) Trichomonas hydrogenosomes contain the NADH dehydrogenase module of mitochondrial complex I. Nature 432: 618–622.
40. Shiflett AM, Johnson PJ (2010) Mitochondrion-related organelles in eukaryotic protists. Annu Rev Microbiol 64: 409–429.
41. Smith A, Johnson P (n.d.) Gene expression in the unicellular eukaryote Trichomonas vaginalis. Res Microbiol 162: 646–654.
42. Dolezal P, Smíd O, Rada P, Zubácová Z, Bursać D, et al. (2005) Giardia mitosomes and trichomonad hydrogenosomes share a common mode of protein targeting. Proc Natl Acad Sci U S A 102: 10924–10929.
43. Drmota T, Proost P, Van Ranst M, Weyda F, Kulda J, et al. (1996) Iron-ascorbate cleavable malic enzyme from hydrogenosomes of Trichomonas vaginalis: purification and characterization. Mol Biochem Parasitol 83: 221–234.
44. Gurskaya NG, Verkhusha VV, Shcheglov AS, Staroverov DB, Chepurnykh TV, et al. (2006) Engineering of a monomeric green-to-red photoactivatable fluorescent protein induced by blue light. Nat Biotechnol 24: 461–465.
45. Shaner NC, Lin MZ, McKeown MR, Steinbach PA, Hazelwood KL, et al. (2008) Improving the photostability of bright monomeric orange and red fluorescent proteins. Nat Methods 5: 545–551.
46. Griffin BA, Adams SR, Tsien RY (1998) Specific covalent labeling of recombinant protein molecules inside live cells. Science 281: 269–272.
47. Yamaguchi K, Inoue S, Ohara O, Nagase T (2009) Pulse-chase experiment for the analysis of protein stability in cultured mammalian cells by covalent fluorescent labeling of fusion proteins. Methods Mol Biol 577: 121–131.
48. Urh M, Hartzell D, Mendez J, Klaubert DH, Wood K (2008) Methods for detection of protein-protein and protein-DNA interactions using HaloTag. Methods Mol Biol 421: 191–209.
49. Westermann B (2010) Mitochondrial fusion and fission in cell life and death. Nat Rev Mol Cell Biol 11: 872–884.

MCB
Journals.ASM.org

Probing the Biology of *Giardia intestinalis* Mitosomes Using *In Vivo* Enzymatic Tagging

Eva Martincová,[a] Luboš Voleman,[a] Jan Pyrih,[a] Vojtěch Žárský,[a] Pavlína Vondráčková,[a] Martin Kolísko,[b] Jan Tachezy,[a] Pavel Doležal[a]

Department of Parasitology, Faculty of Science, Charles University in Prague, Prague, Czech Republic[a]; Centre for Microbial Diversity and Evolution, Department of Botany, University of British Columbia, Vancouver, BC, Canada[b]

Giardia intestinalis **parasites contain mitosomes, one of the simplest mitochondrion-related organelles. Strategies to identify the functions of mitosomes have been limited mainly to homology detection, which is not suitable for identifying species-specific proteins and their functions. An *in vivo* enzymatic tagging technique based on the *Escherichia coli* biotin ligase (BirA) has been introduced to *G. intestinalis*; this method allows for the compartment-specific biotinylation of a protein of interest. Known proteins involved in the mitosomal protein import were *in vivo* tagged, cross-linked, and used to copurify complexes from the outer and inner mitosomal membranes in a single step. New proteins were then identified by mass spectrometry. This approach enabled the identification of highly diverged mitosomal Tim44 (*Gi*Tim44), the first known component of the mitosomal inner membrane translocase (TIM). In addition, our subsequent bioinformatics searches returned novel diverged Tim44 paralogs, which mediate the translation and mitosomal insertion of mitochondrially encoded proteins in other eukaryotes. However, most of the identified proteins are specific to *G. intestinalis* and even absent from the related diplomonad parasite *Spironucleus salmonicida*, thus reflecting the unique character of the mitosomal metabolism. The *in vivo* enzymatic tagging also showed that proteins enter the mitosome posttranslationally in an unfolded state and without vesicular transport.**

Giardia intestinalis causes intestinal infection in diverse vertebrate species, including humans, where it causes the disease giardiasis (1). In addition to its medical and veterinary importance, *Giardia* is an interesting unicellular eukaryote (protist) from cell biology and evolutionary perspectives (2).

The binucleated *Giardia* trophozoite is equipped with eight flagella and an adhesive disc, which mediates attachment to its host's intestine. The interior of the cell is dominated by an endoplasmic reticulum (ER) network (3) and lysosome-like peripheral vacuoles that mediate the uptake and digestion of nutrients (4). There are also Golgi body-like encystation vesicles that distribute the cyst wall material to the cell surface during encystation of the parasite (5).

The mitosomes of *Giardia* are highly adapted forms of mitochondria and are approximately 100 nm in size. These organelles are surrounded by two membranes, but unlike mitochondria, they do not contain DNA. The mitosomal proteome is currently limited to 21 proteins, which primarily participate in iron-sulfur cluster biosynthesis and protein import and folding (6–8). The identification of mitosomal proteins has been accomplished mostly using bioinformatics techniques, such as phylogenetics (9, 10) and hidden Markov model (HMM)-based searches (6, 11), that detect homologous proteins. Thus, in contrast to hydrogenosomes and mitochondria, in which 20 to 50% of proteins have no assigned function (12–14), the vast majority of mitosomal proteins have known functions and orthologs in the mitochondria of other eukaryotes. Attempts to identify the mitosomal proteome using cell fractionation techniques have been largely stymied by the abundance of the ER and cytoskeletal structures in the cell (7). Analogous studies of the proteomes of encystation vesicles and peripheral vacuoles of *Giardia* using sophisticated organelle purification procedures have demonstrated the limits of direct organelle isolation approaches (15). As a result, several essential aspects of the mitosome, such as the nature of the translocase of the inner membrane (TIM) complex or the protein composition of the outer mitosomal membrane, remain unknown.

Here, we addressed the difficulty of the biochemical characterization of giardial mitosomes by employing an *in vivo* enzymatic tagging approach. The highly specific purification of biotinylated mitosomal proteins led to the identification of divergent *Gi*Tim44, the first component of the mitosomal TIM complex. In addition, over 10 novel mitosomal proteins from the mitosomal matrix and the outer mitosomal membrane were also identified, increasing the known mitosomal proteome by one-half. Most of these proteins reflect the unique and unpredictable character of giardial mitosome biology. Moreover, the compartment-specific protein tagging allowed us to identify the mode of mitosomal protein transport.

MATERIALS AND METHODS

Cell culture and fractionation. Trophozoites of *G. intestinalis* strain WB (ATCC 30957) were grown in TY-S-33 medium (16) supplemented with 10% heat-inactivated bovine serum (PAA Laboratories), 0.1% bovine bile, and antibiotics. Cells expressing the dihydrofolate reductase (DHFR)

Received 8 May 2015 **Returned for modification** 18 May 2015
Accepted 3 June 2015
Accepted manuscript posted online 8 June 2015
Citation Martincová E, Voleman L, Pyrih J, Žárský V, Vondráčková P, Kolísko M, Tachezy J, Doležal P. 2015. Probing the biology of *Giardia intestinalis* mitosomes using *in vivo* enzymatic tagging. Mol Cell Biol 35:2864–2874. doi:10.1128/MCB.00448-15.
Address correspondence to Pavel Doležal, pavel.dolezal@natur.cuni.cz.
Supplemental material for this article may be found at http://dx.doi.org/10.1128/MCB.00448-15.

doi:10.1128/MCB.00448-15

fusion protein were grown in medium supplemented with 100 μM pyrimethamine (PM).

Preparation of cell fractions. The cells were harvested by centrifugation at 1,000 × *g* at 4°C for 10 min in ice-cold phosphate-buffered saline (PBS), washed once in SM buffer (250 mM sucrose, 20 mM MOPS [morpholinepropanesulfonic acid], pH 7.4), and resuspended in SM buffer with protease inhibitors (cOmplete, EDTA-free; Roche). Cells were disrupted on ice by sonication with 1-s pulses and an amplitude of 40 for 1 min (Bioblock Scientific Vibra-Cell 72405). The lysate was then centrifuged at 2,750 × *g* for 10 min. The centrifugation step was repeated until the pellet containing unbroken cells, nuclei, and the cytoskeleton was no longer visible. The clear supernatant was centrifuged at 180,000 × *g* at 4°C for 30 min. The resulting high-speed supernatant represented the cytosolic fraction; the high-speed pellet (HSP) containing the mitosomes was resuspended in SM buffer containing protease inhibitors.

Fluorescence microscopy. *G. intestinalis* trophozoites were fixed and immunolabeled as previously described (17). Mitosomal *Gi*Tom40 was detected with a specific polyclonal antibody raised in rabbits (18), and the hemagglutinin epitope (HA tag) was recognized by a rat monoclonal antibody (Roche). The primary antibodies were detected by a donkey Alexa Fluor 594 (red)-conjugated anti-rabbit antibody and Alexa Fluor 594 (red)- or Alexa Fluor 488 (green)-conjugated anti-rat antibodies (Life Technologies), respectively. Alexa Fluor 488 (green)-conjugated streptavidin (Life Technologies) was used to detect biotinylation. Slides were mounted with Vectashield containing DAPI (4′,6-diamidino-2-phenylindole; Vector Laboratories). The slides were imaged with an Olympus Cell-R, IX81 microscope system, and the images were processed using ImageJ 1.41e software (NIH).

Cloning and transfection. The pTG vector was used for *Escherichia coli* biotin ligase (BirA) cloning and protein expression (17). The gene encoding BirA (WP_023308552) was amplified from pET21a-BirA (19). Table S1 in the supplemental material lists all the primers used in this study. To coexpress proteins with BirA, biotin acceptor peptide (BAP) was introduced into the pONDRA vector (6) using a reverse primer for *Gi*Pam18-BAP. This vector carrying the C-terminal BAP was used for the subsequent cloning of the other genes. All *Giardia* genes were amplified from genomic DNA. Mouse DHFR was amplified from pARL2-GDG (20) (kindly provided by Jude Przyborski, Philipps University Marburg). *G. intestinalis* transfection was performed as previously described (6). Briefly, 300 μl of *G. intestinalis* trophozoites (3.3×10^7 cells/ml) was electroporated with a Bio-Rad Gene Pulser using an exponential protocol (U = 350 V; C = 1,000 μF; R = 750 Ω). The transfected cells were grown in medium supplemented with antibiotics (57 μg/ml puromycin and 600 μg/ml G418).

Cross-linking, protein isolation, and mass spectrometry (MS). *G. intestinalis* cells were grown in standard medium supplemented with 50 μM biotin for 24 h prior to harvesting. The cells were harvested and fractionated as described above. The HSP (40 mg) was used for the cross-linking and protein isolation. The pellet was resuspended in PBS (pH 7.4) supplemented with protease inhibitors (Roche) at a final protein concentration of 1.5 mg/ml. Then, a 25 μM concentration of the cross-linker DSP (dithiobis [succinimidyl propionate]; Thermo Scientific) was added, followed by 1 h of incubation on ice. After the incubation, Tris (pH 8) was added at a final concentration of 50 mM, and the sample was incubated at room temperature for 15 min. The sample was centrifuged at 30,000 × *g* for 10 min at 4°C, and the resulting pellet was resuspended in boiling buffer (50 mM Tris, 1 mM EDTA, 1% SDS, pH 7.4) supplemented with protease inhibitors at a final protein concentration of 1.5 mg/ml. The sample was incubated at 80°C for 10 min and was centrifuged at 30,000 × *g* for 10 min at room temperature. The resulting supernatant was diluted 1:10 in incubation buffer (50 mM Tris, 150 mM NaCl, 5 mM EDTA, 1% Triton X-100, pH 7.4) supplemented with protease inhibitors. Then, 200 μl of streptavidin-coupled magnetic beads (Dynabeads MyOne Streptavidin C1; Invitrogen) was washed 3 times with incubation buffer, mixed with the sample, and incubated overnight at 4°C with gentle rotation. The beads were then subjected to the following washes: 3 times for 5 min each in incubation buffer supplemented with 0.1% SDS, once for 5 min in boiling buffer, once for 5 min in washing buffer (60 mM Tris, 2% SDS, 10% glycerol), and twice for 5 min each in incubation buffer supplemented with 0.1% SDS. Finally, proteins were eluted from the beads in SDS-PAGE sample buffer supplemented with 20 mM biotin for 5 min at 95°C.

The samples were analyzed by Western blotting using streptavidin-conjugated Alexa Fluor 488 and were visualized using a Molecular Imager FX imager (Bio-Rad). The eluate was resolved by SDS-PAGE and stained with Coomassie brilliant blue. The gel was cut, destained, trypsin digested, and analyzed on a mass spectrometer.

Mass spectrometry and MS/MS analyses. Spectra were acquired using a (4800 Plus MALDI-TOF/TOF) analyzer (Applied Biosystems/MDS Sciex) equipped with an Nd:YAG laser (355 nm) with a firing rate of 200 Hz. The tandem mass spectrometry (MS/MS) analyses were performed as previously described (21).

Protease protection assay. To determine whether proteins were embedded in the outer mitosomal membrane, 150 μg of the HSP fraction in SM buffer supplemented with protease inhibitors was incubated with 200 μg/ml trypsin for 10 min at 37°C. The control sample also contained 0.1% Triton X-100 to completely digest the proteins of the solubilized organelles. The samples were separated by SDS-PAGE and blotted onto a nitrocellulose membrane, and proteins were detected with antibodies.

To determine whether proteins were in the mitosomal matrix, 1 mg of the HSP fraction was resuspended in 400 μl of either hypotonic buffer (1 mM EDTA, 10 mM MOPS, pH 7.2), isotonic buffer (hypotonic buffer supplemented with 250 mM sucrose), or NaCl buffer (500 mM NaCl, 10 mM Tris, pH 7.4). Pellets were resuspended by gentle pipetting or by sonication with 1-s pulses and amplitude of 60 for 2 times 1 min (Bioblock Scientific Vibra Cell 72405). Subsequently, 100 μl of each sample was treated with a different concentration of proteinase K (PK) and incubated on ice for 20 min. The reaction was stopped by the addition of 2 μl of 1 mM phenylmethanesulfonyl fluoride (PMSF), and the mixture was incubated on ice for 10 min. For the protein precipitation, 20 μl of 100% trichloroacetic acid (TCA) was added, and the samples were incubated on ice for 30 min. The samples were then centrifuged at 30,000 × *g* at 4°C for 30 min. The resulting pellets were washed in acetone and centrifuged at 30,000 × *g* at 4°C for 30 min, air dried, and resuspended in SDS-PAGE sample buffer.

Electron microscopy. For transmission electron microscopy (TEM) studies, *G. intestinalis* cell pellets were fixed for 24 h in 2.5% glutaraldehyde in 0.1 M cacodylate buffer (pH 7.2) and were postfixed in 2% OsO_4 in the same buffer. The fixed samples were dehydrated by passage through an ascending ethanol and acetone series and were embedded in an Araldite-Poly/Bed 812 mixture. Thin sections were cut on a Reichert-Jung Ultracut E ultramicrotome and were stained using uranyl acetate and lead citrate. The sections were examined and photographed with a JEOL JEM-1011 electron microscope. Fine-structure measurements were performed with a Veleta camera and iTEM 5.1 software (Olympus Soft Imaging Solution GmbH).

Bioinformatic analyses. To identify the copurified proteins, their amino acid sequences were analyzed by BLASTP against the NCBI nr database using the following algorithms: HHpred at http://toolkit.tuebingen.mpg.de/hhpred# (22); HMMER3 at http://hmmer.janelia.org/ (23); and I-TASSER at http://zhanglab.ccmb.med.umich.edu/I-TASSER/ (24). The subcellular localization and topology of the proteins were predicted using TargetP at http://www.cbs.dtu.dk/services/ (25) and Phobius at http://phobius.sbc.su.se (26), respectively.

RESULTS

***In vivo* enzymatic tagging in *Giardia intestinalis*.** To gain insights into the composition of protein import pathways and other processes in giardial mitosomes, we took a direct biochemical ap-

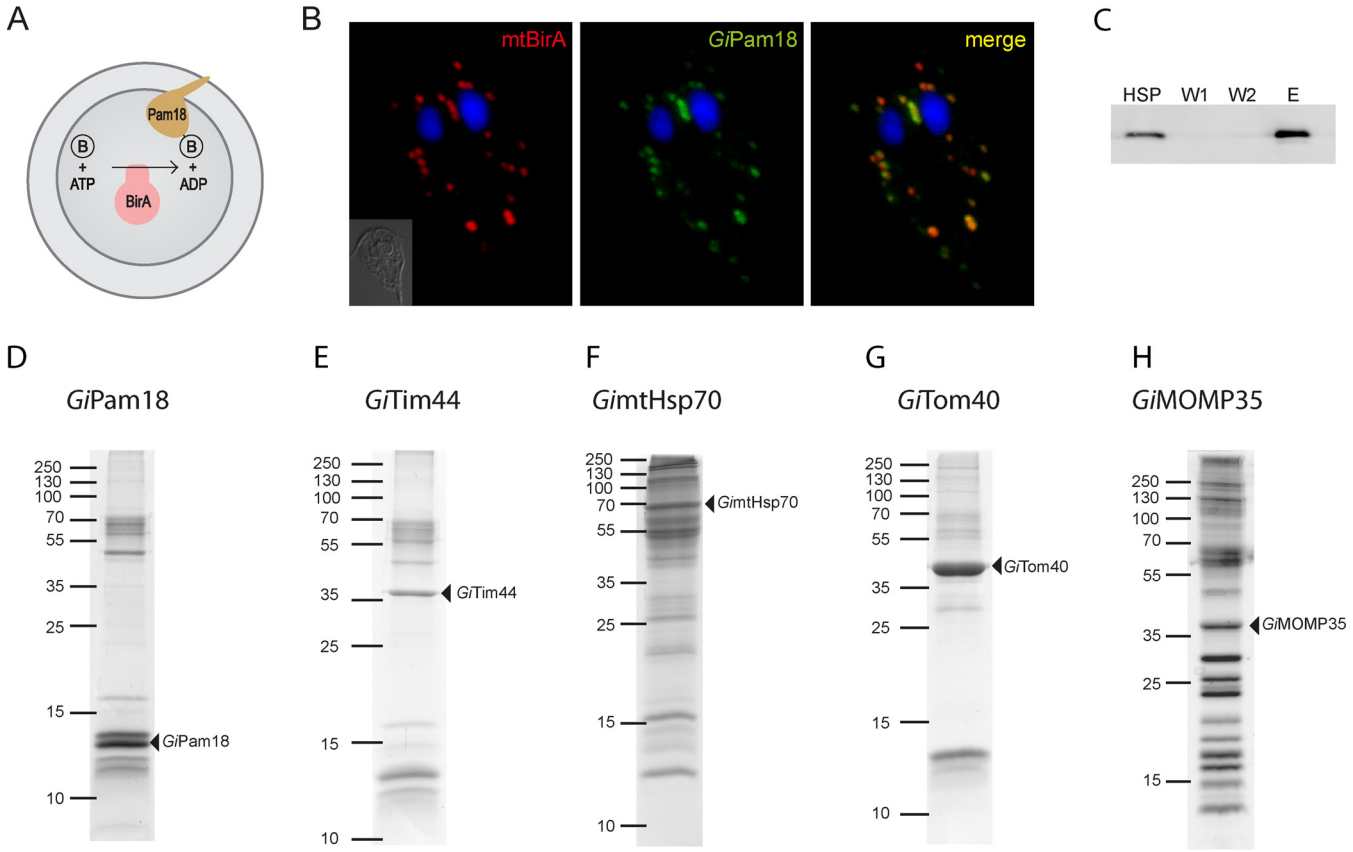

FIG 1 *Gi*Pam18 is biotinylated within mitosomes. (A) Schematic representation of mitosome-specific *in vivo* enzymatic tagging. *E. coli* biotin ligase (BirA) specifically biotinylates the biotin acceptor peptide when present in the same compartment. B, biotin. (B) BAP-tagged *Gi*Pam18 was successfully biotinylated by mtBirA. Cells were stained with an anti-HA tag antibody (red) and streptavidin-conjugated Alexa Fluor 488 (green) to detect mtBirA. Nuclei were stained with DAPI (blue). (C) Example of the purification steps (*Gi*Pam18) as analyzed on the Western blot by Alexa Fluor Fluor 488-streptavidin conjugate. (D to H) Protein profiles of the particular eluates from the streptavidin-coupled magnetic beads resolved by SDS-PAGE. The triangles indicate the proteins carrying the BAP tag.

proach involving highly specific protein pulldown assays followed by mass spectrometry analyses. To this end, an *in vivo* enzymatic tagging technique based on the biotin-avidin interaction was introduced into *Giardia*. This tagging relies on the highly specific *E. coli* biotin ligase (BirA), which uses one ATP molecule to catalyze the covalent attachment of biotin to the side chain of lysine within a biotin acceptor peptide (BAP) (27). A chimeric construct composed of *E. coli* BirA preceded by the N-terminal region of mitosomal *Gi*Mge1 and followed by a double HA tag was expressed in *Giardia*. The resulting strain contained mitosomally localized BirA (mtBirA). This construct was cotransformed with a second plasmid carrying a gene encoding mitosomal *Gi*Pam18 with the C-terminal BAP (Fig. 1A). Detection using a fluorescent streptavidin conjugate revealed the specific biotinylation of BAP (Fig. 1B). *Gi*Pam18-BAP-specific biotinylation was confirmed by Western blotting of a *Giardia* trophozoite lysate, which produced a single band of approximately 13 kDa, which corresponded to *Gi*Pam18-BAP. These results demonstrated that BirA remained active when delivered to *Giardia* mitosomes and that no nonspecific biotinylation was detected. Moreover, the use of mitosomal ATP during the biotinylation of the BAP had no apparent effects on mitosomal morphology, mitosomal distribution, or parasite growth.

Search for the TIM components. *Gi*Pam18-BAP was further used to identify putative components of the mitosomal TIM complex. As a part of the PAM complex at the inner mitochondrial membrane, Pam18 interacts with the translocation channel via Tim44 (28). HSPs, which were enriched for mitosomes, were obtained from *Giardia* trophozoites expressing mtBirA and *Gi*Pam18-BAP. The purification of the biotinylated proteins was initially performed under native conditions; however, the resulting eluates contained numerous contaminating proteins (data not shown). Thus, chemical cross-linking and denaturation conditions were used instead. The HSP was treated with a low concentration of the membrane-permeable reversible cross-linker DSP, which is commonly used to identify interacting proteins in various cellular compartments, including mitochondria (29, 30).

Upon cross-linking, the detergent-solubilized samples were passed over streptavidin-coupled magnetic beads, and the resulting protein fractions were analyzed via SDS-PAGE and Western blotting (Fig. 1C and D). The samples were then trypsin cleaved and analyzed by mass spectrometry. Analogous purification experiments were performed in parallel using HSPs isolated from wild-type *Giardia* cells and from *Giardia* cells expressing mtBirA only. These two samples were used as negative controls for the mass spectrometry protein identification. After the results of the negative controls were subtracted, the identified proteins were ordered according to their Mascot score. Although none of the

known mitosomal proteins were present in the negative controls, these proteins were abundant among the hits derived from the *Gi*Pam18-BAP samples. The high specificity of the purification procedures suggests that *Gi*Pam18-interacting partners were present among the top identified proteins. The remainder of the refined data set largely represented proteins of unknown function, and their amino acid sequences were analyzed using homology and topology detection software.

Mitosomes contain highly diverged Tim44. Of the proteins that copurified with *Gi*Pam18-BAP, GL50803_14845 had the highest Mascot score of the unknown proteins (see Fig. S3 in the supplemental material). Although pairwise sequence analyses of GL50803_14845 showed no obvious homology to known protein families, profile-sequence comparisons conducted with HHpred showed clear homology to Tim44, a key component of the TIM complex (Fig. 2A). The mitosomal localization of GL50803_14845, here referred to as *Gi*Tim44, was confirmed by its episomal expression in *Giardia* (Fig. 2B). Further comparisons with mitochondrial and hydrogenosomal Tim44 proteins revealed that *Gi*Tim44 is one of the most divergent Tim44 orthologs identified and that it consists of the C-terminal domain of Tim44, which has been suggested to interact with mitochondrial lipids. However, *Gi*Tim44 lacks recognizable N-terminal domain of Tim44 (Fig. 2C), which binds the import motor molecule mtHsp70 and the core subunit of the protein-conducting channel, Tim23 (31, 32).

The homology model of the C-terminal domain of *Gi*Tim44 indicated that this protein was capable of forming a conserved Tim44 structure containing a hydrophobic cavity, indicating its possible attachment to the mitosomal membrane (Fig. 2F). To test whether mitosomal *Gi*Tim44 interacts with its putative mitochondrial partner, *Gi*mtHsp70, *Giardia* trophozoites coexpressing mtBirA and *Gi*Tim44-BAP were generated. Following chemical cross-linking and purification, the proteins that copurified with *Gi*Tim44-BAP were analyzed by mass spectrometry. Similar to what was seen in the initial experiment, the purified sample was highly enriched for known mitosomal proteins (see Fig. S3 in the supplemental material). The five most highly enriched identified proteins included mitosomal *Gi*mtHsp70 and its nucleotide exchange factor, *Gi*Mge1, which strongly supports the hypothesis that Tim44 and Hsp70 interact within mitosomes.

Distant Tim44 orthologs in eukaryotes. The discovery of a divergent Tim44 in *Giardia* led us to search for other Tim44 orthologs in eukaryotes. Using Tim44-specific HMMs, we identified Tim44 orthologs in two free-living metamonads, *Carpediemonas membranifera* and *Ergobibamus cyprinoides*. However, no Tim44 orthologs were identified in the fish parasite *Spironucleus salmonicida* or in the group Euglenozoa, which includes medically important trypanosomes and leishmania.

Surprisingly, the HMMs identified two mitochondrial proteins, MRLP45 and Mba1, as belonging to the Tim44 protein family (Fig. 2C and D). Whereas MRLP45 is a subunit of the mitochondrial ribosome (33), Mba1 serves as a mitochondrial ribosome receptor during the membrane insertion of mitochondrially translated proteins (34). Their distribution in eukaryotes suggests that both proteins represent independent paralogs of Tim44 that are specialized for mitochondrial protein translation (Fig. 2D).

Search for the translocase of the TOM components. To identify outer mitosomal membrane components, *Gi*Tom40-BAP was coexpressed with the cytosolic version of BirA (cytBirA). As a result, mitosome-specific biotinylation was observed (see Fig. S1 in the supplemental material). Employing the same strategy as the one used for *Gi*Pam18 and *Gi*Tim44, the proteins obtained by *Gi*Tom40-BAP purification were identified using mass spectrometry. The proteins obtained from wild-type *Giardia* cells and *Giardia* cells expressing cytBirA only were subtracted from the data set.

Because *Gi*Tom40 is the only known outer mitosomal membrane protein, the specificity of the purification procedure could not be determined. Nevertheless, the absence of mitosomal matrix proteins among the most significant hits (see Fig. S3 in the supplemental material) indicated that a distinct subset of mitosomal proteins was obtained. However, the previously identified mitosomal protein GL50803_14939 was found among the hits (7) (see Fig. S3 in the supplemental material). According to transmembrane topology predictors, GL50803_14939 contains two transmembrane domains in its N-terminal region. To determine whether the protein is embedded in the outer or inner mitosomal membrane, an HSP isolated from *Giardia* expressing C-terminally HA-tagged GL50803_14939 was subjected to a protease protection assay. Similar to *Gi*Tom40, GL50803_14939 was sensitive to protease activity even without the addition of detergent, which suggests that GL50803_14939 is inserted into the outer membrane (Fig. 3A). Taken together, these data suggest that GL50803_14939, here referred to as mitosomal outer membrane protein 35 (*Gi*MOMP35), is anchored by two N-terminal transmembrane domains in the outer mitosomal membrane and that its C-terminal domain is in the cytosol. Whether the transmembrane domains of *Gi*MOMP35 are also responsible for its mitosomal targeting was tested by analyzing the expression of an N-terminally truncated version of the protein. Indeed, the removal of the transmembrane domains resulted in the cytosolic localization of the truncated *Gi*MOMP35 (see Fig. S2A in the supplemental material).

The function of the exposed soluble domain could not be predicted using bioinformatic analyses, which revealed no significant similarity of the domain to any known protein families. To examine the function of *Gi*MOMP35, we attempted to overexpress the full-length protein using a strong promoter (ornithine carbamoyltransferase) (35). However, a stable *Giardia* line could not be established after numerous attempts, indicating that the overexpression of *Gi*MOMP35 was lethal. Milder *Gi*MOMP35 overexpression (using the 5′ untranslated region [5′UTR] of glutamate dehydrogenase as a promoter) allowed a stable line of *Giardia* transformants to be established and inspected for mitosome-related defects. Approximately one half of the cells retained typical mitosomal distribution and morphology (Fig. 3B), whereas the other half exhibited dramatic membrane protrusions and aggregation (Fig. 3C to E).

Further analyses indicated that *Gi*Tom40 colocalized with these elongated structures (Fig. 3C). However, these structures were largely devoid of the mitosomal protein GL50803_9296, which localized to the mitosomal matrix (see Fig. S2B in the supplemental material). When examined with a transmission electron microscope, the structures were observed as tightly packed multimembrane complexes (Fig. 3F). These data suggest that the membrane protrusions corresponded to the enlarged and aggregated outer mitosomal membrane. In contrast, the overexpression of *Gi*MOMP35 did not result in an ER-related phenotype, as illus-

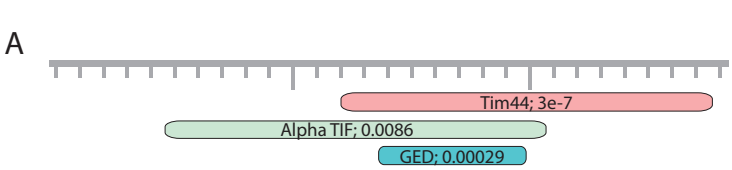

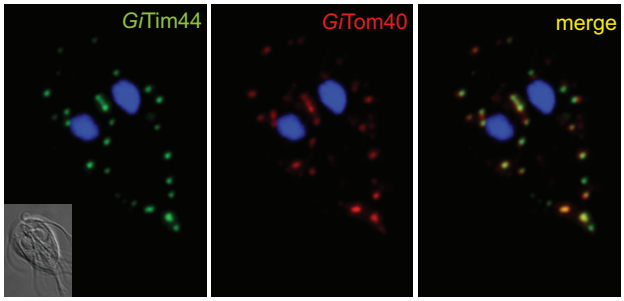

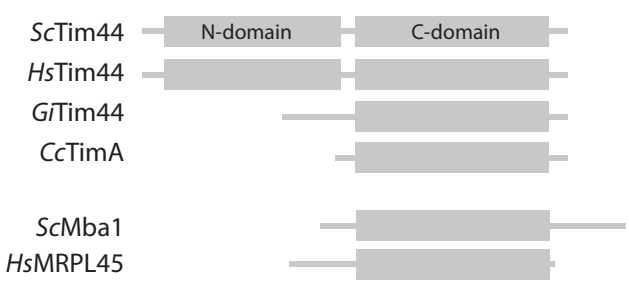

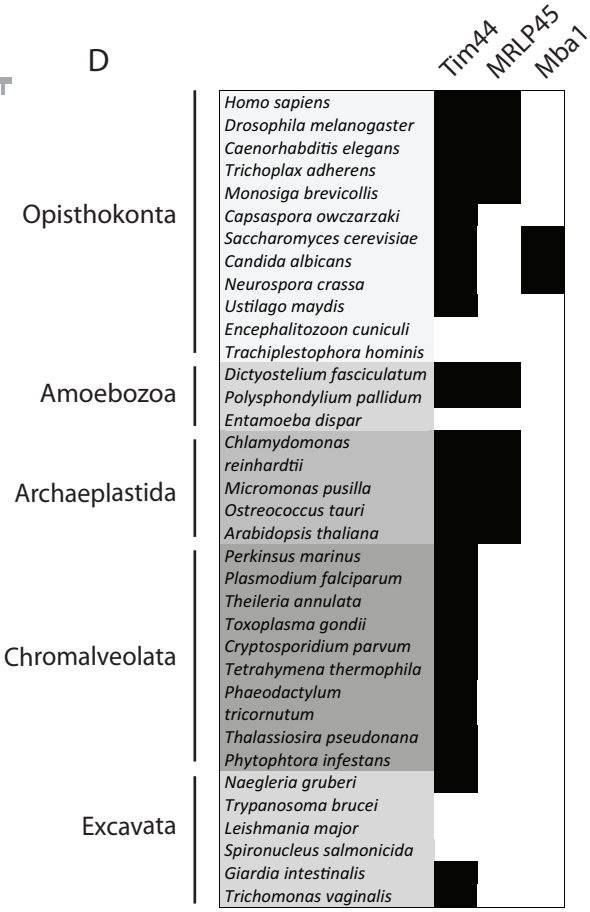

E

```
G.intestinalis     119 ---------- -----LALDF RRLR-SLLPS FDLPHFTENY GIDTLVAILG GYLNIFNTYN PQSYPRQTIA YLLDNCTSKL QKQ-LLEGIQ EHIRKDVDTH FRLHHIRGVK CTGLDLH---  219
C.membranifera     133 -------SQW GKGTELGINV GLVS-AWIP- ---------- --QFVAQIM- ---------- -EAYFMNDVA TLRECCADGA LSI-LLQGLK EQRDKHLSVQ GSTYRIGTTD LARVGG---D  216
E.cyprinoides      135 -----MACDL IGRDTQAAVA AARA-HFDRD FDLHQLQDSA A-AITGELM- ---------- -DAFFAGDVE TVAGLTAEVP RRL-LLDAMR QFLNARIEVT GWTYWAGEPA LRSADVSE-E  234
B.naejangsanensis  56 ---------- --DPALTAAI AGLK-ARDPN FDPHRFLEGA RQAY-ETIV- ---------- -GAYAKGDRE ALRPLLLDKV MGS-FEAGIA AREARGDIES AELVHPPRAD LELATAE--G  147
H.sapiens          281 DKVTDLLGGL FSKTEMSEVL TELL-RVDPA FDKDRFLKQC ENDIIPNVLL ---------- -EAMISGELD ILKDWQYEAT YSQ-LAHFIQ QAKALGLQFH SRILDIDNVD LAMGKMM--E  384
S.cerevisiae       259 NKV----GGF FAETESSRVY SQFK-LMDPT FSNESFTRHL REYIVPEILL ---------- -EAYVKGDVK VLKKWFSEAP FNV-YAAQQK IFKEQDVYAD GRILDIRGVE IVSAKLLAPQ  360
A.thaliana         301 --IQDMNEKF LKETDSASTY KELR-SRDPS FSLPDEAAEI EEVIKF-VLL ---------- -NAYSEGDVE TLKKYCSKEV IER-CTAERT AVQTHGVLFD NKLLHISEVS VSVTKMM--G  402
N.gruberi          348 EDIPDTEADI SSTSENALAM GAFK-KRDPR FDLDLLLVTM RTLTIPEIM- ---------- -SAYFNDDAH TLKKFVSESC YRQVFFPRIQ EFVHTKIKYD AKLLHVEDVM LYTTRYD--A  452
P.falciparum       302 -------GKL FGETELAAAL REMK-MIDKN FKLSELMYLF EYVISKHIV- ---------- -ESYLIGDEF TLRLHCGSSA FNS-LNASIT LKKKKVFLD TNVLIYKNHF LKGAQRME-E  400
T.vaginalis        156 NASSVVVSKL TQPSKEQLVQ MSIQ-MYYPT FTISEFKQWI EKSFLPVLL- ---------- -ERYLRGNIK QLEELTSQQV AKE-RQLAVV QFLSNRLIIR TKLLSITDVD IMGFDFT--N  259
D.fasciculatum     362 GTIAGFVGGY TSSPALTKFY FDYRDLIMPG FEFNKFLPIA KSKFIPEFL- ---------- -EIVFANDVD GLEDFCGETL HKM-LSGIIA ANEAGHKVFD GKIVKIDTLD FMGINES--E  466

G.intestinalis     219 ---SMELHFT AILTGAYAVT NRS---GQTV NGGYNKSRD- -YLVDYSYRY YNGK------ ---------- WLLSALKMSI LSISAKPTYF Y 286
C.membranifera     217 DRFTLTVNET --LSHFFRVN LPR---GHCL HGS-KKGRDY TYTATISPEK GQWVDLTEGD AKIEVR---- WMLTDIHAET VDYVANKEE- - 295
E.cyprinoides      235 GVESFFAVT --LSQLYAAT RAGEHGPELL HGSLRRGTDF EYVFKLRPAG EPRAIVGRG- -NQGPTR--- WIVSALLAPT LDATLEPRGA T 318
B.naejangsanensis  148 DRALAKVREL --AEVRGSLT PSG---GETV TEE----RRT AEIWTFERRL G--------- -TSDPN---- WALARVEPAA A--------- - 205
H.sapiens          385 QGEVVLTTTQ --AQLVMVVR NPK---GEVV EGDPDKYLRM LYVWAICRDQ DEL------- -NPYAA---- WRLLDISASS TEQIL----- - 452
S.cerevisiae       361 DIEVLVVGCR --AQEINLYR KKKT--GEIA AGDEANILMS SYAMVFIRDP EQIDD----- -DETEG---- WKILEFVRGG SRQFT----- - 431
A.thaliana         403 DSPIITAKFQ --TQEIYCVR DEN---GEIQ EGGQDTIHTV YEEWAMQQVE T----TELGE DAIYPI---- WRLREMCRNG VQALI----- - 474
N.gruberi          453 GNPALVISCA --VQYIHCMK NEA---GEIV EGGPKDIRKE NQMWIIKQDE S--------- -QETDD---- WYVSEVSMLN ADAVK----I V 520
P.falciparum       401 SSPWFIFTFH --TQQINCLK NKN---DEII EGKIDDIREV VYTIALSEHP E--------- -PCKEGLLYP YIVREFAIIG NTPSW----- - 470
T.vaginalis        260 RMPSILVRCS --ADHTNEVI TMNS--GTIV EGGPQDICHT DFIVVLTIDA S--------- -KQTPR---- WIASELRPDS TSNRI----- - 326
D.fasciculatum     467 NREETYFSFL VVVHHTYCIR LYQ---FEIV EGGDHEIIKT QMIVHMSVDT D--------- -LNEFG---- WCVSKLDVHP SESIY----- L 535
```

F

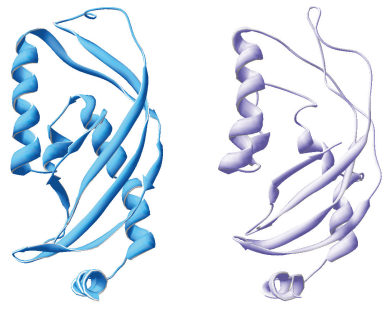

ScTim44 GiTim44

trated by the lack of colocalization between the ER and the enlarged mitosomes (Fig. 3E).

As an alternate means of investigating the function of *Gi*MOMP35, the cross-linked BAP-tagged protein was purified and subjected to mass spectrometry. As expected, *Gi*Tom40 was included in the significant hits; however, the obtained data set contained no clear indication of the function of *Gi*MOMP35 (see Fig. S3 in the supplemental material).

Newly identified mitosomal proteins. In addition to *Gi*Tim44 and *Gi*MOMP35, a number of other proteins of unknown function were identified from the pulldown experiments. The proteins that coprecipitated with BAP-tagged mitosomal Hsp70 (*Gi*mtHsp70) were added to the data sets derived from the *Gi*Pam18, *Gi*Tim44, *Gi*Tom40, and *Gi*MOP35 coimmunoprecipitations, and the data were analyzed together (Fig. 1D to H). *Gi*mtHsp70 is thought to be a central component of mitosomal metabolism and to participate in protein import and iron-sulfur cluster assembly.

Seventeen proteins (see Table S2 in the supplemental material) were subcloned into *Giardia* expression vectors to verify their mitosomal localization. These proteins were selected according to three criteria: (i) the protein copurified with more than one target molecule, (ii) the identification of the protein was highly significant, or (iii) homology predictors showed an affiliation with a particular protein family. Using this approach, mitosomal localization was confirmed for 13 of the proteins, including 3 with dual localization (Fig. 4). The localization of one protein (GL50803_92741) could not be confirmed because no viable transformants were obtained after three independent transfections. Particular attention was paid to GL50803_27910 and GL50803_16424. The first represents an ortholog of rhodanese, a protein involved in various aspects of sulfur metabolism (36), including the repair of iron-sulfur clusters (37). The latter was the only protein identified in all the pulldown experiments performed in this study (see Fig. S3 in the supplemental material); i.e., GL50803_16424 coprecipitated with the outer membrane, the inner membrane, and the matrix proteins, which might indicate its complicated topology. Moreover, the episomal expression of GL50803_16424 often but not always resulted in the formation of enlarged structures at the mitosomal sites (Fig. 4). Strikingly, this protein appears to be a member of the myelodysplasia-myeloid leukemia factor 1-interacting protein (Mlf1IP) family, which has been considered exclusive to metazoans (38). For the remainder of the confirmed mitosomal proteins, no recognizable homology could be identified. Moreover, with the exception of GL50803_27910, GL50803_3491, and GL50803_16424, these proteins appear to lack orthologs, even in other metamonad species; thus, they currently represent *Giardia*-specific molecules (see Table S3 in the supplemental material).

Mode of mitosomal protein import. Compartment-specific biotinylation allows one to determine whether a given protein is transported into an organelle co- or posttranslationally. To this end, we generated a *Giardia* strain expressing a cytosolic version of BirA (cytBirA) (Fig. 5). The ability of cytBirA to biotinylate the BAP on a mitosomal protein indicates that the protein is transported posttranslationally. Indeed, the biotinylation of *Gi*Tim44-BAP was observed upon coexpression with cytBirA (Fig. 5A). Similarly, the use of compartment-specific biotinylation allowed us to assess whether the reported presence of a SNARE protein, Sec20, in the mitosomes (39) indicated the fusion of secretory vesicles with the mitosomal surface. However, because no biotinylation of the mitosomal proteins was observed when BirA was targeted to the ER (data not shown), the integration of mitosomes into the secretory pathway could not be confirmed. The posttranslational transport of mitosomal proteins raised the question of whether these proteins are required to retain their unfolded state during import. To address that question, a chimeric construct encoding mitosomal *Gi*Mge1, mouse dihydrofolate reductase (DHFR), and a C-terminal HA tag was expressed in *Giardia*. The DHFR domain is a classical experimental substrate used in protein translocation studies due to its ability to fold upon the addition of a folate analog (40). Usually, the use of folate analogs requires the experiment to be performed *in vitro* on isolated organelles due to the effect of these analogs to the endogenous enzyme (40). However, *Giardia* lacks DHFR and instead relies on the purine salvage pathway (41), which allows for the *in vivo* use of DHFR-containing constructs. The localization of the chimeric protein was examined in cells incubated with or without the folate analog pyrimethamine (PM). As expected, in the absence of the folate analog, the targeting information on *Gi*Mge1 mediated the efficient delivery of this protein to the mitosomes (Fig. 5B). In contrast, the addition of PM resulted in an entirely cytosolic localization (Fig. 5C). These results demonstrate that the protein must remain unfolded before and during its import into mitosomes.

DISCUSSION

The *Giardia* mitosome remains one of the least well characterized forms of mitochondria. This is especially true for its biogenesis pathways, which ensure that the organelle maintains its integrity and functions. The aim of this study was to identify new mitosomal proteins, which might have diverged from known proteins beyond the sensitivity of homology detection algorithms or have been replaced by lineage-specific components. Because mitosomes represent one of the smallest membrane-bound cellular compartments of eukaryotes (42), biochemical approaches using cell fractionation techniques are highly challenging (7). The *in vivo* enzymatic tagging approach utilizing *E. coli* BirA introduced in this study allows proteins of interest to be purified and their transport through cellular organelles and their subcompartments to be monitored.

First, two key proteins involved in mitosomal protein import, which reside in different mitosomal membranes, were used to

FIG 2 A Tim44 homolog is present in giardial mitosomes. (A) HHpred analysis of GL50803_14845 shows the presence of a Tim44 domain. (B) HA-tagged *Giardia* Tim44 (*Gi*Tim44) localizes to mitosomes. Green, anti-HA antibody; red, anti-*Gi*Tom40 antibody; blue, nuclei stained with DAPI. (C) Domain structure of Tim44 orthologs in eukaryotes and bacteria. *Sc*, *Saccharomyces cerevisiae*; *Hs*, *Homo sapiens*; *Gi*, *Giardia intestinalis*; *Cc*, *Caulobacter crescentus*. (D) Distribution of Tim44 paralogs in eukaryotes. (E) Protein sequence alignment of *Gi*Tim44 with the C-terminal domains of Tim44 orthologs from *Carpediemonas membranifera*, *Ergobibamus cyprinoides*, *Brevundimonas naejangsanensis*, *Homo sapiens*, *Saccharomyces cerevisiae*, *Arabidopsis thaliana*, *Naegleria gruberi*, *Plasmodium falciparum*, *Trichomonas vaginalis*, and *Dictyostelium discoideum*. The sequences were aligned using MAFFT at http://mafft.cbrc.jp/alignment/server/. The residues involved in forming a hydrophobic pocket are framed in red (57). (F) Model of the C-terminal domain of *Gi*Tim44 obtained by Swiss-Model (58) using human Tim44 as a template (48).

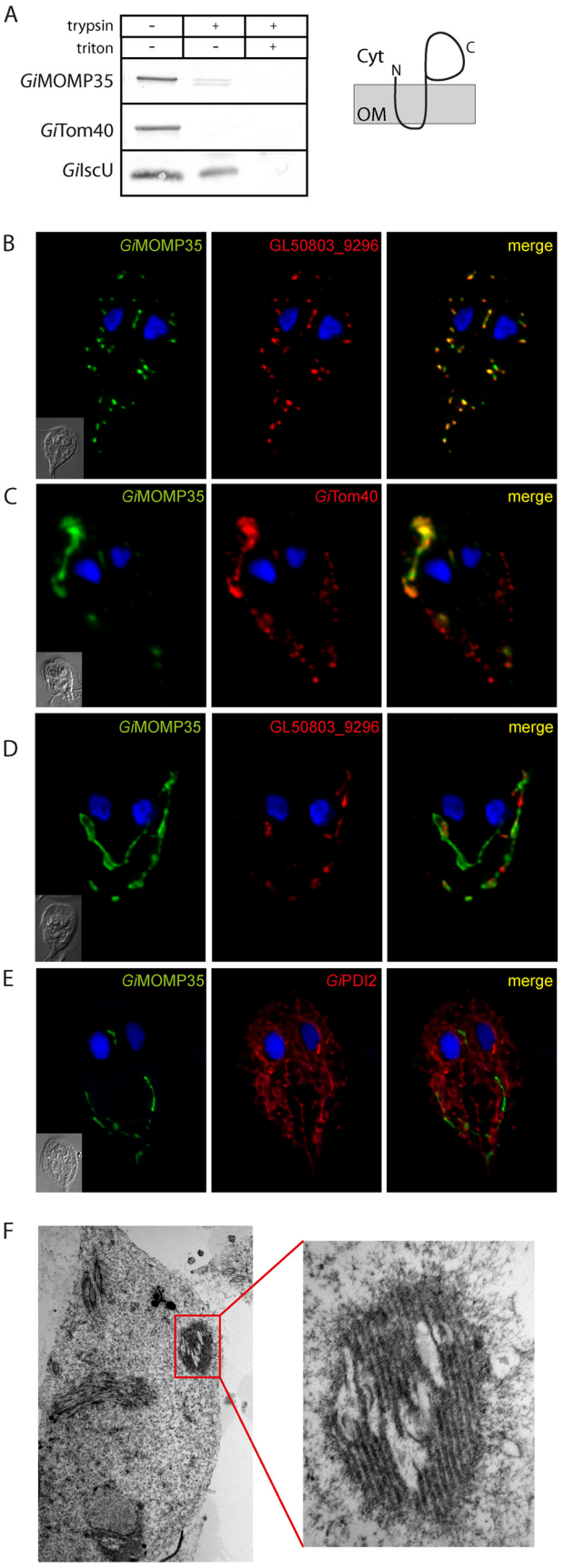

search for new mitosomal components. *Gi*Pam18 was the best available candidate to identify putative TIM components in mitosomes. The protein identified with this approach, *Gi*Tim44, represents one of the most diverged eukaryotic Tim44 proteins. The homology of *Gi*Tim44 is limited to the C-terminal membrane interaction domain, an arrangement reminiscent of the distant Tim44 ortholog found exclusively in alphaproteobacteria (43). However, despite the absence of the N-terminal domain, which has been shown to mediate an interaction with mtHsp70 (31), *Gi*mtHsp70 was found among the most significant proteins that copurified with *Gi*Tim44. This finding may indicate that the interaction between these proteins is conserved in mitosomes, although it is mediated by different amino acid residues. Unfortunately, no protein translocase candidate was found among the obtained data set, which lacked polytopic membrane proteins. This absence was likely due to the experimental conditions used, particularly the cross-linking chemistry and the preparation of samples for mass spectrometry (44). A customized procedure will be necessary to identify such proteins.

Using *Gi*Tim44 as a query, related sequences were found in metamonads such as *C. membranifera* and *E. cyprinoides*. Surprisingly, no Tim44 ortholog was identified in the recently published genome of the hydrogenosome-bearing fish parasite *S. salmonicida* (45). According to further HMM-based searches, Tim44 has been lost several times in the evolution of eukaryotes. Previous reports have shown that this protein is absent from Entamoeba (46) and microsporidian species (47), which also carry highly adapted mitosomes. Strikingly, the Tim44 protein is also missing from the entire group of kinetoplastida, which contain complex aerobic mitochondria. However, our Tim44-specific HMM identified additional new Tim44 paralogs in the mitochondria of opisthokonts, amoebozoa, and plants. Specifically, the mitochondrial proteins MRLP45 and Mba1 participate in mitochondrial translation and membrane protein insertion, respectively (33, 34). MRLP45 is a component of the large subunit of the mitoribosome, the structure of which was recently been resolved (33). The structure of MRLP45 clearly demonstrates its homology to the C-terminal domain of Tim44 (48). Although Mba1 is not a mitoribosome component, it binds the large subunit of the mitoribosome and cooperates with OxaI in the membrane insertion of mitochondrially translated proteins (34). Despite the differences in the molecular architecture of the complexes containing MRLP45 and Mba1, it is likely that these proteins perform analogous functions.

FIG 3 *Gi*MOMP35 is an outer mitosomal membrane protein. (A) Protease protection assay of high-speed pellets isolated from *Giardia* expressing HA-tagged *Gi*MOMP35. After incubation with trypsin, the samples were immunolabeled with antibodies against the HA tag, the outer membrane protein *Gi*Tom40, and the matrix protein *Gi*IscU. The sensitivity of *Gi*MOMP35 to the protease indicates its outer membrane localization. The drawing shows the suggested topology of *Gi*MOMP35. Cyt, cytosol; OM, outer mitosomal membrane. (B) Cells expressing HA-tagged *Gi*MOMP35 were stained with an anti-HA tag antibody (green) and an anti-GL50803_9296 antibody (red). Nuclei were stained with DAPI (blue). In addition to exhibiting typical mitosomal morphology (B), approximately 50% of the observed trophozoites contained elongated tubular structures (C to E). These structures colocalized with *Gi*Tom40 (red) (C); however, only a small fraction exhibited costaining for GL50803_9296 (red) (D). The structures were devoid of the ER marker *Gi*PDI2 (red) (E). These data indicate that the elongated tubular structures represent an enlarged outer mitosomal membrane. Under transmission electron microscopy, the structures appeared as organized membrane layers (F).

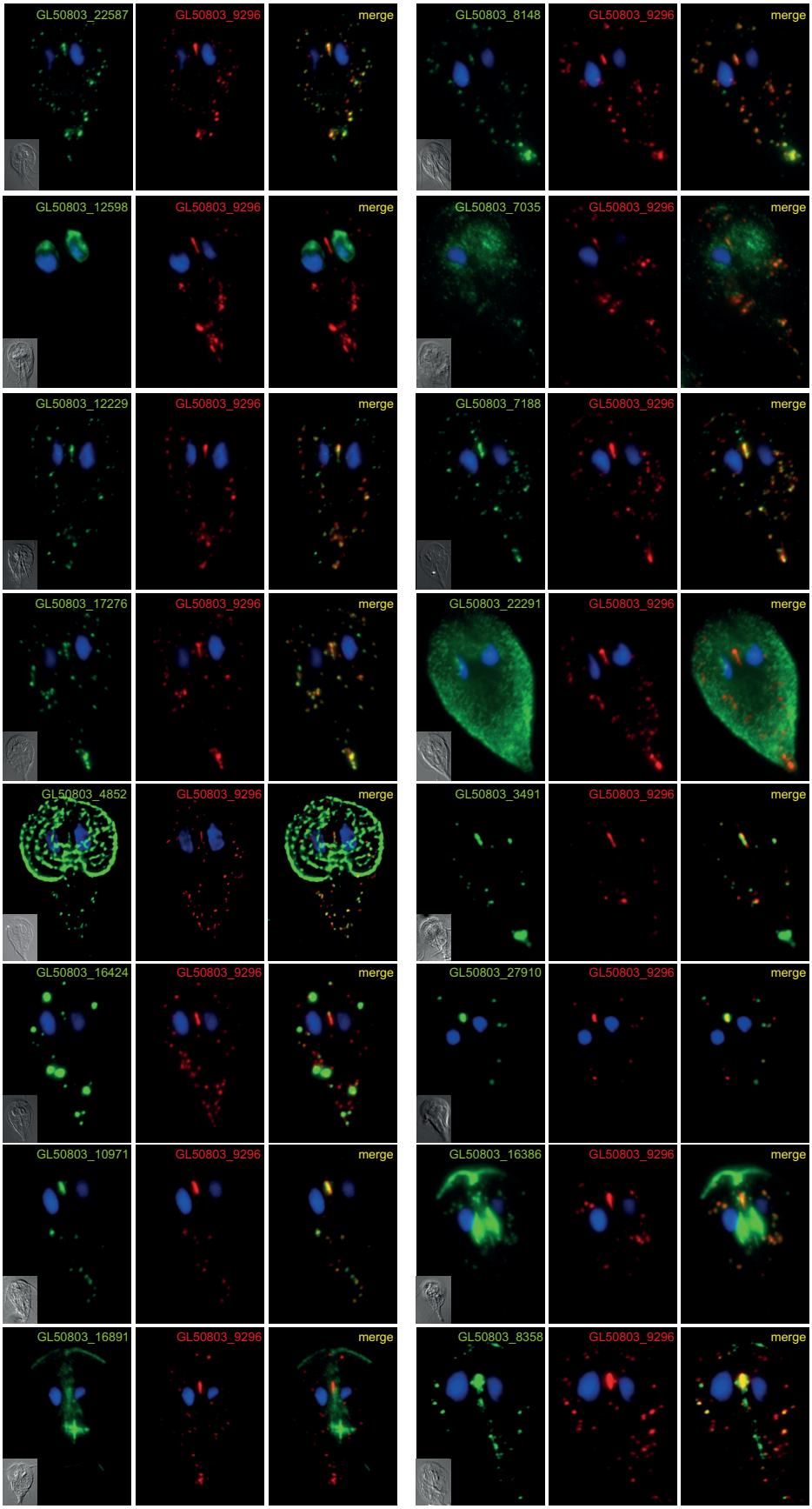

FIG 4 Localization of putative mitosomal proteins. Selected HA-tagged proteins were expressed in *Giardia*, and their cellular localization was determined using immunofluorescence microscopy. The cells were stained with anti-HA tag (green) and anti-GL50803_9296 (red) antibodies. Nuclei were stained with DAPI (blue).

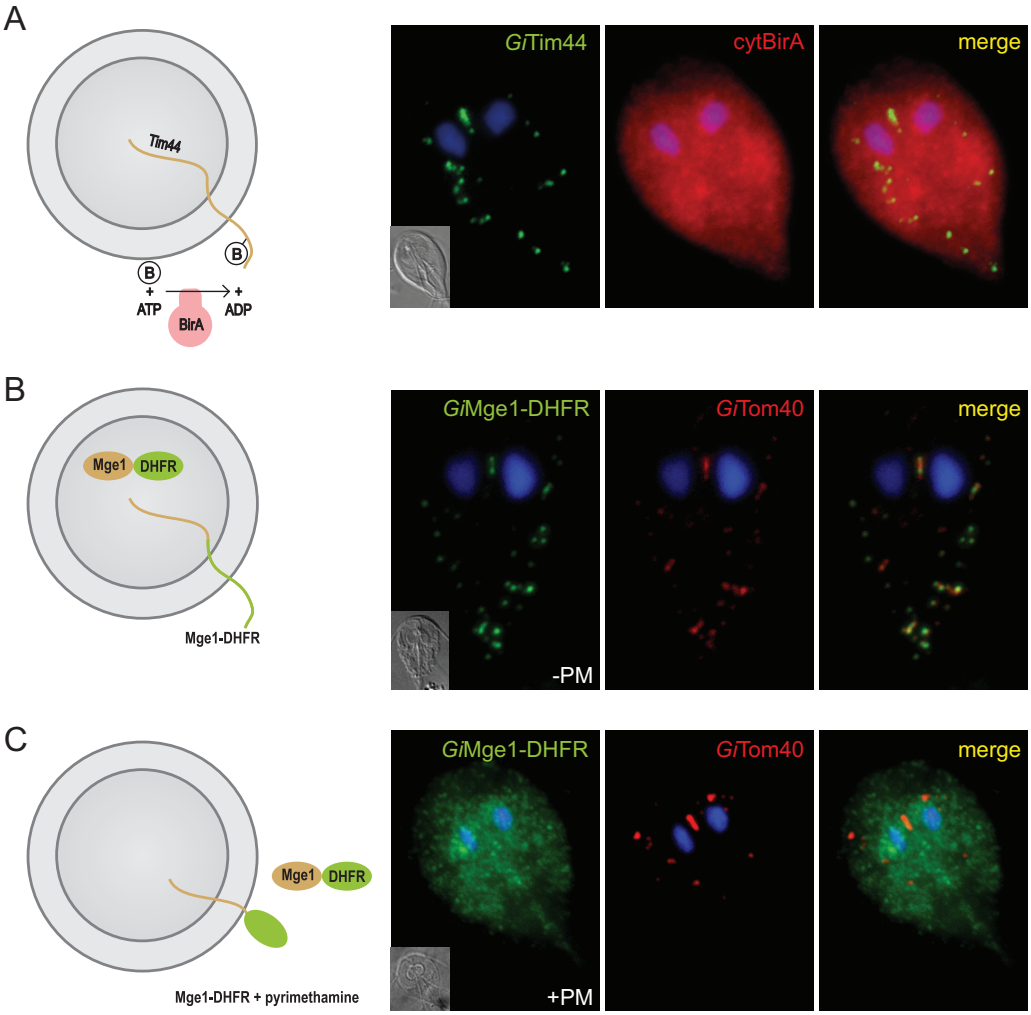

FIG 5 Mitosomal proteins are transported posttranslationally and in an unfolded state. BAP-tagged *Gi*Tim44 was coexpressed with cytosolic BirA (cytBirA), and the biotinylation of the tag was observed using fluorescence microscopy. Cells were stained with an anti-HA tag antibody (red) to detect cytBirA and with streptavidin-conjugated Alexa Fluor 488 (green) to detect the biotinylation of the BAP tag. Nuclei were stained with DAPI (blue). (A) A fusion protein of mouse DHFR, mitosomal *Gi*Mge1, and a C-terminal HA tag was expressed in *Giardia*. (B and C) The localization of the chimeric construct was assessed in the absence (B) or presence (C) of 100 μM pyrimethamine (+PM), which induces the folding of the DHFR domain. The cells were stained with anti-HA (green) and anti-*Gi*Tom40 antibodies (red). Nuclei were stained with DAPI (blue).

The only known outer mitosomal membrane protein has been *Gi*Tom40. This eukaryotic porin is a hallmark of all mitochondria (49), in which it constitutes the general import pore (18, 50) and interacts with the components of the SAM and ERMES complexes (51). The purification of *Gi*Tom40 led to the identification of *Gi*MOMP35. The protein had already been identified in giardial mitosomes, but neither its localization within the mitosome nor its topology had been determined (7). According to our results, the *Gi*MOMP35 protein is anchored in the outer mitosomal membrane with its C-terminal domain exposed to the cytosol. The phenotype of mitochondrial aggregation triggered by the overexpression of *Gi*MOMP35 is reminiscent of the overexpression of some of the outer membrane proteins involved in protein import (52) or mitochondrial dynamics (53). However, without further characterization of its C-terminal domain, the exact function of *Gi*MOMP35 in mitosome biology will remain unknown. This protein is exclusive to *Giardia*; no related sequences have been found in *S. salmonicida* or in other parasitic or free-living metamonads.

Due to the presence of Tom40 in the outer mitosomal membrane, the occurrence of Sam50 was expected (54). Sam50 is an essential component of the SAM complex, the β-barrel protein folding machine (55) that is considered an important evolutionary feature linking mitochondria to Gram-negative bacteria (56). Despite the omnipresence of Sam50 in eukaryotes, no ortholog has been identified in the *Giardia* genome (18) or among the proteins that copurified with *Gi*Tom40 or *Gi*MOMP35 in the present work. Surprisingly, while missing in the *G. intestinalis* and *S. salmonicida* genomes, Sam50 orthologs are present in the expressed sequence tag (EST) data of *C. membranifera* and *E. cyprinoides* (M. Kolísko and A. J. Roger, unpublished results). This strongly suggests that the unique loss of Sam50 in the evolution of eukaryotes occurred in the common ancestor of diplomonads.

However, 5 of the 13 novel mitosomal proteins seem to be

specific to the outer mitosomal membrane, as these were exclusive to *Gi*Tom40- and *Gi*MOMP35-derived data sets. Further investigation of these proteins may bring more information on the biogenesis of the outer mitosomal membrane as well as on the interaction between the mitosomes and other cellular organelles.

In general, the identification of novel mitosomal proteins, the vast majority of which are specific to *Giardia*, demonstrates that metabolic processes other than the formation of iron-sulfur clusters occur in mitosomes. The presence of a rhodanese ortholog indicates the existence of additional sulfur metabolism at a minimum. In addition, the striking presence of an Mlf1IP ortholog in mitosomes may shed light on the exact function of the protein, for which a precise role has not been assigned in the Metazoa.

In addition to the identification of new proteins, the techniques used in this study enabled us to demonstrate that proteins maintain an unfolded state while traveling to mitosomes post-translationally. However, no sign of mixing of the ER and mitosome lumina was detected. The reported mitosomal localization of *Giardia* Sec20 ortholog indicated that a vesicular transport may play a role in mitosomal protein import (39). Our data on the localization of the endogenous Sec20 (not shown in this work) using specific polyclonal antibody indicate that its mitosomal localization is a result of experimental artifact, a phenomenon often observed for the overexpression of tail-anchored proteins. These results provide new evidence that mitosomal biogenesis follows the same rules as mitochondrial biogenesis despite the absence of some of the core components.

Taken together, the data presented here demonstrate that techniques such as *in vivo* enzymatic tagging are extremely valuable tools to investigate the biology of organelles as small as *Giardia* mitosomes. The identification of *Giardia*-specific proteins also demonstrates that our current concept of mitosomes as highly simplified mitochondria may not entirely reflect the true biology of these organelles. Future studies will likely reveal yet-unknown mitosomal functions.

ACKNOWLEDGMENTS

We thank Veronika Klápštová, Vladimíra Najdrová, and Zuzana Drašnarová for valuable technical assistance.

This work was funded by a grant from the Czech Science Foundation (P305-10-0651), by the European Regional Development Fund to the Biomedicine Center of the Academy of Sciences and Charles University (CZ.1.05/1.1.00/02.0109), and by a grant from Charles University Grant Agency (98214).

REFERENCES

1. **Adam RD.** 2001. Biology of Giardia lamblia. Clin Microbiol Rev **14:**447–475. http://dx.doi.org/10.1128/CMR.14.3.447-475.2001.
2. **Ankarklev J, Jerlström-Hultqvist J, Ringqvist E, Troell K, Svärd SG.** 2010. Behind the smile: cell biology and disease mechanisms of Giardia species. Nat Rev Microbiol **8:**413–422. http://dx.doi.org/10.1038/nrmicro2317.
3. **Hehl AB, Marti M.** 2004. Secretory protein trafficking in Giardia intestinalis. Mol Microbiol **53:**19–28. http://dx.doi.org/10.1111/j.1365-2958.2004.04115.x.
4. **Lanfredi-Rangel A, Attias M, de Carvalho TM, Kattenbach WM, De Souza W.** 1998. The peripheral vesicles of trophozoites of the primitive protozoan Giardia lamblia may correspond to early and late endosomes and to lysosomes. J Struct Biol **123:**225–235. http://dx.doi.org/10.1006/jsbi.1998.4035.
5. **Konrad C, Spycher C, Hehl AB.** 2010. Selective condensation drives partitioning and sequential secretion of cyst wall proteins in differentiating Giardia lamblia. PLoS Pathog **6:**e1000835. http://dx.doi.org/10.1371/journal.ppat.1000835.
6. **Dolezal P, Smíd O, Rada P, Zubácová Z, Bursać D, Suták R, Nebesárová J, Lithgow T, Tachezy J.** 2005. Giardia mitosomes and trichomonad hydrogenosomes share a common mode of protein targeting. Proc Natl Acad Sci U S A **102:**10924–10929. http://dx.doi.org/10.1073/pnas.0500349102.
7. **Jedelský PL, Doležal P, Rada P, Pyrih J, Smíd O, Hrdý I, Sedinová M, Marcinčiková M, Voleman L, Perry AJ, Beltrán NC, Lithgow T, Tachezy J.** 2011. The minimal proteome in the reduced mitochondrion of the parasitic protist Giardia intestinalis. PLoS One **6:**e17285. http://dx.doi.org/10.1371/journal.pone.0017285.
8. **Regoes A, Zourmpanou D, León-Avila G, van der Giezen M, Tovar J, Hehl AB.** 2005. Protein import, replication, and inheritance of a vestigial mitochondrion. J Biol Chem **280:**30557–30563. http://dx.doi.org/10.1074/jbc.M500787200.
9. **Roger AJ, Svärd SG, Tovar J, Clark CG, Smith MW, Gillin FD, Sogin ML.** 1998. A mitochondrial-like chaperonin 60 gene in Giardia lamblia: evidence that diplomonads once harbored an endosymbiont related to the progenitor of mitochondria. Proc Natl Acad Sci U S A **95:**229–234. http://dx.doi.org/10.1073/pnas.95.1.229.
10. **Tachezy J, Sánchez LB, Müller M.** 2001. Mitochondrial type iron-sulfur cluster assembly in the amitochondriate eukaryotes Trichomonas vaginalis and Giardia intestinalis, as indicated by the phylogeny of IscS. Mol Biol Evol **18:**1919–1928. http://dx.doi.org/10.1093/oxfordjournals.molbev.a003732.
11. **Likic VA, Dolezal P, Celik N, Dagley M, Lithgow T.** 2010. Using hidden markov models to discover new protein transport machines. Methods Mol Biol **619:**271–284. http://dx.doi.org/10.1007/978-1-60327-412-8_16.
12. **Sickmann A, Reinders J, Wagner Y, Joppich C, Zahedi R, Meyer HE, Schönfisch B, Perschil I, Chacinska A, Guiard B, Rehling P, Pfanner N, Meisinger C.** 2003. The proteome of Saccharomyces cerevisiae mitochondria. Proc Natl Acad Sci U S A **100:**13207–13212. http://dx.doi.org/10.1073/pnas.2135385100.
13. **Schneider RE, Brown MT, Shiflett AM, Dyall SD, Hayes RD, Xie Y, Loo JA, Johnson PJ.** 2011. The Trichomonas vaginalis hydrogenosome proteome is highly reduced relative to mitochondria, yet complex compared with mitosomes. Int J Parasitol **41:**1421–1434. http://dx.doi.org/10.1016/j.ijpara.2011.10.001.
14. **Panigrahi AK, Ogata Y, Zíková A, Anupama A, Dalley RA, Acestor N, Myler PJ, Stuart KD.** 2009. A comprehensive analysis of Trypanosoma brucei mitochondrial proteome. Proteomics **9:**434–450. http://dx.doi.org/10.1002/pmic.200800477.
15. **Wampfler PB, Tosevski V, Nanni P, Spycher C, Hehl AB.** 2014. Proteomics of secretory and endocytic organelles in Giardia lamblia. PLoS One **9:**e94089. http://dx.doi.org/10.1371/journal.pone.0094089.
16. **Keister DB.** 1983. Axenic culture of Giardia lamblia in TYI-S-33 medium supplemented with bile. Trans R Soc Trop Med Hyg **77:**487–488. http://dx.doi.org/10.1016/0035-9203(83)90120-7.
17. **Martincová E, Voleman L, Najdrová V, De Napoli M, Eshar S, Gualdron M, Hopp CS, Sanin DE, Tembo DL, Van Tyne D, Walker D, Marcinčiková M, Tachezy J, Doležal P.** 2012. Live imaging of mitosomes and hydrogenosomes by HaloTag technology. PLoS One **7:**e36314. http://dx.doi.org/10.1371/journal.pone.0036314.
18. **Dagley MJ, Dolezal P, Likic VA, Smid O, Purcell AW, Buchanan SK, Tachezy J, Lithgow T.** 2009. The protein import channel in the outer mitosomal membrane of Giardia intestinalis. Mol Biol Evol **26:**1941–1947. http://dx.doi.org/10.1093/molbev/msp117.
19. **Howarth M, Takao K, Hayashi Y, Ting AY.** 2005. Targeting quantum dots to surface proteins in living cells with biotin ligase. Proc Natl Acad Sci U S A **102:**7583–7588. http://dx.doi.org/10.1073/pnas.0503125102.
20. **Gehde N, Hinrichs C, Montilla I, Charpian S, Lingelbach K, Przyborski JM.** 2009. Protein unfolding is an essential requirement for transport across the parasitophorous vacuolar membrane of Plasmodium falciparum. Mol Microbiol **71:**613–628. http://dx.doi.org/10.1111/j.1365-2958.2008.06552.x.
21. **Rada P, Doležal P, Jedelský PL, Bursac D, Perry AJ, Šedinová M, Smíšková K, Novotný M, Beltrán NC, Hrdý I, Lithgow T, Tachezy J.** 2011. The core components of organelle biogenesis and membrane transport in the hydrogenosomes of Trichomonas vaginalis. PLoS One **6:**e24428. http://dx.doi.org/10.1371/journal.pone.0024428.
22. **Söding J, Biegert A, Lupas AN.** 2005. The HHpred interactive server for protein homology detection and structure prediction. Nucleic Acids Res **33:**W244–W248. http://dx.doi.org/10.1093/nar/gki408.
23. **Eddy SR.** 2011. Accelerated profile HMM searches. PLoS Comput Biol **7:**e1002195. http://dx.doi.org/10.1371/journal.pcbi.1002195.

24. **Zhang Y.** 2008. I-TASSER server for protein 3D structure prediction. BMC Bioinformatics **9:**40. http://dx.doi.org/10.1186/1471-2105-9-40.
25. **Krogh A, Larsson B, von Heijne G, Sonnhammer EL.** 2001. Predicting transmembrane protein topology with a hidden Markov model: application to complete genomes. J Mol Biol **305:**567–580. http://dx.doi.org/10.1006/jmbi.2000.4315.
26. **Käll L, Krogh A, Sonnhammer ELL.** 2007. Advantages of combined transmembrane topology and signal peptide prediction—the Phobius web server. Nucleic Acids Res **35:**W429–W432. http://dx.doi.org/10.1093/nar/gkm256.
27. **Howarth M, Ting AY.** 2008. Imaging proteins in live mammalian cells with biotin ligase and monovalent streptavidin. Nat Protoc **3:**534–545. http://dx.doi.org/10.1038/nprot.2008.20.
28. **Chacinska A, van der Laan M, Mehnert CS, Guiard B, Mick DU, Hutu DP, Truscott KN, Wiedemann N, Meisinger C, Pfanner N, Rehling P.** 2010. Distinct forms of mitochondrial TOM-TIM supercomplexes define signal-dependent states of preprotein sorting. Mol Cell Biol **30:**307–318. http://dx.doi.org/10.1128/MCB.00749-09.
29. **Tieu Q, Okreglak V, Naylor K, Nunnari J.** 2002. The WD repeat protein, Mdv1p, functions as a molecular adaptor by interacting with Dnm1p and Fis1p during mitochondrial fission. J Cell Biol **158:**445–452. http://dx.doi.org/10.1083/jcb.200205031.
30. **Yoon Y, Krueger EW, Oswald BJ, McNiven MA.** 2003. The mitochondrial protein hFis1 regulates mitochondrial fission in mammalian cells through an interaction with the dynamin-like protein DLP1. Mol Cell Biol **23:**5409–5420. http://dx.doi.org/10.1128/MCB.23.15.5409-5420.2003.
31. **Merlin A, Voos W, Maarse AC, Meijer M, Pfanner N, Rassow J.** 1999. The J-related segment of tim44 is essential for cell viability: a mutant Tim44 remains in the mitochondrial import site, but inefficiently recruits mtHsp70 and impairs protein translocation. J Cell Biol **145:**961–972. http://dx.doi.org/10.1083/jcb.145.5.961.
32. **Ting S-Y, Schilke BA, Hayashi M, Craig EA.** 2014. Architecture of the TIM23 inner mitochondrial translocon and interactions with the matrix import motor. J Biol Chem **289:**28689–28696. http://dx.doi.org/10.1074/jbc.M114.588152.
33. **Brown A, Amunts A, Bai X-C, Sugimoto Y, Edwards PC, Murshudov G, Scheres SHW, Ramakrishnan V.** 2014. Structure of the large ribosomal subunit from human mitochondria. Science **346:**718–722. http://dx.doi.org/10.1126/science.1258026.
34. **Ott M, Prestele M, Bauerschmitt H, Funes S, Bonnefoy N, Herrmann JM.** 2006. Mba1, a membrane-associated ribosome receptor in mitochondria. EMBO J **25:**1603–1610. http://dx.doi.org/10.1038/sj.emboj.7601070.
35. **Lauwaet T, Davids BJ, Torres-Escobar A, Birkeland SR, Cipriano MJ, Preheim SP, Palm D, Svärd SG, McArthur AG, Gillin FD.** 2007. Protein phosphatase 2A plays a crucial role in Giardia lamblia differentiation. Mol Biochem Parasitol **152:**80–89. http://dx.doi.org/10.1016/j.molbiopara.2006.12.001.
36. **Cipollone R, Ascenzi P, Visca P.** 2007. Common themes and variations in the rhodanese superfamily. IUBMB Life **59:**51–59. http://dx.doi.org/10.1080/15216540701206859.
37. **Bonomi F, Pagani S, Cerletti P, Cannella C.** 1977. Rhodanese-mediated sulfur transfer to succinate dehydrogenase. Eur J Biochem **72:**17–24. http://dx.doi.org/10.1111/j.1432-1033.1977.tb11219.x.
38. **Ohno K, Takahashi Y, Hirose F, Inoue YH, Taguchi O, Nishida Y, Matsukage A, Yamaguchi M.** 2000. Characterization of a Drosophila homologue of the human myelodysplasia/myeloid leukemia factor (MLF). Gene **260:**133–143. http://dx.doi.org/10.1016/S0378-1119(00)00447-9.
39. **Elias EV, Quiroga R, Gottig N, Nakanishi H, Nash TE, Neiman A, Lujan HD.** 2008. Characterization of SNAREs determines the absence of a typical Golgi apparatus in the ancient eukaryote Giardia lamblia. J Biol Chem **283:**35996–36010. http://dx.doi.org/10.1074/jbc.M806545200.
40. **Eilers M, Schatz G.** 1986. Binding of a specific ligand inhibits import of a purified precursor protein into mitochondria. Nature **322:**228–232.
41. **Wang CC, Aldritt S.** 1983. Purine salvage networks in Giardia lamblia. J Exp Med **158:**1703–1712. http://dx.doi.org/10.1084/jem.158.5.1703.
42. **van der Giezen M, Tovar J.** 2005. Degenerate mitochondria. EMBO Rep **6:**525–530. http://dx.doi.org/10.1038/sj.embor.7400440.
43. **Clements A, Bursac D, Gatsos X, Perry AJ, Civciristov S, Celik N, Likic VA, Poggio S, Jacobs-Wagner C, Strugnell RA, Lithgow T.** 2009. The reducible complexity of a mitochondrial molecular machine. Proc Natl Acad Sci U S A **106:**15791–15795. http://dx.doi.org/10.1073/pnas.0908264106.
44. **Schey KL, Grey AC, Nicklay JJ.** 2013. Mass spectrometry of membrane proteins: a focus on aquaporins. Biochemistry **52:**3807–3817. http://dx.doi.org/10.1021/bi301604j.
45. **Xu F, Jerlström-Hultqvist J, Einarsson E, Astvaldsson A, Svärd SG, Andersson JO.** 2014. The genome of Spironucleus salmonicida highlights a fish pathogen adapted to fluctuating environments. PLoS Genet **10:**e1004053. http://dx.doi.org/10.1371/journal.pgen.1004053.
46. **Dolezal P, Dagley MJ, Kono M, Wolynec P, Likić VA, Foo JH, Sedinová M, Tachezy J, Bachmann A, Bruchhaus I, Lithgow T.** 2010. The essentials of protein import in the degenerate mitochondrion of Entamoeba histolytica. PLoS Pathog **6:**e1000812. http://dx.doi.org/10.1371/journal.ppat.1000812.
47. **Waller RF, Jabbour C, Chan NC, Celik N, Likic VA, Mulhern TD, Lithgow T.** 2009. Evidence of a reduced and modified mitochondrial protein import apparatus in microsporidian mitosomes. Eukaryot Cell **8:**19–26. http://dx.doi.org/10.1128/EC.00313-08.
48. **Handa N, Kishishita S, Morita S, Akasaka R, Jin Z, Chrzas J, Chen L, Liu Z-J, Wang B-C, Sugano S, Tanaka A, Terada T, Shirouzu M, Yokoyama S.** 2007. Structure of the human Tim44 C-terminal domain in complex with pentaethylene glycol: ligand-bound form. Acta Crystallogr D Biol Crystallogr **63:**1225–1234. http://dx.doi.org/10.1107/S0907444907051463.
49. **Zarsky V, Tachezy J, Dolezal P.** 2012. Tom40 is likely common to all mitochondria. Curr Biol **22:**R479–R481; author reply, R481–R482. http://dx.doi.org/10.1016/j.cub.2012.03.057.
50. **Baker KP, Schaniel A, Vestweber D, Schatz G.** 1990. A yeast mitochondrial outer membrane protein essential for protein import and cell viability. Nature **348:**605–609. http://dx.doi.org/10.1038/348605a0.
51. **Yamano K, Tanaka-Yamano S, Endo T.** 2010. Mdm10 as a dynamic constituent of the TOB/SAM complex directs coordinated assembly of Tom40. EMBO Rep **11:**187–193. http://dx.doi.org/10.1038/embor.2009.283.
52. **Yano M, Kanazawa M, Terada K, Namchai C, Yamaizumi M, Hanson B, Hoogenraad N, Mori M.** 1997. Visualization of mitochondrial protein import in cultured mammalian cells with green fluorescent protein and effects of overexpression of the human import receptor Tom20. J Biol Chem **272:**8459–8465. http://dx.doi.org/10.1074/jbc.272.13.8459.
53. **Rojo M, Legros F, Chateau D, Lombès A.** 2002. Membrane topology and mitochondrial targeting of mitofusins, ubiquitous mammalian homologs of the transmembrane GTPase Fzo. J Cell Sci **115:**1663–1674.
54. **Dolezal P, Likic V, Tachezy J, Lithgow T.** 2006. Evolution of the molecular machines for protein import into mitochondria. Science **313:**314–318. http://dx.doi.org/10.1126/science.1127895.
55. **Kozjak V, Wiedemann N, Milenkovic D, Lohaus C, Meyer HE, Guiard B, Meisinger C, Pfanner N.** 2003. An essential role of Sam50 in the protein sorting and assembly machinery of the mitochondrial outer membrane. J Biol Chem **278:**48520–48523. http://dx.doi.org/10.1074/jbc.C300442200.
56. **Gentle I, Gabriel K, Beech P, Waller R, Lithgow T.** 2004. The Omp85 family of proteins is essential for outer membrane biogenesis in mitochondria and bacteria. J Cell Biol **164:**19–24. http://dx.doi.org/10.1083/jcb.200310092.
57. **Josyula R, Jin Z, Fu Z, Sha B.** 2006. Crystal structure of yeast mitochondrial peripheral membrane protein Tim44p C-terminal domain. J Mol Biol **359:**798–804. http://dx.doi.org/10.1016/j.jmb.2006.04.020.
58. **Biasini M, Bienert S, Waterhouse A, Arnold K, Studer G, Schmidt T, Kiefer F, Cassarino TG, Bertoni M, Bordoli L, Schwede T.** 2014. SWISS-MODEL: modelling protein tertiary and quaternary structure using evolutionary information. Nucleic Acids Res **42:**W252–W258. http://dx.doi.org/10.1093/nar/gku340.

Voleman et al. BMC Biology (2017) 15:27
DOI 10.1186/s12915-017-0361-y

BMC Biology

RESEARCH ARTICLE Open Access

Giardia intestinalis mitosomes undergo synchronized fission but not fusion and are constitutively associated with the endoplasmic reticulum

Luboš Voleman[1], Vladimíra Najdrová[1], Ásgeir Ástvaldsson[2], Pavla Tůmová[3], Elin Einarsson[2], Zdeněk Švindrych[4], Guy M. Hagen[4], Jan Tachezy[1], Staffan G. Svärd[2] and Pavel Doležal[1*]

Abstract

Background: Mitochondria of opisthokonts undergo permanent fission and fusion throughout the cell cycle. Here, we investigated the dynamics of the mitosomes, the simplest forms of mitochondria, in the anaerobic protist parasite *Giardia intestinalis*, a member of the Excavata supergroup of eukaryotes. The mitosomes have abandoned typical mitochondrial traits such as the mitochondrial genome and aerobic respiration and their single role known to date is the formation of iron–sulfur clusters.

Results: In live experiments, no fusion events were observed between the mitosomes in *G. intestinalis*. Moreover, the organelles were highly prone to becoming heterogeneous. This suggests that fusion is either much less frequent or even absent in mitosome dynamics. Unlike in mitochondria, division of the mitosomes was absolutely synchronized and limited to mitosis. The association of the nuclear and the mitosomal division persisted during the encystation of the parasite. During the segregation of the divided mitosomes, the subset of the organelles between two *G. intestinalis* nuclei had a prominent role. Surprisingly, the sole dynamin-related protein of the parasite seemed not to be involved in mitosomal division. However, throughout the cell cycle, mitosomes associated with the endoplasmic reticulum (ER), although none of the known ER-tethering complexes was present. Instead, the ER–mitosome interface was occupied by the lipid metabolism enzyme long-chain acyl-CoA synthetase 4.

Conclusions: This study provides the first report on the dynamics of mitosomes. We show that together with the loss of metabolic complexity of mitochondria, mitosomes of *G. intestinalis* have uniquely streamlined their dynamics by harmonizing their division with mitosis. We propose that this might be a strategy of *G. intestinalis* to maintain a stable number of organelles during cell propagation. The lack of mitosomal fusion may also be related to the secondary reduction of the organelles. However, as there are currently no reports on mitochondrial fusion in the whole Excavata supergroup, it is possible that the absence of mitochondrial fusion is an ancestral trait common to all excavates.

* Correspondence: pavel.dolezal@natur.cuni.cz
[1]Department of Parasitology, Faculty of Science, Charles University, Průmyslová 595, Vestec 252 42, Czech Republic
Full list of author information is available at the end of the article

Background

The mitochondria of opisthokonts are dynamic cellular compartments that undergo constant fusion and division events [1]. These processes control mitochondrial morphology and ensure that the mitochondrial network remains homogenous across the cell [2].

GTPases from the dynamin superfamily have a central role in controlling mitochondrial dynamics. The division apparatus relies on the function of the soluble dynamin-related protein Drp1/Dnm1 [3], which is recruited to the mitochondrial surface by several membrane-anchored proteins, such as Fis1 and Mff [4, 5]. The opposing fusion processes require the membrane-anchored, dynamin-related proteins mitofusins/Fzo1 [6] and Opa1/Mgm1 [7] in the outer and inner mitochondrial membranes, respectively. However, information on the fusion and its apparatus is limited to animals and fungi. Whether mitochondria of other lineages of eukaryotes also fuse remains largely unknown.

Recent studies have shown the prominent role of the endoplasmic reticulum (ER) tubules in mitochondrial dynamics in fungal and mammalian cells [8–11]. Different molecular tethers between the ER and the mitochondria have been functionally described in both fungi [11–14] and mammalian cells [15], although for the latter the data have been questioned recently [16].

The transformation of endosymbiotic alphaproteobacteria into current-day mitochondria involved a redesign of their division apparatus. The bacterial divisome complex, which is built around the polymers of a tubulin ortholog, the GTPase FtsZ, has been entirely replaced in the mitochondria of many eukaryote lineages by proteins of the dynamin superfamily [17]; yet, eukaryotes that have preserved the original FtsZ-based machinery can still be found in all eukaryotic supergroups [18, 19].

Our detailed understanding of the molecular background of mitochondrial dynamics in opisthokonts is in sharp contrast to what is known about the rest of eukaryotic diversity. So far only a handful of eukaryotic species have been shown to employ dynamin-related proteins for mitochondrial division. Of the Excavata supergroup, which comprises a large collection of protist taxons, these include the parasitic kinetoplastid *Trypanosoma brucei* [20, 21] and the parabasalid *Trichomonas vaginalis,* the latter of which carries mitochondria-related organelles (MRO) known as hydrogenosomes [22]. Mitochondrial fusion has not been examined in any Excavata species so far, and neither have the orthologs of components of the fusion machinery been identified [23, 24].

Mitosomes represent the simplest form of MROs, which have independently arisen through convergent simplification in several protist lineages that inhabit oxygen-poor environments [25, 26]. While mitosomes have retained a double membrane, they have abandoned their mitochondrial genome and have dramatically reduced their proteome [27, 28].

Giardia intestinalis is an intestinal protist parasite of humans and other vertebrates and has been studied for a number of its unique cellular features, including the mitosomes [29, 30]. About 40–50 tiny mitosome vesicles are stably present in the active, motile stage of the parasite (trophozoite), with a prominent array of the organelles, referred to as central mitosomes, between the two nuclei of the trophozoite cell [31–33]. Mitosomes do not produce ATP, and their only identified metabolic role is in the formation of iron–sulfur clusters [29].

In this study, we investigated the dynamics of *G. intestinalis* mitosomes. We show that mitosomes are extremely steady organelles that do not fuse, and that their division is uniquely synchronized with mitosis. Mitosomes also divide in the encysting cell; thus, the infectious cyst contains two sets of organelles, which may facilitate rapid cytokinesis upon excystation in a newly infected host. Surprisingly, *G. intestinalis* mitosomes seems not to rely on dynamin-related protein during division but they associate with the ER throughout the cell cycle. The regions of contact between these two organelles are enriched for the lipid metabolic enzyme long-chain acyl-CoA synthetase 4 (LACS4), suggesting that the contacts define the sites of the lipid transport to the mitosomes.

Results

Mitosomes undergo neither fusion nor division during interphase

The distribution of mitosomes in *G. intestinalis* trophozoites was followed using immunofluorescence and live-cell microscopy. As shown previously, each cell contains an array of multiple central mitosomes between the two nuclei and peripheral mitosomes that are spread throughout the cytoplasm (Fig. 1a). The superimposed images of multiple trophozoites showed that the mitosomes are plentiful at the lateral and posterior regions of the cell. Apart from between the two nuclei, the central region and the anterior end of the cell are devoid of mitosomes and low in mitosome number, respectively.

The live-cell fluorescence microscopy is hampered by weak fluorescence of green fluorescent protein (GFP) and its derivatives, which require the presence of oxygen to form the fluorescent tripeptide. Therefore, to follow the mitosomal dynamics in live cells, attached *G. intestinalis* trophozoites were observed using Halo-ligand-labeled mitosomal IscU [31]. The number of independent observations (e.g., Fig. 1b) showed no changes in the distribution or morphology of the organelles. This result suggests that mitosomes do not undergo division during interphase. Moreover, the lack of observable fusion

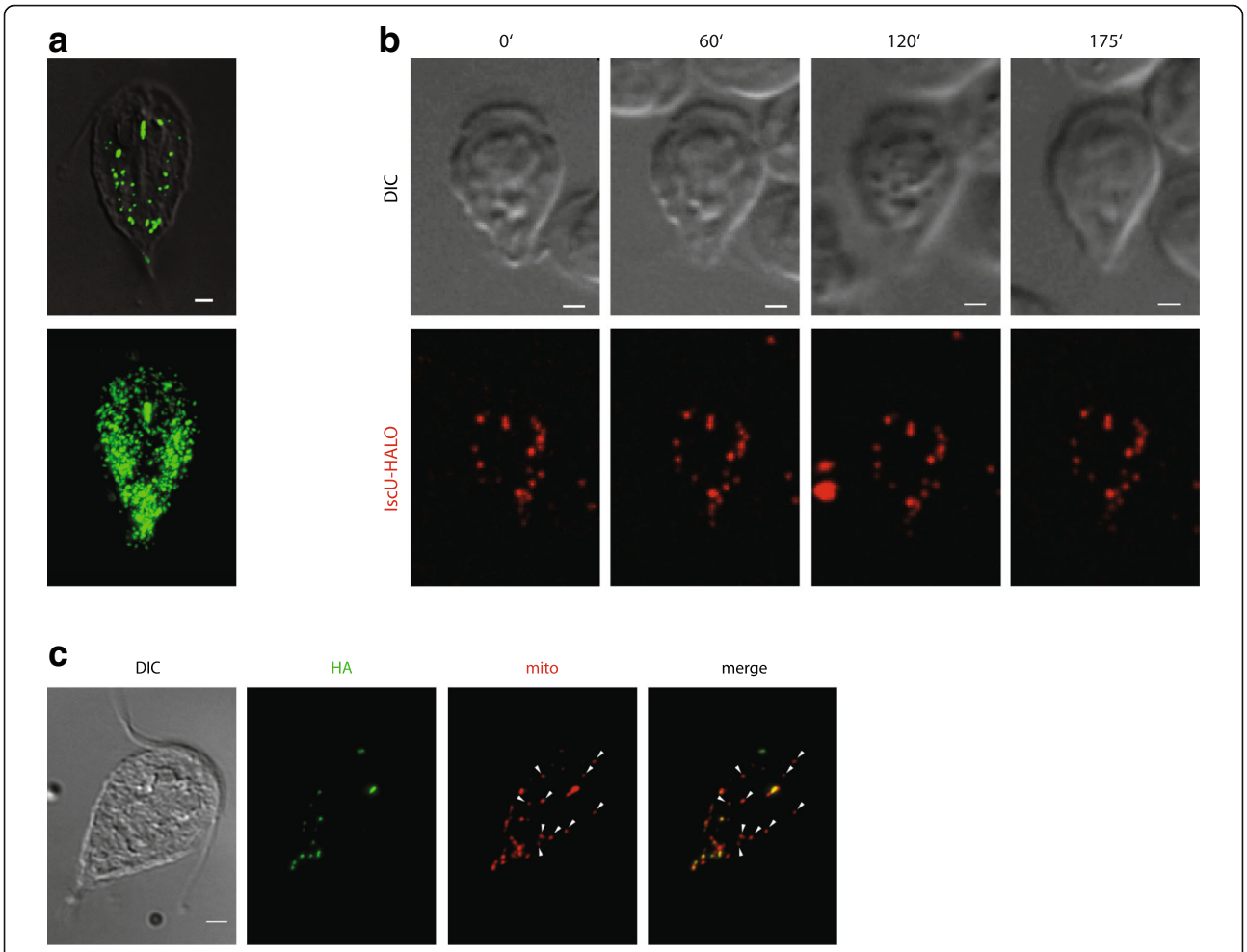

Fig. 1 Mitosomes are stable organelles during interphase. **a** *G. intestinalis* trophozoites were fixed and immunolabeled with an anti-GL50803_9296 antibody. While the upper image shows a single *G. intestinalis* cell, the lower image represents the superposition of 25 imaged cells and shows areas of frequent and scarce mitosomal localization. **b** *G. intestinalis* cells expressing IscU-Halo were stained with the TMR Halo ligand and observed in medium containing 2% agarose under a confocal microscope equipped with a spinning disc. Still images (maximal projections of Z-stacks) from a time-lapse movie are shown with times indicated. Corresponding differential interference contrast (*DIC*) images are shown. Note that the number and distribution of organelles does not change during the indicated period of time. Scale bars, 2 μm. **c** *G. intestinalis* cells expressing human influenza hemagglutinin (*HA*)-tagged IscU were fixed and immunolabeled with an anti-GL50803_9296 antibody and anti-HA antibody. The *arrowheads* indicate mitosomes lacking the recombinant protein

among the mitosomes indicated that this behavior is either much less frequent or even absent in *G. intestinalis.*

We tested if the parasite responds to changes in metabolic conditions by varying the mitosome number by incubating cells in either iron-rich or iron-depleted media. The key proteins in *Giardia* energy metabolism, such as pyruvate:ferredoxin oxidoreductase (PFO) and 4Fe-4S ferredoxin, carry iron–sulfur clusters in their active sites [34]. Considering that synthesis of iron–sulfur clusters occurs exclusively in the mitosomes [29], up-regulation of the biosynthetic iron–sulfur cluster proteins [35] and an increased number of mitosomes could be expected to occur as a way to compensate for a lack of iron–sulfur proteins. However, no change in mitosome morphology or number was observed in iron-depleted cells (Fig. 2d).

Similarly, the cells were also grown with increasing concentrations of metronidazole, a 5-nitroimidazole antibiotic used to treat infections of anaerobic organisms including *Giardia* [36]. The compound is activated by electron transfer from low-redox-potential electron donors such as ferredoxins [37] and, for instance, induces morphological changes to hydrogenosomes of *Trichomonas vaginalis* [38, 39]. Mitosomes contain 2Fe-2S ferredoxin and are likely a place of metronidazole activation; however, the presence of metronidazole did not trigger any mitosome-related phenotype, even at lethal metronidazole concentrations (Fig. 2d).

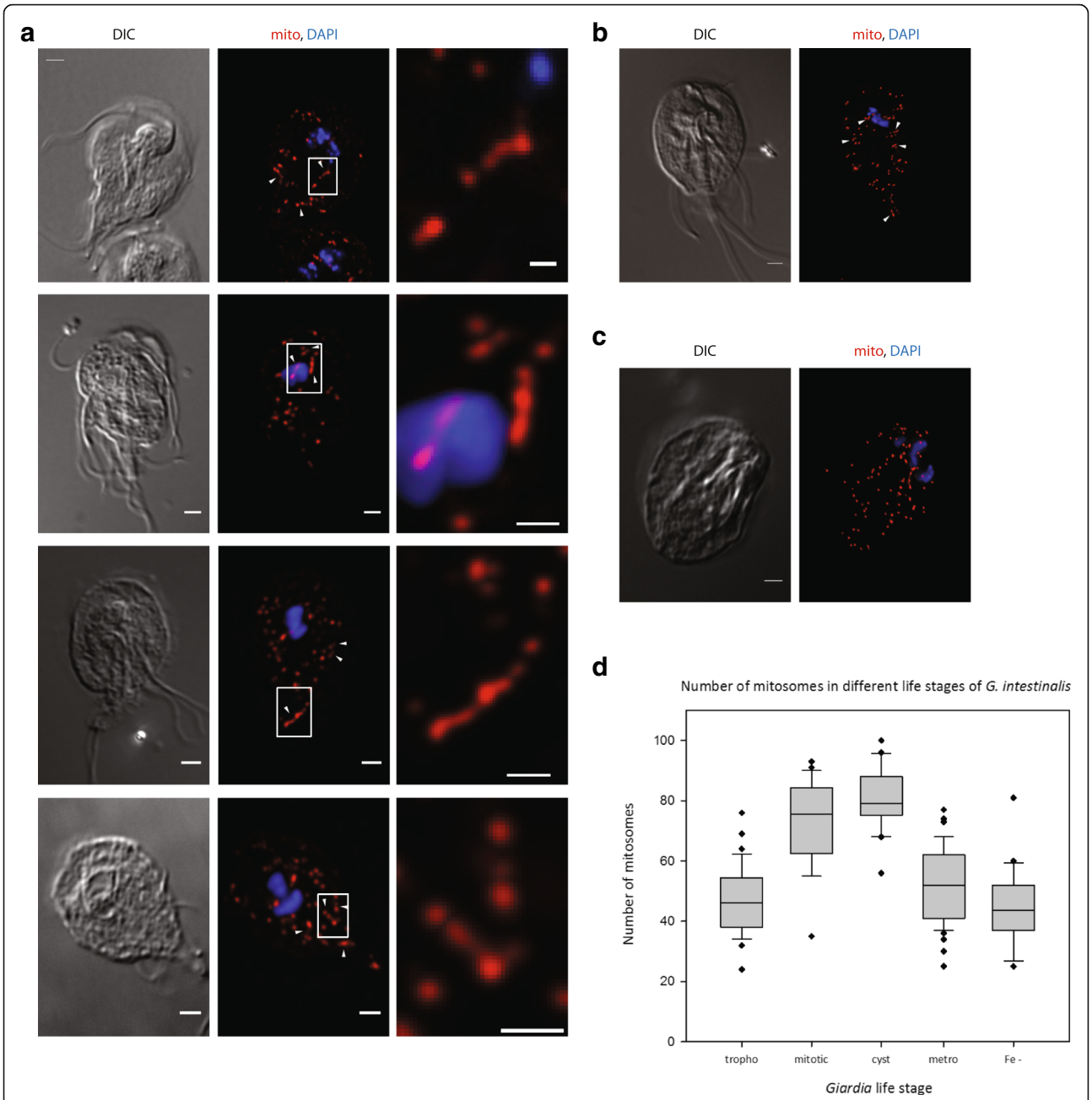

Fig. 2 Mitosomes divide during mitosis. **a** A *G. intestinalis* culture was enriched for mitotic trophozoites by albendazole treatment (100 ng/ml) for 6 h at 37 °C. The cells were washed twice in warm medium and fixed, and the mitosomes were immunolabeled with an anti-GL50803_9296 antibody (*red*) and stained for nuclei with DAPI (*blue*). The image represents a deconvolved maximal projection of the Z-stack. Corresponding differential interference contrast (*DIC*) images are shown. Scale bar, 2 μm. An inset of the dividing organelle is shown on the *right*. *Arrowheads* indicate dumbbell-shaped dividing mitosomes. Scale bar, 0.5 μm. *G. intestinalis* cells were induced to encyst in vitro and the mitosomes were immunolabeled. **b** Encysting cell. **c** Completed cyst stage. **d** The mitosome numbers in *Girdia* cells in different cell/life stages, grown under metabolic stress (metronidazole/iron chelator). *tropho* trophozoite, *mitotic* mitotic cell, *cyst* cyst stage of *G. intestinalis*, *metro G. intestinalis* cells treated with 5 μM metronidazole, *Fe G. intestinalis* cells treated with 300 μM 2,2′-Bipyridyl (DIP). Statistical calculations were carried out using 30–50 cells in SigmaPlot. The *vertical lines* represent the mean values, the *gray boxes* depict the range in which 90% of the values fall, and the error bars depict the standard deviations. *Black dots* represent values outside the standard deviation range

Mitosomal heterogeneity supports the lack of fusion

The absence of observable mitosomal fusions suggested that the organelles could exhibit some degree of heterogeneity. In animal and fungal cells, experimental abolition of mitochondrial fusion leads to fragmentation of the mitochondrial network and functional and morphological heterogeneity of the individual mitochondrial compartments [40, 41].

Uniformity of mitosomes was inspected by immunolocalization of the endogenous mitosomal protein GL50803_9296 [33] and the episomally encoded human influenza hemagglutinin (HA)-tagged mitosomal protein IscU. The fluorescence signals of both proteins co-localized to the same organelles in most instances but in every cell individual mitosomes were positive only for the endogenous protein (Fig. 1c). While the heterogeneity illustrates that the synthesis and/or the transport of the episomally expressed protein is not as efficient as that of the endogenous one, it also indicates that individual mitosomes did not fuse to homogenize their protein content.

Mitosomes divide during mitosis

The lack of observable mitosomal division during interphase suggested that mitosomes might divide during mitosis. Live-cell microscopy of mitotic *G. intestinalis* cells is hampered by the rapid movement of the detached dividing cells, in which the adhesive disc depolymerizes. Nevertheless, observation of individual cells passing through mitosis indicated that mitosomes may divide during this stage of the cell cycle (Additional files 1, 2, 3 and 4). Thus, fixed *G. intestinalis* cultures enriched for mitotic cells were instead examined by immunofluorescence microscopy. To enrich the mitotic cells, starvation [42] as well as albendazole-dependent [43] methods were used. While both methods provided the same results concerning mitosomal dynamics, the latter was used owing to a higher degree of synchrony.

In contrast to interphase cells, mitotic cells were found to contain a variety of elongated dividing mitosomes whose morphology ranged from dumbbell-shaped to thread-like structures (Fig. 2a). Importantly, these mitosomes were found across the whole cytoplasm and were usually dumbbell-shaped, which is a typical configuration for dividing vesicular structures [44–46]. This observation suggests that the individual mitosomes undergo independent and synchronized divisions during mitosis.

Mitotic *G. intestinalis* cells were further studied to identify a possible connection between mitosomal division and a particular phase of mitosis. The dividing organelles were found during all phases of mitosis (Fig. 3b, Additional file 5) with the number of mitosomes gradually increasing toward telophase (Additional file 5). The only exception was the central mitosomes (Fig. 3a). The division of the central organelles, which are arranged as an array localized closely to the basal bodies [47], occurred exclusively in prophase, before the basal bodies moved toward the opposite spindle poles [48] (Fig. 3b). Sister arrays of mitosomes were often positioned to form a V-shaped structure (Fig. 3a,), which likely represented the early separation of two sets of central mitosomes.

To further follow the separation of the central mitosomes, the cells were co-labeled for centrin, a basal body marker [49]. After their division the mitosomes remained associated with the basal bodies throughout the course of mitosis (Fig. 3b).

The prominent character of the central mitosomes was tested by the expression of a synthetic linker composed of the outer mitosomal membrane protein GiMOMP35 at the N-terminus [33], a central HA-tag, and the C-terminal SNARE protein GiQb4, which has been suggested to participate in membrane fusions on the cell periphery [50]. The topology of the construct was designed to dislocate the mitosomes by linking them to the peripheral endomembrane vesicles (Fig. 3c). Indeed, the expression of the synthetic linker dramatically perturbed the overall distribution of the mitosomes. Of about 40 peripheral mitosomes, only several large structures remained. These structures were positive for the synthetic linker and very likely represented mitosomal aggregates induced upon the linker expression (Fig. 3c). However, the central mitosomes remained largely unaffected by the expression of the linker (Fig. 3c). This could be explained by the association of the central mitosomes with the karyomastigont (structural complex of the basal bodies and the nuclei), which minimized the effect of the linker expression. Moreover, the linker also induced rearrangement of the ER network as documented by co-labeling by the ER marker protein, protein disulfide isomerase 2 (PDI2) [51]. Notably, the co-localization of the mitosome- and the ER-specific markers suggests that chimeric compartments may have been formed in these cells.

G. intestinalis undergoes DNA replication and nuclear division during the process of encystation, when tetranucleated 16 N cysts are formed [52]. To follow mitosomal dynamics during encystation, *G. intestinalis* cells were induced to encyst in vitro, and the cells were then fixed and immunolabeled. Similarly to mitotic trophozoites, the encysting cells were found to contain elongated mitosomes that often adopted a dumbbell shape, suggesting that mitosomes divide during encystation (Fig. 2b). Later encystation stages with the characteristic oval shape of the cyst were devoid of dividing mitosomes. However, these cells contained approximately twice as many mitosomes as the trophozoites (Fig. 2c, d). Collectively, these data show that, in addition to two pairs of nuclei, *G. intestinalis* cysts contain a double set of mitosomes, which enable the parasite to undergo rapid cell division during excystation in a new host.

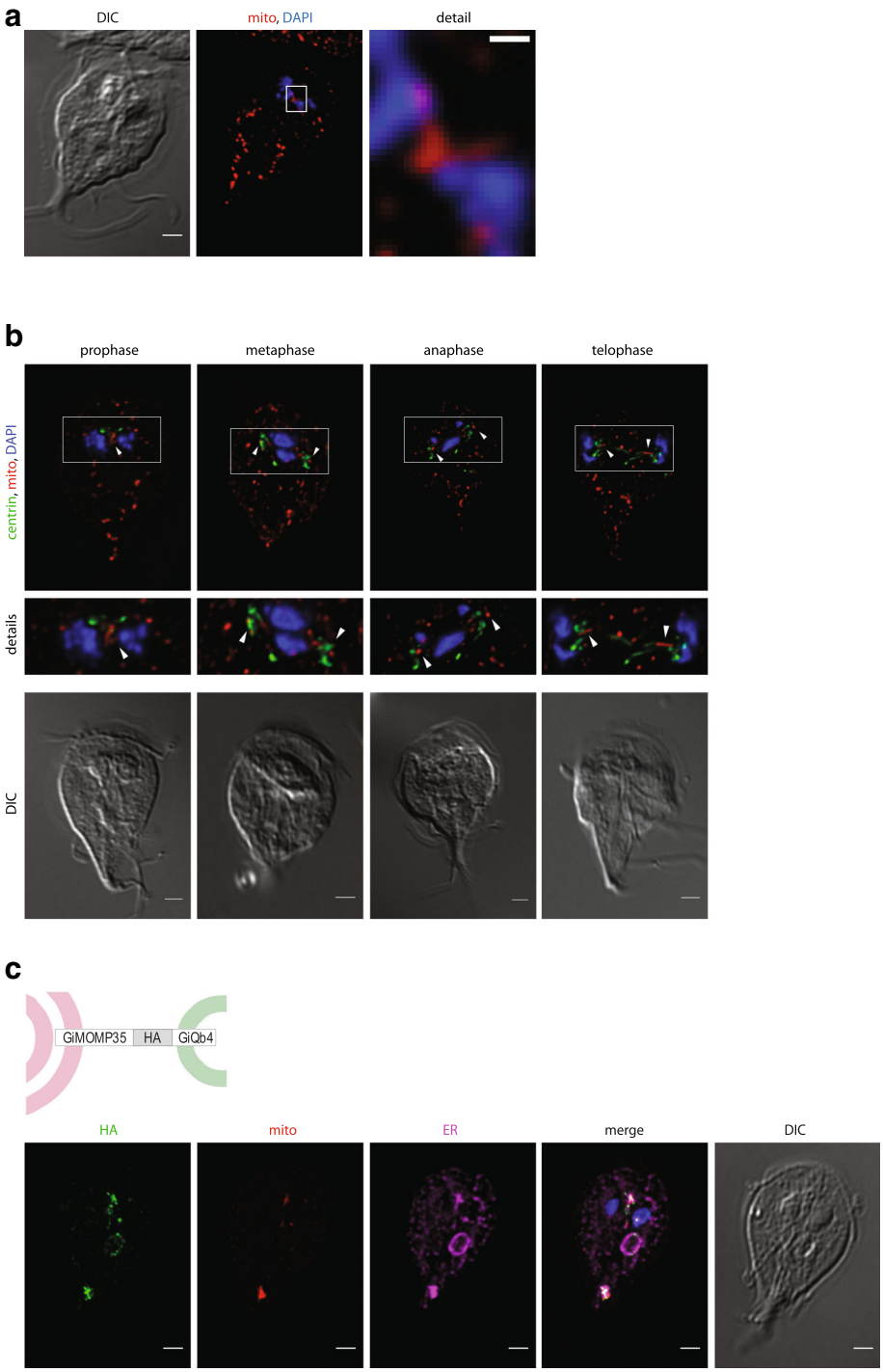

Fig. 3 Central mitosomes divide during prophase and associate with *G. intestinalis* karyomastigont. **a** Mitosomes of mitotic cells were immunolabeled with an anti-GL50803_9296 antibody. The division of the central mitosome could be observed only during prophase as a prominent V-shaped arrangement before the segregation of the daughter kinetosomes and chromosomes. **b** *G. intestinalis* cells expressing C-terminally human influenza hemagglutinin (*HA*)-tagged centrin were enriched for mitotic cells by albendazole treatment. The cells were fixed and immunolabeled with anti-HA (*green*) and anti-GL50803_9296 antibodies (*red*). The nuclei were stained with DAPI (*blue*). *Arrowheads* indicate separation of the central mitosomes coupled with division of the basal bodies. Scale bars, 2 μm. **c** Expression of the synthetic linker composed of the outer mitosomal membrane protein GiMOMP35 and GiQb4 SNARE protein induces aggregation of the mitosomes to the cell periphery and the formation of the endoplasmic reticulum–mitosome chimeras. The cells were fixed and immunolabeled with anti-HA (*green*), anti-GL50803_9296 antibodies (*red*), and anti-PDI2 antibodies (*magenta*). The nuclei were stained with DAPI (*blue*). *DIC* differential interference contrast microscopy

The single dynamin-related protein in *G. intestinalis* is not involved in mitosomal division

Mitochondrial division is mediated by dynamin-related proteins [53] or by the ancestral bacterial FtsZ-based machinery [18]. Moreover, the actin cytoskeleton was recently found to participate in mitochondrial division, possibly by inducing initial mitochondrial constrictions [54]. Thus, the roles of *G. intestinalis* dynamin-related protein (GlDRP) [55] and actin (GiActin) [56] in mitosomal division were investigated.

G. intestinalis cells were transformed with a plasmid carrying HA-tagged GlDRP. In addition to the mitosomal and ER markers, the mitotic trophozoites were immunolabeled with the anti-HA antibody (Additional file 6). Most of the cellular dynamin was localized to the cytoplasmic membrane, where it takes part in the endosomal-lysosomal system of the peripheral vacuoles [55, 57]. However, there was no direct indication that GlDRP plays a role in mitosomal division. To further examine the possible role of GlDRP in mitosomal division, an HA-tagged, K43E-mutated version of GlDRP was introduced into *G. intestinalis* (Fig. 4a, Additional file 7). This mutation abolishes GTPase activity and causes a dominant negative effect in *G. intestinalis* [55]. Provided that encystation of *G. intestinalis* also involves mitosomal division, the K43E GlDRP was cloned behind the promoter region of cyst wall protein 1, expression of which is induced upon the encystation stimuli. As reported previously [55], the presence of K43E GlDRP resulted in the inability of the trophozoites to complete encystation (Fig. 4b). This phenotype supported the establishment of a dominant

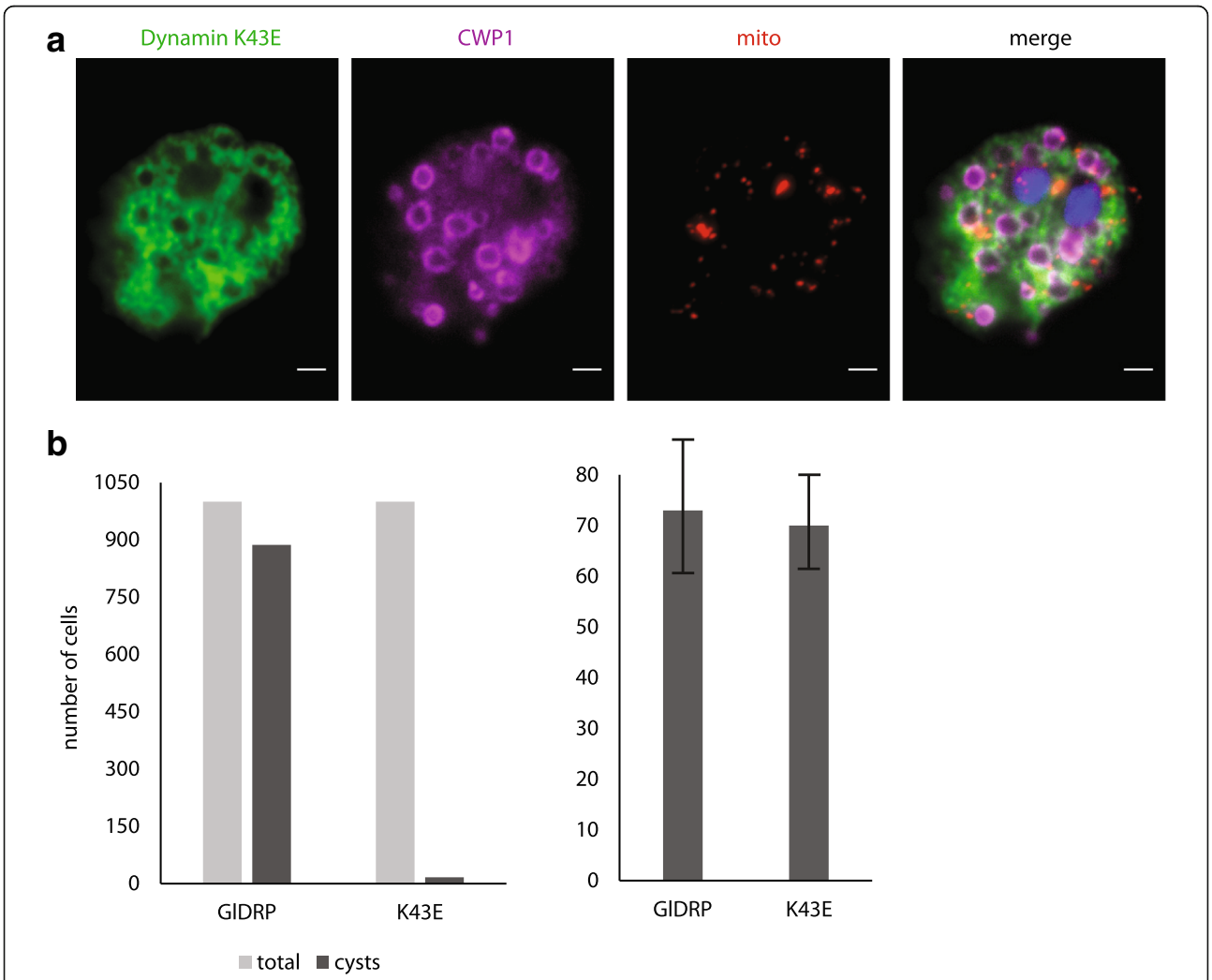

Fig. 4 The single dynamin-related protein of *G. intestinalis* (*GiDRP*) is not involved in the division of mitosomes. **a** *G. intestinalis* cells expressing human influenza hemagglutinin (*HA*)-tagged K43E GlDRP were immunolabeled using anti-HA antibody (*green*), anti-GL50803_9296 antibody *(red*), and anti-CWP1 antibody (*magenta*). One layer of the whole Z-stack is shown. Scale bar, 2 μm. **b** *G. intestinalis* trophozoites were subjected to in vitro encystation and the number of formed cysts and the number of mitosomes within these cells were determined. For the latter, 50 encysting cells were used for the calculation. The error bars depict the standard deviations

negative effect of K43E GlDRP in *G. intestinalis*. However, the affected encysting cells contained twice as many mitosomes as trophozoites. This strongly suggests that GlDRP is not involved in the division of mitosomes (Fig. 4b).

It has previously been shown that GiActin localizes to the axonemes and flagella, nuclei and the cortex of the trophozoites [56]. An inspection of the mitotic cells showed no association between the dividing mitosomes and GiActin (Additional file 8).

The mitosomes associate with the endoplasmic reticulum

Dynamin-related proteins are not the only effectors of mitochondrial division. Recent data from mammalian

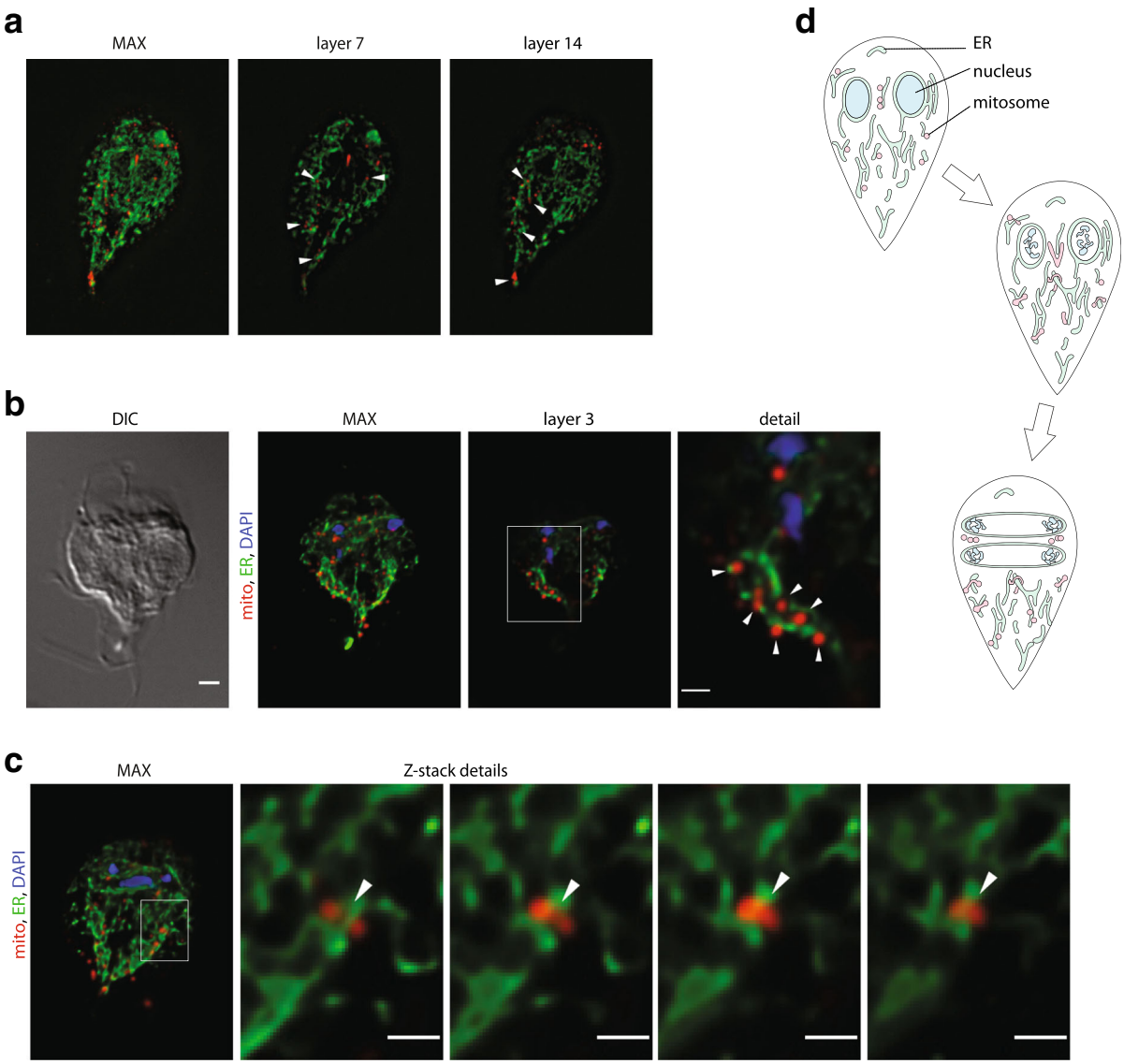

Fig. 5 Mitosomes associate with the endoplasmic reticulum (*ER*) throughout the life cycle. **a** *G. intestinalis* trophozoites were fixed and immunolabeled using anti-GL50803_9296 (*red*) and anti-PDI2 antibodies (*green*) and observed using structured illumination microscopy (SIM). The maximal projection of the Z-stack of SIM images and selected Z-layers are shown. **b** *G. intestinalis* trophozoites enriched for mitotic cells by albendazole treatment were fixed and immunolabeled using anti-GL50803_9296 (*red*) and anti-PDI2 antibodies (*green*). The nuclei were stained with DAPI (*blue*). The images represent deconvolved maximal projections of the Z-stacks. Corresponding differential interference contrast (*DIC*) images are shown. Scale bars, 2 μm and 0.5 μm. **c** Ring-like mitosomal structures around the ER tubules. **d** Schematic representation of the ER–mitosome association and the mitosomal division synchronized with mitosis in *G. intestinalis*: *top*, the interphase cell with no observable mitosomal dynamics; *middle*, upon entry into mitosis, central and peripheral mitosomes start to divide; *bottom*, division of the central mitosomes completes during prophase as the divided organelles segregate along with the divided basal bodies to the opposite spindle poles. The peripheral organelles continue to divide throughout all mitotic stages

and yeast cells have revealed the fundamental role of the ER–mitochondria connections in the dynamics of the mitochondrial network and the positioning of the mitochondrial division sites [8–10]. So far only limited data are available about whether such connections are present outside the supergroup of Opisthokonta, where animals and fungi belong. We tested if such associations also occur in *G. intestinalis*, which belongs to the Excavata [58].

In order to visualize the distribution of the ER and the mitosomes, interphase trophozoite cells were co-labeled for the ER marker PDI2 [51] and the mitosomal marker GL50803_9296 [33]. The double labeling revealed a very close association between the ER tubules and the vast majority of the mitosomes in every cell (Fig. 5a). When compared to the mitochondrial networks of mammals and yeasts, the association appears even more prominent owing to the vesicular morphology of the mitosomes.

The two organelles remained associated during mitosomal division (Fig. 5b). Moreover, the dividing mitosomes elongated along the ER tubules, which indicates that the ER may serve as a platform for mitosomal division (Fig. 5c, d).

The mitosome-associated endoplasmic reticulum is enriched for long-chain fatty acid CoA ligase 4

Several different molecular tethers mediate the association between the ER and the mitochondria. Fungi employ an ER–mitochondria tethering complex known as ERMES (ER–mitochondria encounter structure) consisting of four different components: Mdm10 and Mdm34 in the mitochondrial membrane, and the cytosolic Mdm12 and Mmm1 in the ER [11]. Analogous interactions seem to be mediated by the recently described ER membrane protein complex (EMC) [59] and Lam6 protein [13, 14], whose unifying function is interorganellar lipid transport. Animal mitochondria were shown to rely on the interactions between mitofusin 2 anchored in both the ER membrane and the outer mitochondrial membrane [15]. However, the function of this interaction has recently been questioned [16]. Importantly, all these structures have limited evolutionary distributions and none of them is present in metamonads, including *G. intestinalis* [60, 61]. In addition, several proteins are enriched in the so-called mitochondria-associated membranes (MAMs), a specific region of the ER, which comes into contact with mitochondria and mainly accommodates lipid and fatty acid metabolic enzymes [62].

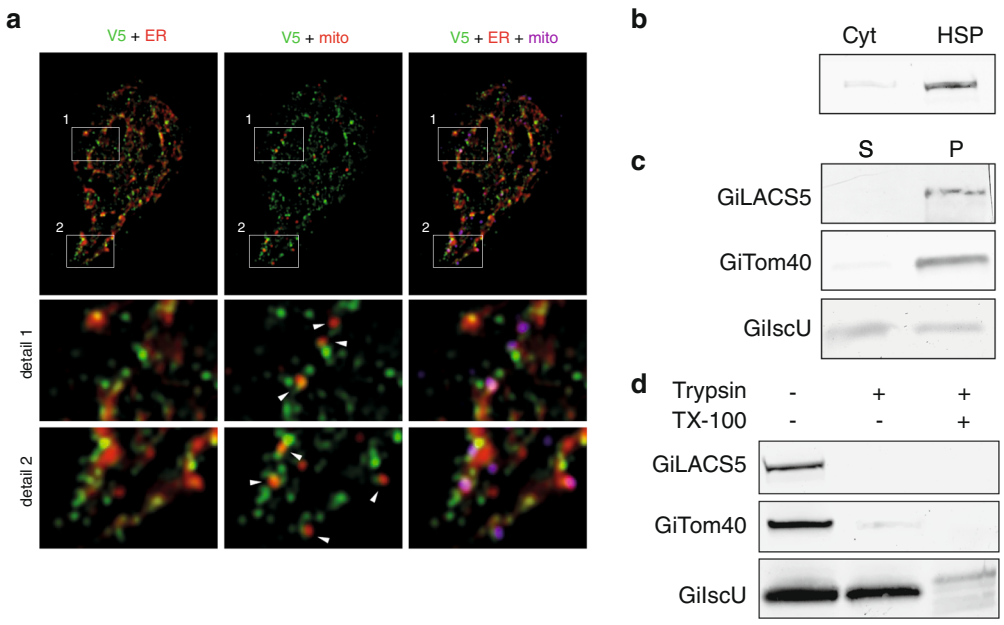

Fig. 6 GiLACS4 populates the endoplasmic reticulum (*ER*)–mitosome contact sites. **a** *G. intestinalis* cells expressing V5-tagged GiLACS were fixed and immunolabeled using anti-V5 tag, anti-GL50803_9296, and anti-PDI2 antibodies. *Left*: V5 in *green* and PDI2 in *red*; *Middle*: V5 in *green* and GL50803_9296 in *red*; *Right*: V5 in *green*, PDI2 in *red* and GL50803_9296 in *magenta*. The cells were observed by structured illumination microscopy (SIM). The *arrows* indicate spots where the mitosomal signal meets the V5-tagged GiLACS4. **b** The cells were fractionated and the high-speed pellet (*HSP*) and cytosolic fraction were immunolabeled with anti-V5 antibody. **c** The HSP fraction was subjected to sodium carbonate extraction and the resulting fractions immunolabeled with anti-V5 (GiLACS4), anti-IscU, and anti-Tom40 antibodies. S - soluble fraction, P - membrane bound fraction. **d** The HSP fraction was treated with trypsin with or without the presence of 1% Triton. The samples were immunolabeled with anti-V5 (GiLACS4), anti-IscU, and anti-Tom40 antibodies

Of the 21 known MAM marker proteins summarized in [62], our bioinformatic searches revealed a single candidate in the *G. intestinalis* genome: long-chain acyl-CoA synthetase 4, hereafter referred to as GiLACS4 [63]. GiLACS4 expressed with a C-terminal V5 tag localized to specific regions of the ER network (Fig. 6a). Importantly, GiLACS4 was also localized proximal to the mitosomes (Fig. 6a). Accordingly, the protein was present in the high-speed pellet fraction, which was enriched for both the ER and the mitosomes (Fig. 6b). Upon sodium carbonate treatment, GiLACS4 was retained in the pellet fraction, which indicates its insertion into the membrane (Fig. 6c). However, on trypsin treatment, the protein was exposed to the cytoplasm (Fig. 6d). Altogether, these data suggest that the mitosome–ER contact sites are occupied by the fatty acid activating enzyme, GiLACS4 (Fig. 7).

Discussion

Mitosomes represent one of the most derived forms of mitochondria and are found in diverse anaerobic eukaryotes [25, 64]. During the course of mitochondrial evolution, the proteome of the mitosomes has shrunk to just a handful of proteins [27], whose sole role is the biosynthesis of iron–sulfur clusters [29, 33]. The mitosomes are devoid of the mitochondrial genome and cristae but have retained two organellar membranes. The stable number of mitosomes in *G. intestinalis* trophozoites indicates that their inheritance must be a controlled process, although alternate stochastic scenarios have also been suggested [32].

Mitochondrial dynamics, as studied in detail in fungal and animal cells, are controlled by dedicated molecular machineries governing both fusion and fission [1]. However, information on the mitochondrial dynamics outside Opisthokonta is scarce.

One of the striking characters of mitosomal dynamics is the synchrony between mitosis and mitosomal division. In our experiments, we have shown that both the central and the peripheral mitosomes divide exclusively during mitosis.

Earlier reports showed that the central mitosomes localize near the basal bodies and the axonemes between the two nuclei [47]. The division of this subpopulation of mitosomes occurs only in prophase and the daughter organelles then follow the separation of the chromosomes to the opposite spindle poles. The privileged localization of the central mitosome suggested that they may represent "germline" organelles, of which the peripheral organelles are derived upon mitosis [32, 65]. However, we show that the peripheral organelles also divide simultaneously during mitosis, including mitosis during encystation. This suggests that a mitosis-dependent signal for mitosomal division must exist in *G. intestinalis.*

Such overall harmonization of mitosomal division and mitosis has not been reported, to our knowledge, in any other eukaryote. In several instances a functional link between mitochondrial division and the cell cycle has been demonstrated, including for the mitochondria of kinetoplastids [66] and apicomplexans [67]. However, these organisms carry just a single mitochondrion, which, in the case of kinetoplastids, is even physically connected to the basal body of the flagellum [66]. Analogous behavior can be expected in other protists that carry a single mitochondrion, such as jakobids [68], where the organelle is often localized next to the cell nucleus.

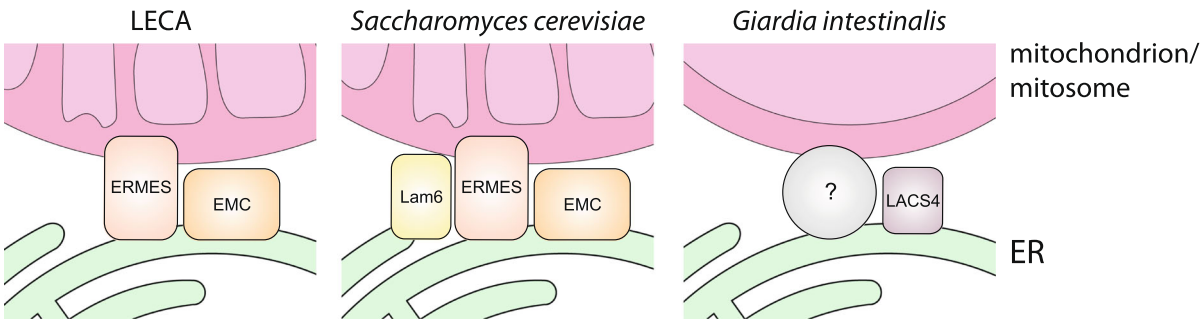

Fig. 7 The evolution of mitochondrial dynamics in Excavata. A schematic representation of the occurrence of the mitochondrial fission and fusion machinery and the endoplasmic reticulum (*ER*)–mitochondria tethering complexes. The patchy phylogenetic distribution of FtsZ-based machinery [19] suggests that dynamin-based division of mitochondria appeared later in the evolution of eukaryotes and was not present in the last eukaryotic common ancestor (*LECA*). While both systems can be found in Excavata, *G. intestinalis* does not use either of them for the division of mitosomes. The lack of observable mitochondrial fusion and the responsible molecular machinery in Excavata indicates that the lack of fusion is an ancestral trait. The components of both recently described ER-tethering complexes can be found in all five supergroups of eukaryotes and thus they were likely present in the LECA [76]. Despite the secondary loss of these complexes, *G. intestinalis* mitosomes maintain association with the ER throughout the cell cycle, indicating the presence of yet unknown tethering mechanisms, perhaps including lipid metabolism enzymes such as LACS4. *ERMES* endoplasmic reticulum–mitochondria encounter structure, *EMC* endoplasmic reticulum membrane protein complex

What is the functional meaning of such synchronized division? We propose that the lack of mitosomal dynamics and the synchronized mitosomal division actually represent two sides of the same coin. The absence of dynamics in the interphase cell disqualifies the stochastic segregation of the organelles. Thus, harnessing the mitosomal and the nuclear division allows the cell to control the organelle number just before cytokinesis.

During the course of evolution, the FtsZ-based division machinery of the bacterial ancestor of mitochondrion has disappeared from most of the eukaryotes and has been replaced by the scission machinery driven by dynamin-related proteins. However, certain organisms from all supergroups of eukaryotes have preserved this ancestral division complex [19, 69], which suggests that the transition to the eukaryote-specific dynamin-based machinery occurred independently on numerous occasions. The group of Excavata to which *G. intestinalis* belongs comprises a great diversity of protists with a variety of mitochondrial forms, ranging from the single reticulate mitochondrion of kinetoplastids to the anaerobic vesicular forms known as hydrogenosomes and mitosomes of metamonads. So far, the division machinery has been characterized to some detail in mitochondria of *Trypanosoma brucei* [20, 21] and hydrogenosomes of *Trichomonas vaginalis* [22]. Here, dynamin-related proteins have been shown to participate in organelle division. Similarly to *Trypanosoma brucei*, the *G. intestinalis* genome encodes only for a single dynamin-related protein (GlDRP). This protein has been shown to function during the encystation process [55]. Indeed, we could show that its function is necessary for the completion of encystation, yet the presence of the dominant negative form of GlDRP did not affect the division of mitosomes, which is in contrast to the recent finding of Rout et al. [70]. However, while our data suggest that dynamin-related proteins are not involved in mitosomal division, it is also possible that the level of the dominant negative form of dynamin capable of preventing encystation is not sufficient to interfere with mitosomal division. Considering that neither of the outer membrane DRP1 recruitment factors, such as Mff and Fis1 [2], is present in the *G. intestinalis* genome, the responsible mitosome division machinery remains entirely unknown. This also includes the absence of GiActin at the dividing organelles.

Instead, mitosomes maintain a vital connection to the ER throughout the cell cycle and the association becomes more prominent during mitosomal division. While the nature of the connection is unknown, we have shown that the ER–mitochondria interface is populated by the fatty acid activating enzyme LACS4. Thus, it is likely that the ER–mitosomal association enables lipid and/or fatty acid transport between the compartments as documented for the mitochondria of animals and fungi [12, 62]. Unfortunately, direct biochemical characterization of the mitosome-associated ER membrane fraction is not feasible owing to the lack of procedures enabling specific organelle purification [27]. A recently developed technique involving in vivo biotinylation and cross-linking of the target protein [33] enables the bypassing of such experimental limitations, although optimization toward the native purification conditions will be required.

The bridging complexes between mitochondria and the ER include the ERMES and the EMC complexes [11, 59]. The ERMES complex was originally described in *Saccharomyces cerevisiae* as the first bona fide structure specialized in tethering the mitochondrial and ER membranes [11]. The complete set of four ERMES components can be found across all supergroups of eukaryotes, although is missing in most Excavata species [60]. The EMC is more conserved among eukaryotes, but it is missing in all metamonads including *G. intestinalis* and *Trichomonas vaginalis* [61]. Considering that both the ERMES and the EMC were likely present in the last eukaryotic common ancestor (LECA), it is highly probable that they were lost in *G. intestinalis* and perhaps all metamonads.

Our data suggest that the overall dynamics of mitosomes in *G. intestinalis* is secondarily reduced down to organelle division. The mitosomes do not manifest any observable dynamics in the interphase cells, as their number and morphology remained constant upon metabolic stress induced by 5-nitroimidazole or under iron deficiency, which affects their single metabolic function of the iron–sulfur clusters formation. By contrast, highly enlarged hydrogenosomes appear in *Trichomonas vaginalis* treated with 5-nitroimidazole (metronidazole) and other drugs [39], and the organelles undergo distinct transformation upon the lack of iron ions [71].

Interestingly, mitosomal fusion was not observed in our experiments. While it is possible that the organelles fuse under very low frequency, the process is not efficient enough to provide a homogeneous population of mitosomes. Moreover, the *G. intestinalis* genome does not encode orthologs of the mitochondrial membrane fusion proteins identified in opisthokonts [6, 7]. It is, however, important to note that other lineages of eukaryotes, including Archaeplastida (e.g., *Arabidopsis thaliana*), which exhibit mitochondrial fusion, also do not rely on opisthokont machinery [72].

Nevertheless, the absence of mitochondrial fusion seems to be common to the whole supergroup of Excavata, as it has not been observed in any studied species so far. Neither have the orthologs of components governing the mitochondrial membrane(s) fusion been identified. Taken together, it is plausible that mitochondrial fusion appeared independently in other lineages of

eukaryotes outside Excavata, perhaps employing different, lineage-specific molecular machinery. Whether the lack of mitochondrial fusion concerns also the LECA awaits further and more complex comparative analyses.

Although simple in their shape and function, the mitosomes of *G. intestinalis* show unique and sophisticated dynamics, which seem to be a mosaic of evolutionarily conserved traits and lineage-specific inventions. Nevertheless, an understanding of the molecular machinery responsible for mitosomal division and its synchrony as well as the nature of the ER–mitosome connections poses exciting possibilities for future research.

Conclusion

The mitochondria of animals and fungi undergo constant cycles of division and fusion during the cell cycle. Here, we show that the minimalist MROs known as mitosomes have dramatically simplified their dynamics. In the anaerobic protist *G. intestinalis*, mitosomes divide only during mitosis and remain steady during interphase. In contrast to mitochondria, we propose that mitosomes do not fuse but, similar to mitochondria, maintain a close connection to the ER. We propose that harnessing the nuclear and mitosomal division is a strategy evolved to bypass the lack of mitochondrial fusion.

Methods

G. intestinalis cultivation and transfection

G. intestinalis cells (strain WB) were cultured in TYI-S-33 medium supplemented with 10% heat-inactivated adult bovine serum (GE Healthcare, Chicago, IL, USA), 0.1% bovine bile (Sigma-Aldrich, St. Louis, MO, USA), and appropriate antibiotics at 37 °C. Cells were electroporated using a previously published modified protocol [73]. Briefly, 300 μL of cell culture at an approximate concentration of 3.3×10^7 cells/mL was electroporated with 50 μg of a circular plasmid using a Bio-Rad Gene Pulser (BioRad, Hercules, CA, USA) with the exponential protocol (350 V, 1000 μF, 750 Ω). Transformants were maintained under selection with 57 μg/mL of puromycin (Gold Biotechnology, St. Louis, MO, USA) and/or 0.56 mg/mL G418 (Gold Biotechnology, St. Louis, MO, USA). For iron-starvation experiments, cells were incubated in TYI-S-33 medium without ferric ammonium citrate and supplemented with 2,2'-dipyridyl (Sigma-Aldrich, St. Louis, MO, USA) to a final concentration of 300 μM. The cell culture was maintained for several passages under these conditions.

Enrichment of mitotic cells

Two approaches for cell synchronization were tested: the starvation [42] and the albendazole-dependent [43] methods. Both methods provided the same results concerning the mitosomal dynamics. However, the albendazole treatment had a much greater effect on cell synchrony and therefore was used in the study. Trophozoites from the late log phase were incubated in growth medium supplemented with 100 ng/mL of albendazole (Sigma-Aldrich, St. Louis, MO, USA) for 6 h at 37 °C [43]. After incubation, the albendazole-affected unattached cells were discarded and the unaffected adherent pre-mitotic cells were washed twice with pre-warmed, fresh, drug-free medium and then detached from the tube by cooling on ice for 10 min. The cells were then allowed to proliferate on slides in the drug-free conditions for 9–14 min, fixed, and permeabilized as described below.

G. intestinalis encystation

In vitro encystation was performed as previously described [74]. Briefly, log-phase cells were incubated at 37 °C for 18 h in TYI:GS3 media at pH 7.8 that was supplemented with 5 mg/mL bovine bile (Sigma-Aldrich, St. Louis, MO, USA) and 0.546 mg/mL lactic acid (Sigma-Aldrich, St. Louis, MO, USA). After incubation, the medium was replaced with TYI-S-33 medium and the cells were incubated at 37 °C for several hours until they started to produce cysts. The cysts were then fixed with 1% paraformaldehyde for 30 min at room temperature and placed on slides.

Immunofluorescent labeling

For the immunofluorescence, trophozoites were incubated on slides in TYI-S-33 medium for 15 min at 37 °C, fixed in ice-cold methanol for 5 min, and permeabilized in ice-cold acetone for 5 min. The blocking and the immunolabeling steps were all performed in a humid chamber using a solution of 0.25% bovine serum albumin (BSA)(Sigma-Aldrich, St. Louis, MO, USA), 0.25% fish gelatin (Sigma-Aldrich, St. Louis, MO, USA), and 0.05% Tween 20 (Sigma-Aldrich, St. Louis, MO, USA) in phosphate-buffered saline (PBS) for 1 h each. The primary antibodies used in this work included rat anti-HA monoclonal IgG antibody (Roche, Basel, Switzerland, 1:1000 dilution), mouse anti-actin polyclonal antibody (gift from Alex Paredez, University of Washington, 1:250 dilution) [56], rabbit anti-GL50803_9296 polyclonal antibody (1:2000 dilution) [33], and mouse anti-GiPDI2 polyclonal antibody (a gift from Adrian Hehl, University of Zurich, 1:2000 dilution) [51]. The secondary antibodies included Alexa Fluor 488-conjugated goat anti-rat monoclonal IgG antibody (Invitrogen, Eugene, OR, USA, batch number 1476598, cat. number A-21208, RRID: AB_141709; 1:1000 dilution), Alexa Fluor 647-conjugated goat anti-mouse monoclonal IgG antibody (Invitrogen, Eugene, OR, USA, batch number 1511346, cat. number A-21235, RRID: AB_141693; 1:1000 dilution), Alexa Fluor 594-conjugated goat anti-rabbit monoclonal IgG antibody (Invitrogen, Eugene, OR, USA, batch number 1454437, cat. number, A-21207, RRID: AB_141637; 1:1000 dilution), and Alexa Fluor 488-conjugated goat anti-mouse

monoclonal IgG antibody (Invitrogen, Eugene, OR, USA, batch number 1562298, cat. number A-21202, RRID: AB_141607; 1:1000 dilution). Three 5-min washes in PBS were performed after each immunolabeling step. Slides were mounted in Vectashield (Vector Laboratories, Burlingame, CA, USA) containing DAPI.

The cysts were fixed in 1% paraformaldehyde for 30 min at 37 °C and spun down at 1000 × *g* for 5 min at room temperature. The cysts were then washed in 1× PEM buffer (100 mM PIPES pH 6.9, 1 mM EGTA, and 0.1 mM $MgSO_4$), resuspended in 1× PEM buffer, and placed on cover slips. Cell permeabilization was performed using 0.2% Triton X-100 (Sigma-Aldrich, St. Louis, MO, USA) for 20 min. The cover slips were then washed three times with 1 mL of 1× PEM and incubated with anti-GL50803_9296 rabbit polyclonal antibody (1:2000 dilution) in 1× PEMBALG [100 mM PIPES pH 6.9, 1 mM EGTA, 0.1 mM $MgSO_4$, 1% BSA, 0.1% NaN_3, 100 mM lysine, and 0.5% cold-water fish skin gelatin (Sigma-Aldrich, St. Louis, MO, USA)] for 1 h. After three 5-min washes in 1× PEM, the slides were incubated with Alexa Fluor 594-conjugated goat anti-rabbit IgG antibody in 1× PEMBALG for 1 h. After three 5-min washes in 1× PEM, the slides were mounted in Vectashield containing DAPI.

For live-cell imaging experiments, trophozoites expressing an IscU-Halo tag fusion product [31] were incubated in growth medium supplemented with the TMR Halo ligand (Promega, Madison, WI, USA, 1:1000 dilution) for 1 h at 37 °C. To wash away unbound TMR ligand, the cells were washed twice with pre-warmed fresh medium and incubated for 30 min at 37 °C. After incubation, the cells were placed on ice for 10 min. The cells were then transferred to a microscope dish and observed using a confocal microscope.

Imaging

Static images were acquired on an Olympus IX-81 microscope using a UPlanSApo 100×/1.4 numerical aperture (NA) oil-immersion objective. Z-stacks of images ranging between 0.23 and 0.25 μm were captured using an ORCA C4742-80-12AG monochromatic CCD camera (Hamamatsu, Shizuoka, Japan). Fluorescence was excited with a xenon arc burner-containing MT20 illumination system (Olympus, Tokyo, Japan), and emitted light was collected through a multiband emission filter. Imaging was controlled with the Olympus Cell-R software. Images were deconvolved using SVI Huygens software with the CMLE algorithm. Maximum intensity projections and brightness/contrast corrections were performed in FIJI ImageJ.

Structured illumination microscopy (SIM) imaging was also performed on a commercial 3D N-SIM microscope (inverted Nikon Eclipse Ti-E, Nikon, Tokyo, Japan) equipped with a Nikon CFI SR Apo TIRF objective (100× oil, NA 1.49). A structured illumination pattern projected into the sample plane was created on a diffraction grating block (100 EX V-R 3D-SIM) for laser wavelengths of 488, 561, and 647 nm. Excitation and emission light was separated using filter cubes with the appropriate filter sets SIM488 (excitation 470–490 nm, emission 500–545 nm), SIM561 (excitation 556–566 nm, emission 570–640 nm) and SIM647 (excitation 590–650 nm, emission 663–738 nm). Emission light was projected through a 2.5× relay lens onto the chip of an electron-multiplying charge-coupled device (EMCCD) camera (Andor iXon Ultra DU897, 10 MHz at 14-bit, 512 × 512 pixels). Three-color Z-stacks (Z-step: 120 nm) were acquired using NIS-Elements AR software (Laboratory Imaging). Laser intensity, electron-multiplying gain, and camera exposure time were set independently for each excitation wavelength. The intensity of the fluorescence signal was held within the linear range of the camera. Fifteen images (three rotations and five phase shifts) were recorded for every plane and color. SIM data were processed in NIS-Elements AR. Before sample measurement, the symmetry of the point spread function was checked with 100 nm red fluorescent beads (580/605, Carboxylate-Modified Microspheres, Molecular Probes, Eugene, OR, USA) mounted in Prolong Diamond Antiface Mountant (Molecular Probes, Eugene, OR, USA), and optimized by adjusting the objective correction collar. The live-imaging differential interference contrast (DIC) microscopy time series and confocal fluorescence images were acquired on an Olympus IX-81 microscope equipped with a Yokogawa CSU-X1 spinning disc unit and an Andor DU-897 EMCCD camera using an UPlanSApo 60×/1.35 NA oil-immersion objective (Olympus, Tokyo, Japan). Fluorescence was excited with a 561-nm laser (Coherent Inc., Santa Clara, CA, USA) and collected through a multiband emission filter (Semrock FF01-440/521/607/700). Typical Z-stacks were captured with a 0.5-μm Z-axis step. After imaging, images were processed in FIJI ImageJ software.

Plasmid construction and cloning

The *G. intestinalis* dynamin gene (GL50803_14373) and 250 base pairs of its 5′ untranslated region (UTR) were amplified together from *G. intestinalis* genomic DNA using the primers 5′-CATGGATATCACAACGAGGC TTTAAGCC-3′ and 5′-CATGATGCATGTCCTTCTT GGCAAGGTC-3′, which contain EcoRV and NsiI restriction sites, respectively. The resulting product was cloned as an EcoRV/NsiI fragment into an EcoRV/PstI-linearized pTG vector. The *G. intestinalis* centrin gene (GL50803_6744) and 300 bp of its 5′ UTR were amplified together from *G. intestinalis* genomic DNA using the primers 5′-CATGGATATCTGCCCATGGCTATGG TGT-3′ and 5′-CATGCTGCAGATAGAGGGACGTGC

GGCG-3′, which contain EcoRV and PstI restriction sites, respectively. The resulting product was cloned as an EcoRV/PstI fragment into an EcoRV/PstI-linearized pTG vector.

To generate mutant K43E dynamin (GL50803_14373), the mutation was introduced by site-directed mutagenesis using the primers 5′-CATGACGCGTTATGTCTC AGATAGACAAG-3′ and 5′-CTCCAAAACCGATGA CTCTCCCGCAGA-3′, and 5′-TCCCAATCTGCGGG AGAGTCATCGGTT-3′ and 5′-CATGGCGGCCGCT CCTTTCTTGGCAAGGTC-3′. The resulting product was cloned as an MluI/NotI fragment into a MluI/NotI-linearized pPAC vector.

The N-terminally HA-tagged gene for GiQb4 was amplified from *G. intestinalis* genomic DNA using primers 5′-CTAGGGATCCATGTACCCATACGATGTTCCAGATT ACGCTGAAGAGATAGAATGTTCACTCA-3′ and 5′-G CTAGTCGACTCAATATCTGATCTCTGA-3′ containing BamHI/SalI restriction sites, respectively. Resulting product was cloned as a BamHI/SalI fragment to a BamHI/XhoI-linearized pONDRA plasmid containing the gene for GiMOMP35 [27].

Cell fractionation

G. intestinalis cells were collected in ST buffer containing protease inhibitors TLCK and Leupeptine. The cells were sonicated by 1-s pulses at amplitude 40 until all the cells were completely lysed. The lysate was centrifuged at 2.680 × *g* for 20 min at 4 °C. The supernatant was centrifuged at 180.000 × *g* for 30 min at 4 °C. The resulting supernatant was considered as the cytosolic fraction while the pellet were considered as the high-speed pellet (HSP) fraction.

Sodium carbonate extraction

For sodium carbonate extraction, 50 μL of the cellular HSP fraction was mixed with 200 μL of freshly made 100 mM Na_2CO_3 (pH 11) and incubated on ice for 30 min. The sample was mixed vigorously every 2 min. After incubation, the sample was centrifuged at 100,000 × *g* for 30 min at 4 °C. The supernatant was then mixed with TCA (trichloracetic acid) to a final concentration of 20% and incubated on ice for 30 min. The pellet (1) was kept on ice. After incubation with TCA, the supernatant was centrifuged at 30,000 × *g* for 10 min at 4 °C. The pellet (2) was rinsed with 0.5 mL of ice-cold acetone and centrifuged at 30,000 × *g* for 10 min at 4 °C. Both pellets were mixed with 50 μL of 1 × SDS (sodium dodecyl sulfate) sample buffer and incubated at 95 °C until dissolved.

Trypsin treatment

For treatment with trypsin, 20 μL of the cellular HSP fraction containing 150 μg of proteins was mixed with trypsin (5 mg/mL) or trypsin and 1% Triton X-100 as follows: (1) 20 μL HSP + 30 μL SM (sucrose, MOPS) buffer; (2) 20 μL HSP + 28 μL SM buffer + 2 μL trypsin; and (3) 20 μL HSP + 23 μL SM buffer + 5 μL Triton X-100.

All samples were incubated for 10 min at 37 °C and boiled in 50 μL of 1 × SDS sample buffer at 95 °C for 5 min.

Determination of enzymatic activities

All enzyme activities were assayed spectrophotometrically at 25 °C. The activity of PFO was assayed as the rate of methyl viologen reduction monitored at 600 nm. The assay was performed under anaerobic conditions using pyruvate as a substrate for PFO as described in [75].

Additional files

Additional file 1: Dividing mitosomes in mitotic *G. intestinalis*. *G. intestinalis* culture expressing IscU-Halo was enriched for mitotic trophozoites by albendazole treatment (100 ng/mL) for 6 h at 37 °C. The cells were washed twice in warm medium and stained by Halo-TMR ligand and observed under a microscope. The images are representative of the sequence submitted as movie files (Additional files 2, 3, and 4). (EPS 7706 kb)

Additional file 2: Movie of the dividing *Giardia* – IscU-Halo. (AVI 5339 kb)

Additional file 3: Movie of the dividing *Giardia* – DIC. (AVI 4615 kb)

Additional file 4: Movie of the dividing *Giardia* – merged channels. (AVI 11947 kb)

Additional file 5: Peripheral mitosomes divide during all stages of mitosis. (**A**) *G. intestinalis* culture was enriched for mitotic trophozoites by albendazole treatment (100 ng/mL) for 6 h at 37 °C. The cells were washed twice in warm medium and fixed, and the mitosomes were immunolabeled with an anti-GL50803_9296 antibody (red) and stained for nuclei with DAPI (blue). The image represents a deconvolved maximal projection of the Z-stack. Corresponding DIC images are shown. Scale bar, 2 μm. Arrowheads point at dividing mitosomes. (**B**) The number of mitosomes in particular stages of mitosis was determined using fixed cells. The data show a gradual increase in mitosome number during mitosis. Thirty cells of each mitotic stage were used for the statistics. The error bars represent the standard deviations. (EPS 4730 kb)

Additional file 6: Distribution of dynamin in mitotic *G. intestinalis* cells. *G. intestinalis* expressing HA-tagged GlDRP was enriched for mitotic trophozoites. The cells were immunolabeled using anti-GL50803_9296 antibody (red), anti-PDI2 antibody (magenta), and anti-HA antibody (green). Selected layers of the Z-stack are shown with the corresponding DIC image. Scale bar, 2 μm. (EPS 2840 kb)

Additional file 7: The expression of K43E GlDRP in *G. intestinalis*. The cell lysate of the encysting cells was probed for the presence of HA-tagged K43E GlDRP. The arrow points toward the expected size of the protein on the western blot. (EPS 3276 kb)

Additional file 8: Distribution of actin in mitotic *G. intestinalis*. *G. intestinalis* culture was enriched for mitotic trophozoites. (**A**) The cells were immunolabeled using anti-GL50803_9296 antibody (red) and anti-GiActin antibody (green). The image represents the deconvolved maximal projection of the Z-stack (MAX). (**B**) The cells were immunolabeled using the anti-PDI2 antibody (red) and anti-GiActin antibody (green). The images represent the deconvolved maximal projection of the Z-stack (MAX) and two selected layers. Corresponding DIC images are shown. Scale bar, 2 μm. (EPS 5063 kb)

Acknowledgements

We would like to thank Jeremy G. Wideman for helpful comments and suggestions to the manuscript, and Ivan Hrdy for his help with the biochemical characterization of *G. intestinalis* maintained in iron-deficient conditions.

Funding
This project was funded by a grant from the Czech Science Foundation GA13-29423S awarded to PD, by a grant from the Charles University Grant Agency (579012) awarded to LV, and by the PRIMUS/SCI/34 grant from the Charles University awarded to PD. This work was further supported by the Ministry of Education, Youth and Sports of CR within the National Sustainability Program II (Project BIOCEV-FAR) LQ1604 and by the project BIOCEV (CZ.1.05/1.1.00/02.0109). We acknowledge the Imaging Methods Core Facility at BIOCEV, supported by the Czech-BioImaging large RI project (LM2015062 funded by the Ministry of Education, Youth and Sports, CR), for their support with obtaining scientific data presented in this paper.

Availability of data and materials
All data generated or analyzed during this study are included in this published article and its Additional files.

Authors' contributions
LV, PD, SGS, and JT designed the experiments; LV, PD, VN, PT, ZŠ, AA, EE, and PT performed the experiments; LV, PD, GMH, and ZŠ analyzed the data; LV and PD wrote the manuscript. All authors read and approved the final manuscript.

Competing interests
The authors declare that they have no competing interests.

Consent for publication
Not applicable.

Ethics approval and consent to participate
Not applicable.

Publisher's Note

Author details
[1]Department of Parasitology, Faculty of Science, Charles University, Průmyslová 595, Vestec 252 42, Czech Republic. [2]Department of Cell and Molecular Biology, BMC, Uppsala University, Uppsala, Sweden. [3]Institute of Immunology and Microbiology, First Faculty of Medicine, Charles University and General University Hospital, Prague, Czech Republic. [4]Institute of Cellular Biology and Pathology, First Faculty of Medicine, Charles University, Prague, Czech Republic.

Received: 8 December 2016 Accepted: 1 March 2017
Published online: 03 April 2017

References

1. Labbé K, Murley A, Nunnari J. Determinants and functions of mitochondrial behavior. Annu Rev Cell Dev Biol. 2014;30:357–91.
2. Mishra P, Chan DC. Mitochondrial dynamics and inheritance during cell division, development and disease. Nat Rev Mol Cell Biol. 2014;15:634–46.
3. Bleazard W, McCaffery JM, King EJ, Bale S, Mozdy A, Tieu Q, Nunnari J, Shaw JM. The dynamin-related GTPase Dnm1 regulates mitochondrial fission in yeast. Nat Cell Biol. 1999;1:298–304.
4. Mozdy AD, McCaffery JM, Shaw JM. Dnm1p GTPase-mediated mitochondrial fission is a multi-step process requiring the novel integral membrane component Fis1p. J Cell Biol. 2000;151:367–80.
5. Otera H, Wang C, Cleland MM, Setoguchi K, Yokota S, Youle RJ, Mihara K. Mff is an essential factor for mitochondrial recruitment of Drp1 during mitochondrial fission in mammalian cells. J Cell Biol. 2010;191:1141–58.
6. Hales KG, Fuller MT. Developmentally regulated mitochondrial fusion mediated by a conserved, novel, predicted GTPase. Cell. 1997;90:121–9.
7. Wong ED, Wagner JA, Gorsich SW, McCaffery JM, Shaw JM, Nunnari J. The dynamin-related GTPase, Mgm1p, is an intermembrane space protein required for maintenance of fusion competent mitochondria. J Cell Biol. 2000;151:341–52.
8. Friedman JR, Lackner LL, West M, DiBenedetto JR, Nunnari J, Voeltz GK. ER tubules mark sites of mitochondrial division. Science. 2011;334:358–62.
9. Murley A, Lackner LL, Osman C, West M, Voeltz GK, Walter P, Nunnari J. ER-associated mitochondrial division links the distribution of mitochondria and mitochondrial DNA in yeast. Elife. 2013;2:e00422.
10. Rowland AA, Voeltz GK. Endoplasmic reticulum–mitochondria contacts: function of the junction. Nat Rev Mol Cell Biol. 2012;13:607–25.
11. Kornmann B, Currie E, Collins SR, Schuldiner M, Nunnari J, Weissman JS, Walter P. An ER-mitochondria tethering complex revealed by a synthetic biology screen. Science. 2009;325:477–81.
12. AhYoung AP, Jiang J, Zhang J, Khoi Dang X, Loo JA, Zhou ZH, Egea PF. Conserved SMP domains of the ERMES complex bind phospholipids and mediate tether assembly. Proc Natl Acad Sci U S A. 2015;112:E3179–88.
13. Murley A, Sarsam RD, Toulmay A, Yamada J, Prinz WA, Nunnari J. Ltc1 is an ER-localized sterol transporter and a component of ER-mitochondria and ER-vacuole contacts. J Cell Biol. 2015;209:539–48.
14. Elbaz-Alon Y, Eisenberg-Bord M, Shinder V, Stiller SB, Shimoni E, Wiedemann N, Geiger T, Schuldiner M. Lam6 Regulates the Extent of Contacts between Organelles. Cell Rep. 2015;12:7–14.
15. de Brito OM, Scorrano L. Mitofusin 2 tethers endoplasmic reticulum to mitochondria. Nature. 2008;456:605–10.
16. Filadi R, Greotti E, Turacchio G, Luini A, Pozzan T, Pizzo P. Mitofusin 2 ablation increases endoplasmic reticulum–mitochondria coupling. Proc Natl Acad Sci. 2015;112:E2174–81.
17. Adams DW, Errington J. Bacterial cell division: assembly, maintenance and disassembly of the Z ring. Nat Rev Microbiol. 2009;7:642–53.
18. Beech PL, Nheu T, Schultz T, Herbert S, Lithgow T, Gilson PR, McFadden GI. Mitochondrial FtsZ in a chromophyte alga. Science. 2000;287:1276–9.
19. Leger MM, Petrů M, Žárský V, Eme L, Vlček Č, Harding T, Lang BF, Eliáš M, Doležal P, Roger AJ. An ancestral bacterial division system is widespread in eukaryotic mitochondria. Proc Natl Acad Sci U S A. 2015;112:10239–46.
20. Chanez A-L, Hehl AB, Engstler M, Schneider A. Ablation of the single dynamin of T. brucei blocks mitochondrial fission and endocytosis and leads to a precise cytokinesis arrest. J Cell Sci. 2006;119:2968–74.
21. Morgan GW, Goulding D, Field MC. The single dynamin-like protein of Trypanosoma brucei regulates mitochondrial division and is not required for endocytosis. J Biol Chem. 2004;279:10692–701.
22. Wexler-Cohen Y, Stevens GC, Barnoy E, van der Bliek AM, Johnson PJ. A dynamin-related protein contributes to Trichomonas vaginalis hydrogenosomal fission. FASEB J. 2014;28:1113–21.
23. Niemann M, Wiese S, Mani J, Chanfon A, Jackson C, Meisinger C, Warscheid B, Schneider A. Mitochondrial outer membrane proteome of Trypanosoma brucei reveals novel factors required to maintain mitochondrial morphology. Mol Cell Proteomics. 2013;12:515–28.
24. Schneider RE, Brown MT, Shiflett AM, Dyall SD, Hayes RD, Xie Y, Loo JA, Johnson PJ. The Trichomonas vaginalis hydrogenosome proteome is highly reduced relative to mitochondria, yet complex compared with mitosomes. Int J Parasitol. 2011;41:1421–34.
25. Makiuchi T, Nozaki T. Highly divergent mitochondrion-related organelles in anaerobic parasitic protozoa. Biochimie. 2014;100:3–17.
26. O'Malley MA, Wideman JG, Ruiz-Trillo I. Losing complexity: the role of simplification in macroevolution. Trends Ecol Evol. 2016;31(8):608–21.
27. Jedelský PL, Doležal P, Rada P, Pyrih J, Smíd O, Hrdý I, Sedinová M, Marcinčiková M, Voleman L, Perry AJ, Beltrán NC, Lithgow T, Tachezy J. The minimal proteome in the reduced mitochondrion of the parasitic protist Giardia intestinalis. PLoS One. 2011;6:e17285.
28. Mi-ichi F, Abu Yousuf M, Nakada-Tsukui K, Nozaki T. Mitosomes in Entamoeba histolytica contain a sulfate activation pathway. Proc Natl Acad Sci U S A. 2009;106:21731–6.
29. Tovar J, León-Avila G, Sánchez LB, Sutak R, Tachezy J, van der Giezen M, Hernández M, Müller M, Lucocq JM. Mitochondrial remnant organelles of Giardia function in iron-sulphur protein maturation. Nature. 2003;426:172–6.
30. Ankarklev J, Jerlström-Hultqvist J, Ringqvist E, Troell K, Svärd SG. Behind the smile: cell biology and disease mechanisms of Giardia species. Nat Rev Microbiol. 2010;8:413–22.
31. Martincová E, Voleman L, Najdrová V, De Napoli M, Eshar S, Gualdron M, Hopp CS, Sanin DE, Tembo DL, Van Tyne D, Walker D, Marcinčiková M, Tachezy J, Doležal P. Live imaging of mitosomes and hydrogenosomes by HaloTag technology. PLoS One. 2012;7:e36314.
32. Regoes A, Zourmpanou D, León-Avila G, van der Giezen M, Tovar J, Hehl AB. Protein import, replication, and inheritance of a vestigial mitochondrion. J Biol Chem. 2005;280:30557–63.
33. Martincová E, Voleman L, Pyrih J, Žárský V, Vondráčková P, Kolísko M, Tachezy J, Doležal P. Probing the biology of *Giardia intestinalis* mitosomes using in vivo enzymatic tagging. Mol Cell Biol. 2015;35:2864–74.

34. Brown DM, Upcroft JA, Edwards MR, Upcroft P. Anaerobic bacterial metabolism in the ancient eukaryote Giardia duodenalis. Int J Parasitol. 1998;28:149–64.
35. Sutak R, Dolezal P, Fiumera HL, Hrdy I, Dancis A, Delgadillo-Correa M, Johnson PJ, Müller M, Tachezy J. Mitochondrial-type assembly of FeS centers in the hydrogenosomes of the amitochondriate eukaryote Trichomonas vaginalis. Proc Natl Acad Sci U S A. 2004;101:10368–73.
36. Tejman-Yarden N, Eckmann L. New approaches to the treatment of giardiasis. Curr Opin Infect Dis. 2011;24:451–6.
37. Liu SM, Brown DM, O'Donoghue P, Upcroft P, Upcroft JA. Ferredoxin involvement in metronidazole resistance of Giardia duodenalis. Mol Biochem Parasitol. 2000;108:137–40.
38. Land KM, Clemens DL, Johnson PJ. Loss of multiple hydrogenosomal proteins associated with organelle metabolism and high-level drug resistance in trichomonads. Exp Parasitol. 2001;97:102–10.
39. Benchimol M. The hydrogenosome. In: Hohmann-Marriott MF, editor. The structural basis of biological energy generation. Dordrecht: Springer Netherlands; 2014. p. 419–33.
40. Chen H, Chomyn A, Chan DC. Disruption of fusion results in mitochondrial heterogeneity and dysfunction. J Biol Chem. 2005;280:26185–92.
41. Hermann GJ, Thatcher JW, Mills JP, Hales KG, Fuller MT, Nunnari J, Shaw JM. Mitochondrial fusion in yeast requires the transmembrane GTPase Fzo1p. J Cell Biol. 1998;143:359–73.
42. Gustafsson MGL, Shao L, Carlton PM, Wang CJR, Golubovskaya IN, Cande WZ, Agard DA, Sedat JW. Three-dimensional resolution doubling in wide-field fluorescence microscopy by structured illumination. Biophys J. 2008;94:4957–70.
43. Nohynková E, Tumová P, Kulda J. Cell division of Giardia intestinalis: flagellar developmental cycle involves transformation and exchange of flagella between mastigonts of a diplomonad cell. Eukaryot Cell. 2006;5:753–61.
44. Striepen B, Crawford MJ, Shaw MK, Tilney LG, Seeber F, Roos DS. The plastid of Toxoplasma gondii is divided by association with the centrosomes. J Cell Biol. 2000;151:1423–34.
45. Nishida K, Takahara M, Miyagishima S, Kuroiwa H, Matsuzaki M, Kuroiwa T. Dynamic recruitment of dynamin for final mitochondrial severance in a primitive red alga. Proc Natl Acad Sci U S A. 2003;100:2146–51.
46. Pucadyil TJ, Schmid SL. Real-time visualization of dynamin-catalyzed membrane fission and vesicle release. Cell. 2008;135:1263–75.
47. Hehl AB, Regos A, Schraner E, Schneider A. Bax function in the absence of mitochondria in the primitive protozoan Giardia lamblia. PLoS One. 2007;2:e488.
48. Sagolla MS, Dawson SC, Mancuso JJ, Cande WZ. Three-dimensional analysis of mitosis and cytokinesis in the binucleate parasite Giardia intestinalis. J Cell Sci. 2006;119:4889–900.
49. Meng TC, Aley SB, Svard SG, Smith MW, Huang B, Kim J, Gillin FD. Immunolocalization and sequence of caltractin/centrin from the early branching eukaryote Giardia lamblia. Mol Biochem Parasitol. 1996;79:103–8.
50. Elias EV, Quiroga R, Gottig N, Nakanishi H, Nash TE, Neiman A, Lujan HD. Characterization of SNAREs determines the absence of a typical Golgi apparatus in the ancient eukaryote Giardia lamblia. J Biol Chem. 2008;283:35996–6010.
51. Hehl AB, Marti M. Secretory protein trafficking in Giardia intestinalis. Mol Microbiol. 2004;53:19–28.
52. Bernander R, Palm JE, Svärd SG. Genome ploidy in different stages of the Giardia lamblia life cycle. Cell Microbiol. 2001;3:55–62.
53. Labrousse AM, Zappaterra MD, Rube DA, van der Bliek AM. C. elegans dynamin-related protein DRP-1 controls severing of the mitochondrial outer membrane. Mol Cell. 1999;4:815–26.
54. Korobova F, Ramabhadran V, Higgs HN. An actin-dependent step in mitochondrial fission mediated by the ER-associated formin INF2. Science. 2013;339:464–7.
55. Gaechter V, Schraner E, Wild P, Hehl AB. The single dynamin family protein in the primitive protozoan Giardia lamblia is essential for stage conversion and endocytic transport. Traffic. 2008;9:57–71.
56. Paredez AR, Assaf ZJ, Sept D, Timofejeva L, Dawson SC, Wang C-JR, Cande WZ. An actin cytoskeleton with evolutionarily conserved functions in the absence of canonical actin-binding proteins. Proc Natl Acad Sci U S A. 2011;108:6151–6.
57. Zumthor JP, Cernikova L, Rout S, Kaech A, Faso C, Hehl AB. Static clathrin assemblies at the peripheral vacuole-plasma membrane interface of the parasitic protozoan Giardia lamblia. PLoS Pathog. 2016;12:e1005756.
58. Simpson AGB. Cytoskeletal organization, phylogenetic affinities and systematics in the contentious taxon Excavata (Eukaryota). Int J Syst Evol Microbiol. 2003;53:1759–77.
59. Lahiri S, Chao JT, Tavassoli S, Wong AKO, Choudhary V, Young BP, Loewen CJR, Prinz WA. A conserved endoplasmic reticulum membrane protein complex (EMC) facilitates phospholipid transfer from the ER to mitochondria. PLoS Biol. 2014;12:e1001969.
60. Wideman JG, Gawryluk RMR, Gray MW, Dacks JB. The ancient and widespread nature of the ER-mitochondria encounter structure. Mol Biol Evol. 2013;30:2044–9.
61. Wideman JG. The ubiquitous and ancient ER membrane protein complex (EMC): tether or not? F1000Res. 2015;4:624.
62. Vance JE. MAM (mitochondria-associated membranes) in mammalian cells: lipids and beyond. Biochim Biophys Acta. 2014;1841:595–609.
63. Yichoy M, Duarte TT, Chatterjee ADE, Mendez TL. Lipid metabolism in Giardia : a post-genomic perspective. 2011. p. 267–78.
64. Embley TM, Martin W. Eukaryotic evolution, changes and challenges. Nature. 2006;440:623–30.
65. Dolezal P, Smíd O, Rada P, Zubácová Z, Bursać D, Suták R, Nebesárová J, Lithgow T, Tachezy J. Giardia mitosomes and trichomonad hydrogenosomes share a common mode of protein targeting. Proc Natl Acad Sci U S A. 2005;102:10924–9.
66. Robinson DR, Gull K. Basal body movements as a mechanism for mitochondrial genome segregation in the trypanosome cell cycle. Nature. 1991;352:731–3.
67. Nishi M, Hu K, Murray JM, Roos DS. Organellar dynamics during the cell cycle of Toxoplasma gondii. J Cell Sci. 2008;121:1559–68.
68. Gray MW, Lang BF, Burger G. Mitochondria of protists. Annu Rev Genet. 2004;38:477–524.
69. Kuroiwa T, Nishida K, Yoshida Y, Fujiwara T, Mori T, Kuroiwa H, Misumi O. Structure, function and evolution of the mitochondrial division apparatus. Biochim Biophys Acta. 2006;1763:510–21.
70. Rout S, Zumthor JP, Schraner EM, Faso C, Hehl AB. An interactome-centered protein discovery approach reveals novel components involved in mitosome function and homeostasis in Giardia lamblia. Kumar K, editor. PLoS Pathog. 2016;12:e1006036.
71. Beltrán NC, Horváthová L, Jedelský PL, Šedinová M, Rada P, Marcinčiková M, Hrdý I, Tachezy J. Iron-induced changes in the proteome of Trichomonas vaginalis hydrogenosomes. PLoS One. 2013;8:e65148.
72. Gao H, Sage TL, Osteryoung KW. FZL, an FZO-like protein in plants, is a determinant of thylakoid and chloroplast morphology. Proc Natl Acad Sci U S A. 2006;103:6759–64.
73. Yu DC, Wang AL, Wang CC. Stable coexpression of a drug-resistance gene and a heterologous gene in an ancient parasitic protozoan Giardia lamblia. Mol Biochem Parasitol. 1996;83:81–91.
74. McCaffery JM, Gillin FD. Giardia lamblia: ultrastructural basis of protein transport during growth and encystation. Exp Parasitol. 1994;79:220–35.
75. Vanácová S, Rasoloson D, Rázga J, Hrdý I, Kulda J, Tachezy J. Iron-induced changes in pyruvate metabolism of Tritrichomonas foetus and involvement of iron in expression of hydrogenosomal proteins. Microbiology. 2001;147:53–62.
76. Wideman JG, Muñoz-Gómez SA. The evolution of ERMIONE in mitochondrial biogenesis and lipid homeostasis: an evolutionary view from comparative cell biology. Biochim Biophys Acta. 2016;1861(8 Pt B):900–12.